4 BASE FLOW AND TRANSPORT MODELS

4.1 BASE MODEL FOR THE FLUX MEASUREMENT EXPERIMENT

4.1.1 MODEL DESCRIPTION

Model equations.

The tracer experimental data were analyzed using the HYDRUS-2D software package simulating variably-saturated water flow and solute transport (Šimůnek et al., 1999). The model is based on the Richards equation for flow and the advection-dispersion equation for transport, given by equations (3-8) and (3-9), respectively. The soil water retention and unsaturated hydraulic conductivity functions were described using the van Genuchten (1980) relationships given by equations (3-10) and (3-11), respectively.

Simulation domain and boundary conditions.

Application of Eqs. (3-8) to (3-11) to the field tracer experiment using HYDRUS-2D requires definition of the numerical finite element mesh, the initial and boundary conditions, and the soil hydraulic and solute transport parameters. The simulation domain and the initial and boundary conditions were defined in accordance with the experimental conditions as described in Section 3.2.4.1. We considered an axisymmetrical flow field of 250 cm height and a radius of 30 m (Fig. 4-1). The finite element mesh size was 5 cm in the vertical direction and 10 cm in the horizontal direction everywhere, except near the soil surface and the well boundary where we used a mesh size of 2.5 cm. The bottom boundary was considered as a no-flux boundary for both water flow and solute transport. Along the right boundary, 20 m from the pumping well, we assumed that the water table depth (1.68 m) was not affected by the irrigation, and as such imposed an equilibrium pressure head distribution versus depth for flow and a zero gradient concentration for transport.

The soil surface boundary was divided into four concentric rings (Fig. 4-1). A constant water flux of 4.1 mm h^{-1} was imposed between radii of 2.5 to 2,000 cm, and a zero flux elsewhere. A solute flux with a concentration equal to the concentration of the irrigation water (C_{ir}) was assigned between radii of 2.5 and 10 cm, and between 300 and 2000 cm. Water and solute fluxes were assumed to be zero for radii larger than 2,000 cm. Flux concentrations between 10 and 300 cm near the well where the tracers were applied, were calculated such that they were consistent with the total tracer application rates. We assumed pulse durations of one hour (related to the dissolution times of the solutes) for all tracers, leading to concentrations of the infiltrating water of 26,000, 12,700 and 4,073 g L^{-3} for Br, Cl and PFBA, respectively. The Cl concentration of the irrigation water was 8.75 μg cm^{-3} (Section 3.2.4.1), while no Br and PFBA were present in the irrigation water.

Along the left boundary (at a radius r of 2.5 cm) representing the well, a system-dependent seepage flux boundary was applied through which water can leave the saturated part of the flow domain. Although the model stipulated a potential seepage boundary from the soil surface to 170 cm the "active seepage" zone occurred only near the water table (see Fig. 4-1), depending upon the transient flow conditions during the experiment. This type of boundary condition assumes a zero flux as long as the local pressure head at the soil-well interface is negative (Fig. 4-1). However, a zero pressure head is used as soon as the soil at a point along the boundary becomes saturated. Additionally, a variable flux (Neumann) boundary condition was specified between depths of 175 (the pump installation depth) and 23 cm. The total value of the imposed variable

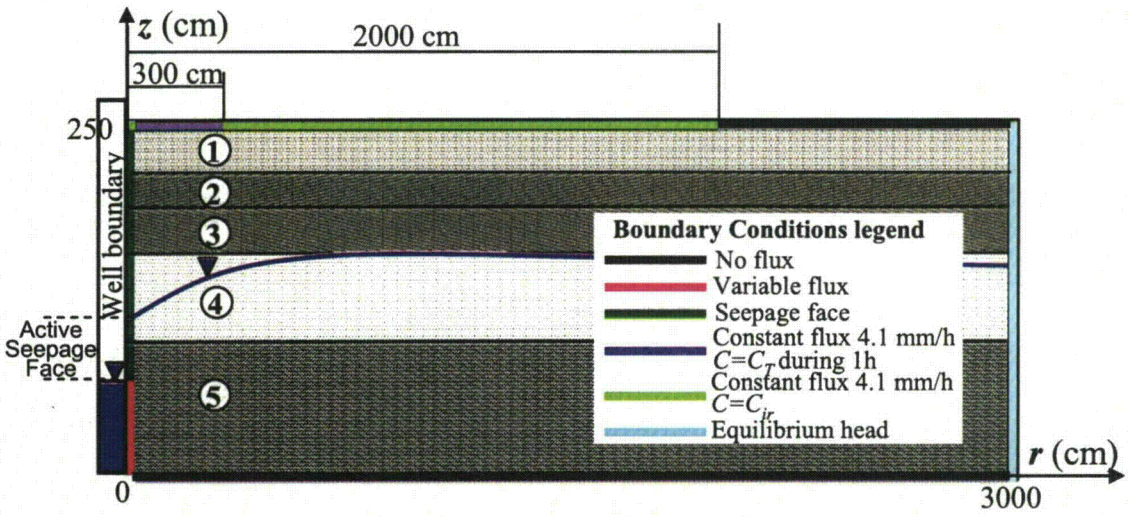

Figure 4-1. Simulation domain and specified boundary conditions (not to scale). Different textures and associated numbers represent the various profile layers. C_T and C_{ir} are the solute concentrations of the infiltrating water.

flux through this boundary was adjusted iteratively during the numerical calculations until the simulated total flow volume to the well matched the measured total volume of pumped water at the end of the simulation period. Finally, a zero concentration gradient was assumed along the left and right boundaries of the transport domain.

As initial condition for the pressure head we used an equilibrium distribution in the profile corresponding to the observed initial water table depth of 1.68 m. The initial concentrations for the transport simulations were zero for Br and PFBA, and 7.3 mg/L for Cl, being the average measured Cl concentration in the saturated zone prior to irrigation.

Calculation of tracer concentrations in the pumping well.

Solute concentrations of the pumped water (C_w) were calculated from a mass balance equation assuming full mixing in the pumping well as follows

$$\pi r_w^2 h_w \frac{dC_w}{dt} = Q_{c(SF)}(t) + Q_{c(VB)}(t) - Q_p(t) C_w \qquad (4\text{-}1)$$

where r_w is the well radius (L), h_w is the mean water level in the well (L), $Q_{c(SF)}$ and $Q_{c(VB)}$ are the mass fluxes (M T^{-1}) of the tracers to the well through the seepage face and variable flux boundaries, respectively, as calculated with HYDRUS-2D, and Q_p is the pumping rate (L^3 T^{-1}).

Model performance.

The goodness-of-fit of the model was evaluated using the coefficient of determination (R^2) and the modified index of agreement (*MIA*) as given by Legates and McCabe (1999):

$$MIA = 1 - \frac{\sum_{i=1}^{n} \left| C_w(t_i) - C_w^{obs}(t_i) \right|}{\sum_{i=1}^{n} \left| C_w(t_i) - \overline{C_w^{obs}} \right| + \sum_{i=1}^{n} \left| C_w^{obs}(t_i) - \overline{C_w^{obs}} \right|}, \qquad (4\text{-}2)$$

where $C_w^{obs}(t_i)$ and $C_w^{obs}(t_i)$ represent the simulated and observed concentrations of the tracer in the pumped water at time t_i, and $\overline{C_w^{obs}}$ is the observed mean concentration. While there is no statistical basis to decide exactly which *MIA* value is a good threshold characterizing the use of an "accurate" model, following Köhne et al. (2005) we assumed simulations with *MIA*>0.75 as being "accurate".

4.1.2 Model calibration and simulations

Inverse solution procedure for the soil hydraulic properties.

Soil hydraulic parameters needed for the calculations were estimated using a combination of one-dimensional and two-dimensional inverse simulations carried out with the HYDRUS-1D (Šimůnek et al., 2005) and HYDRUS-2D (Šimůnek et al., 1999) software packages, respectively, as well as using laboratory measurements of the saturated water content (θ_s) of the various soil horizons. During a first step we used HYDRUS-1D to estimate the hydraulic parameters from observed water contents values that were monitored at different depths in the soil profile 11 m away from the pumping well. By using HYDRUS-1D we assumed that flow in the unsaturated zone this far (11 m) from the pumping well was mainly in the vertical direction, thus considerably minimizing computational times as compared to using HYDRUS-2D. During a second step we used HYDRUS-2D to perform additional calibrations of the saturated hydraulic

conductivity (K_{sat}) of layers 3 to 5 (Fig. 4-1) where water presumably flowed both vertically and horizontally.

For the HYDRUS-1D simulations we assumed a 250-cm deep soil profile consisting of 5 layers consistent with the described lithology of the site: loamy sand (0-28 cm), sandy loam (28-48 cm), sandy loam (48-78 cm), coarse sand (78-140 cm), and gravely sand (142-250 cm). The clay loam horizon (250–350 cm) had an extremely low conductivity and as such was considered to be impermeable and hence not included in the simulations. The sandy loam horizon (30-80 cm) was subdivided into two layers based on the fact that markedly different water contents were observed during steady infiltration at depths of 30 and 50 cm (Fig. 3-49), thus indicating different hydraulic properties. The MCP measured water content at depths of 10, 30, 50, 80, 120 and 150 cm were used to calibrate the flow model, which in total contained 25 hydraulic parameters (the five parameters θ_r, θ_s, α, n and K_{sat} for each of the five layers). To minimize issues of uniqueness in the inverse solution we decreased the number of optimized parameters by using experimentally measured values of the water content at saturation (θ_s), and zero values of the residual water content (θ_r) for all coarse-textured layers (except sandy loam). Thus, we needed to determine three parameters (K_{sat}, α, n) for each of five layers and one θ_r value (for the sandy loam horizon).

The evaporation rate was relatively low, while no rain or irrigation occurred a week prior to the experiment. We therefore assumed that the initial pressure head profile was close to equilibrium with the water table at 1.68 m. The boundary condition at the soil surface defined a water flux of 4.1 mm h^{-1} during the irrigation period. Since the bottom boundary at 250 cm was considered to be impermeable, the water table was likely to rise in some region around the well after irrigation started. As a result, some lateral water flow in the saturated zone occurred, which had to be accounted by a flux through the lower boundary in the one-dimensional HYDRUS-1D simulations. This flux varied with time depending on the position of the water table. To simulate this processes we used the HYDRUS-1D horizontal drain boundary condition with a drain spacing of 22 m (twice the distance from the MCP location to the pumping well). Although this boundary condition does not describe the physical 2D flow system exactly, it was the boundary condition available in HYDRUS-1D that most closely represented our field conditions.

Initial estimates of the α and n parameters for the inverse procedure were based on the assumed initial equilibrium distribution of the pressure head and the observed water contents prior to the experiment, while K_{sat} values were initially estimated from soil textural class and particle size distribution information. We used a sequential inverse procedure by starting the parameter search with the first layer, while assuming that the other parameters were known (the initial estimates) and using observed water contents of the 10 cm depth only. The next step was to find parameters of the second layer by fitting water contents at depths of 0.1 and 0.3 m, and using the parameters of the first layer found at the previous step. The third step was to adjust parameters of layers 1 and 2 simultaneously by fitting measured water contents at depths of 0.1 and 0.3 m. We continued this sequential procedure by gradually increasing the number of layers and hence the number of parameters that were simultaneously estimated. During the final step, the HYDRUS-1D code searched simultaneously for 15 parameters (θ_r for the sandy loam horizon was not changed after the third run).

Soil hydraulic parameters from calibration.

Fig. 4-2 compares MCP-measured water contents at different depth with simulated values obtained with HYDRUS-1D. Good agreement was obtained between the observed and simulated

water contents for all depths except at 0.8 m, where the lowest value of the coefficient of determination (R^2) of 0.877 was obtained. The fluctuations in observed water contents at the four upper observation points may have been caused by non-uniform irrigation during several windy days (Sect. 3.2.4.1). The calculated water content time series clearly describe the propagation of the moisture front into the profile.

Table 4-1 presents the fitted hydraulic parameters obtained using the invoked inverse procedure. A relatively high value of 10 was obtained for the van Genuchten hydraulic parameter n for the fifth layer (gravely sand), which implies very steep water retention curve and an unsaturated hydraulic conductivity curve in which the conductivity decreases very rapidly with decreasing pressure head. While some slight changes in the minimized objective function occurred when the parameter n varied between 8 and 12, the simulated water contents were found not to be sensitive to these changes. We therefore accepted a value of $n = 10$ for the very coarse-textured gravelly sand layer.

Additional calibrations were carried out with the complete two-dimensional axisymmetrical flow model against observed water contents. As a result, we obtained values for the saturated hydraulic conductivity, K_{sat}, of 185, 149 and 52 cm/h for layers 3, 4 and 5, respectively. The maximum difference of these K_{sat} values from those obtained for the 1D problem was for the fifth layer. The calibrated K_{sat} for the 2D problem here was approximately three times smaller than that of 1D problem. The difference likely was a consequence of using an imperfect lower boundary condition in the one-dimensional case. The simulated water contents obtained with HYDRUS-2D were essentially identical to those shown in Fig. 4-2. The coefficient of determination, R^2, for the 2D calibration was 0.858, being slightly smaller than the value of 0.877 obtained with the HYDRUS-1D calibration.

Despite the achieved good fit to the experimental data, we realize that the obtained set of parameters may not be unique and that additional experiments would be helpful to reduce uncertainty in the parameters. Nevertheless, we accepted these values and used them for our simulations for the two-dimensional case. The objective of our study was to obtain an accurate description of the experimental field data (water contents, flow rates, concentrations of the well water), rather than unique soil hydraulic parameters. This since no attempts were made to extrapolate observed data beyond the experimental time period.

2D simulations of water flow and solute transport

Solute transport simulations were carried out for 4 different values of the longitudinal dispersivity, a_L (i.e., 5, 15, 25, and 40 cm). We used the same value for all layers, while assuming in most cases a ratio of 10 between the longitudinal (a_L) and transversal (a_T) dispersivities. This ratio is well within the range of values (5 to 20) reported in previous studies (e.g., Anderson, 1979; Domenico and Schwartz, 1998). Fig. 4-3 compares observed and calculated (using Eq. (4-5) solute breakthrough curves (BTCs) of the tracers in the well. Results are shown for simulations with and without accounting for a seepage face. Neglecting the seepage face boundary caused a delay of a few hours in the arrival of the solute fronts as well as of the maximum concentration. The peak concentrations decreased somewhat, except perhaps for Cl (Fig 4-3b). Since overall agreement with the experimental data was better when the seepage face was included in the simulations, we discuss in what follows only results obtained for simulations with the seepage face boundary.

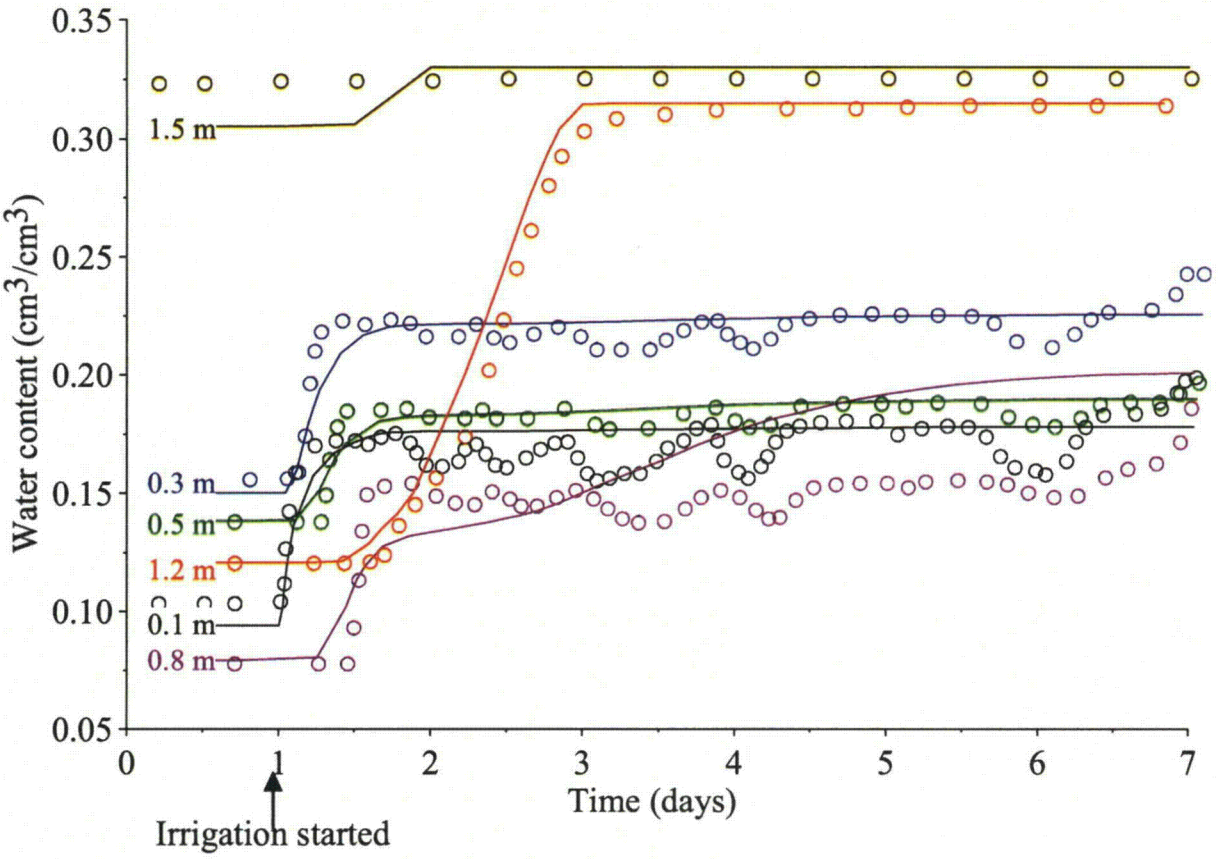

Figure 4-2. Observed (circles) and simulated (lines) soil water contents.

Table 4-1. Unsaturated soil hydraulic parameters inversely estimated using HYDRUS-1D.

N	Layer cm	Parameters				
		θ_s †	θ_r	α , cm^{-1}	n	K_s, cm h^{-1}
1	0-30	0.327	0	0.046	1.62	100
2	30-50	0.351	0.024	0.054	1.46	115
3	50-80	0.260	0	0.054	1.33	113
4	80-150	0.315	0	0.069	1.76	161
5	150-250	0.330	0	0.044	10.00	167

† Experimentally determined.

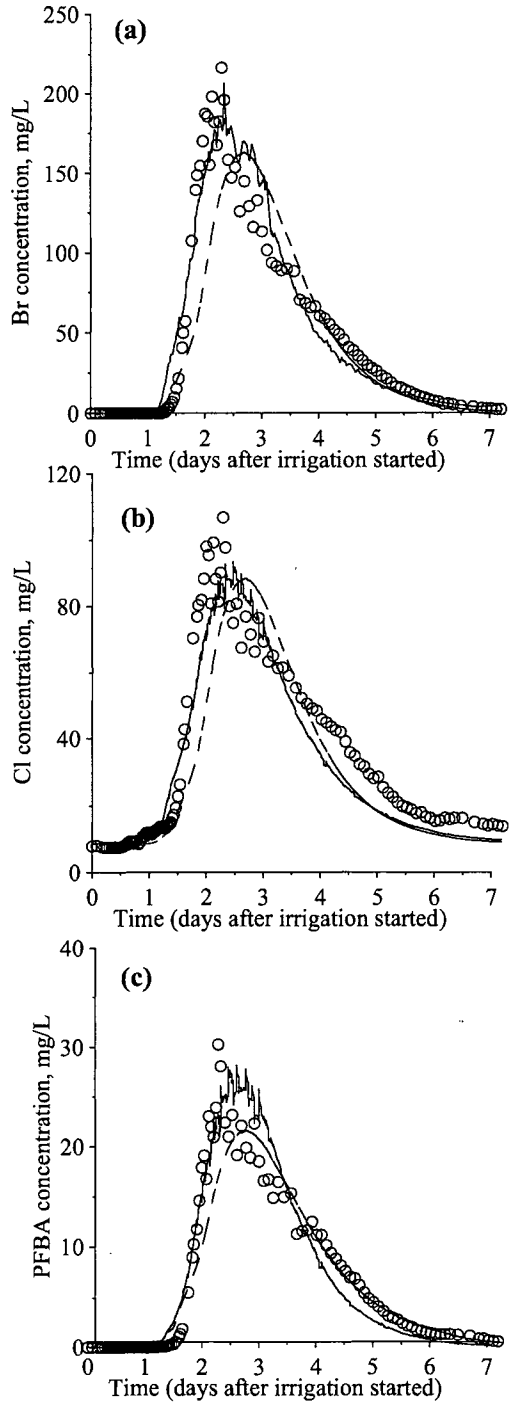

Fig. 4-3. Observed and simulated breakthrough curves of the tracers: (a) Br, (b) Cl and (c) PFBA. Circles – experimental, solid line – simulated with the seepage face boundary, dashed line - simulated without accounting for the seepage face boundary.

The best agreement between observed and simulated BTCs of the tracers in the well was obtained when we used a value of 15 cm for a_L (Fig. 4-3). R^2 values were 0.909, 0.899, and 0.930, and the *MIA* criterion (Eq. 4-6) 0.883, 0.857 and 0.896, for Br, Cl and PFBA, respectively. The model provided a good description of the tracer arrival in the well, but overestimated the arrival time of the maximum concentration by around 8.7%. Simulations with a dispersivity of 5 cm improved the description of the front part of the solute BTCs (especially the initial slope), but caused much lower tails. On the other hand, simulations with a dispersivity of 40 cm described the tails quite well, but resulted in much earlier arrival times and lower maximum concentrations as compared with observed values. Decreasing the ratio a_L/a_T from 10 to 5 did not have an appreciable impact on the simulated BTCs.

The steeper arrival fronts, the more pronounced asymmetrical shape, the earlier concentration peaks, and the longer tails of the observed BTCs as compared with the simulated curves (Fig. 4-3) may indicate enhanced preferential flow or an underestimation of the soil heterogeneity in the simulations (Kung et al., 2000; Buczko and Gerke, 2006). Some of these features probably could be accounted for by invoking a scale-dependent dispersivity in the model. The simulations were conducted with strictly horizontal soil horizons since the extent and spatial distribution of soil heterogeneity were not well known. The variability in the observed concentrations at about the time when the peak concentrations were detected (Fig. 4-3) may have been caused by an unsteady pumping rate (the pumping rate variability was fairly low, but generally increased with time) and because the pump had to be replaced at some point during the experiment (Gish and Kung, 2007).

The sensitivity of the model to the assumed dissolution times of the tracers at the soil surface was tested next. A four-fold decrease or increase in the pulse duration (0.25 or 4 h, respectively), and consequently a four times increase or decrease in the surface boundary concentration (to preserve the injected tracer masses), were found to produce similar results. We additionally tested the effect of having a different thickness of the fifth layer (where most of the well screen was located) by moving the lower boundary of the flow domain up to 2.3 m or down to 2.7 m below the soil surface (Fig. 4-1). Simulation results showed that this did not affect the arrival time of the tracers. The front and back (receding) parts of the BTCs were slightly steeper while the maximum concentration in the well was about 10% larger for the thicker fifth layer (bottom boundary at 2.7 m) as compared with the 2.3-m deep bottom boundary.

Water and solute fluxes at the well boundary

Using HYDRUS-2D we were able to estimate the different water and solute fluxes through the soil-well boundary. Good agreement ($R^2 = 0.944$, *MIA* = 0.961) was obtained between the cumulative water volume flowing to the well (the sum of the cumulative seepage flux and the variable flux at the bottom of the well) and the cumulative pumping volume (Fig. 4-4) during the experiment. The flux through the seepage face in these simulations started approximately 1.2 days after initiating irrigation. The cumulative seepage volume first exceeded the cumulative variable flux (groundwater) after 4.7 days, and at the end of the experiment was about 20% larger than the variable flux. The time period from 1.5 to 3 days when the seepage flux increased mostly, corresponds roughly with the time period when the water content at depths below 0.8 m increased as registered with the MCP probes (Fig. 4-2).

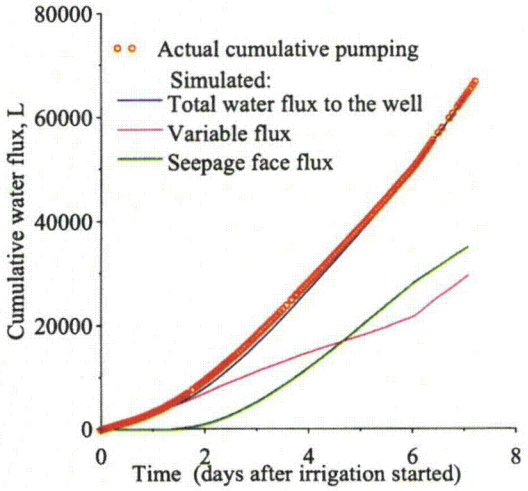

Figure 4-4. Cumulative water fluxes to the well.

The estimated thickness of the seepage face at the time of the peak concentrations was about 35 cm. Thus, if a seepage zone exists it should have a substantial impact on the solute mass flux (Fig. 4-5). Good agreement was obtained between the calculated cumulative fluxes and the mass recoveries of Br (R^2=0.930, *MIA* = 0.964) and PFBA (R^2 = 0.950, *MIA* = 0.969), while the actual mass recovery of Cl significantly exceeded the simulated value after 4 days. This may have been caused by the presence of Cl sources in the unsaturated zone that were not accounted for in the model. All tracers showed much larger simulated mass fluxes through the estimated seepage face than through the variable boundary at the bottom of the well. Hence, solutes appeared to be moving mostly along flow paths close to the water table and then entered the well from the saturated region near the water table. The seepage face is part of the saturated zone (Fig. 4-6a) where most of the flow is horizontal (Fig. 4-6b) and where the tracers first reach the water table (Fig. 4-6c).

Fig. 4-6 shows that the flow patterns in the capillary fringe just above the phreatic surface are also predominantly horizontal, thus shortening solute transport to the well boundary. These findings are consistent with both recent laboratory (Silliman et al., 2003) and field observations (Abit et al., 2008). Still, calculated first arrival times of the tracers to the well were around 40% and 30% earlier (for Br and PFBA, respectively) through the variable flux boundary than through the active seepage face, which became active 1.2 days after irrigation started (Fig. 4-4). Calculated cumulative mass fluxes through the seepage face at the end of simulation period were 8, 4 and 11 times those through the saturated zone, for Br, Cl and PFBA, respectively. The highest ratio between these fluxes was for PFBA since this tracer was applied 7 hours after irrigation was initiated and the Cl was applied. As a result, PFBA arrived at the water table later than the other tracers (i.e., at times when the seepage face was developing and the seepage flux increased). The smallest ratio between the seepage solute flux and the variable flux was for Cl due to its immediate input from the saturated zone having a background concentration of 7.3 mg/L. Our results are very much in agreement with sand box experimental and modeling results by Li et al. (2007) who studied the impact of a seepage face at the unconfined aquifer-lake interface. They found that most of the groundwater and pollutants discharged through a narrow portion near the top of seepage face.

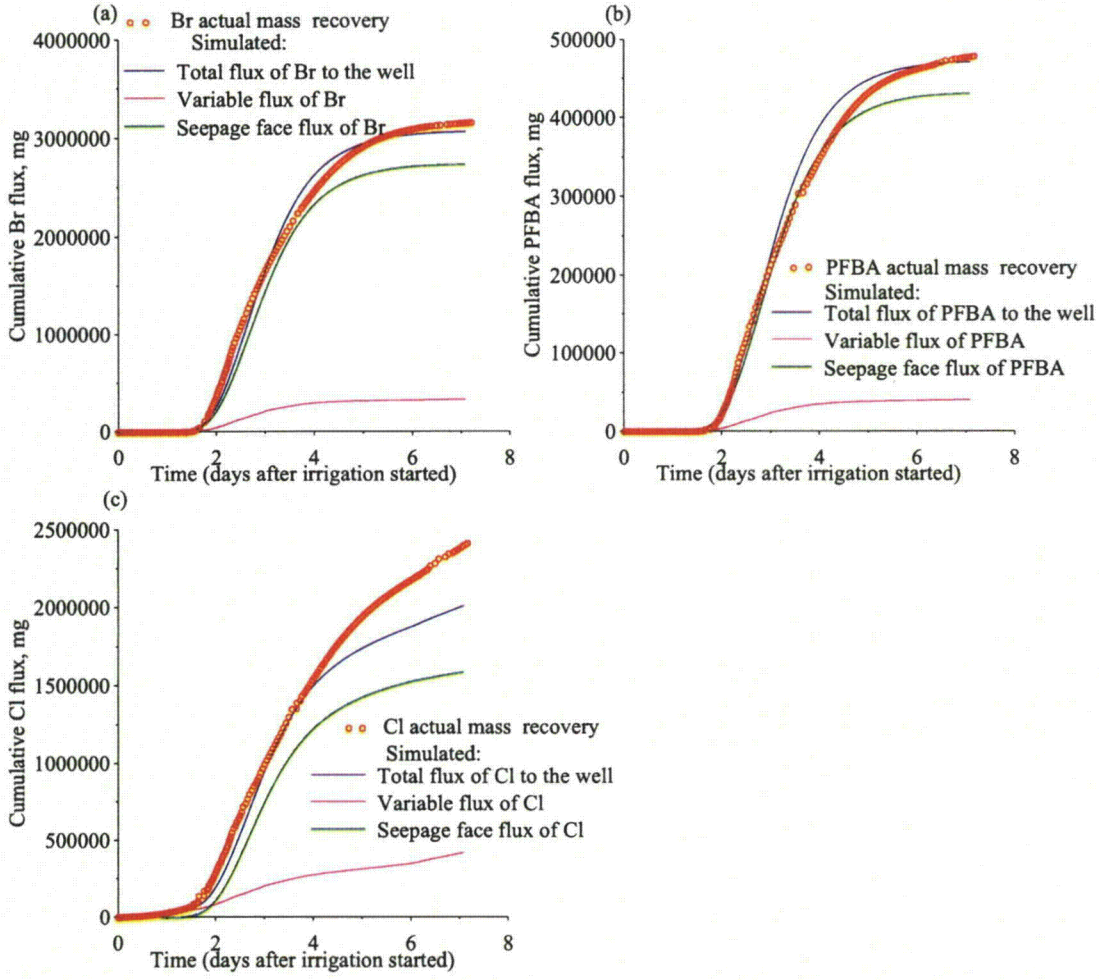

Figure 4-5. Cumulative solute fluxes of (a) Br, (b) Cl and (c) PFBA to the well.

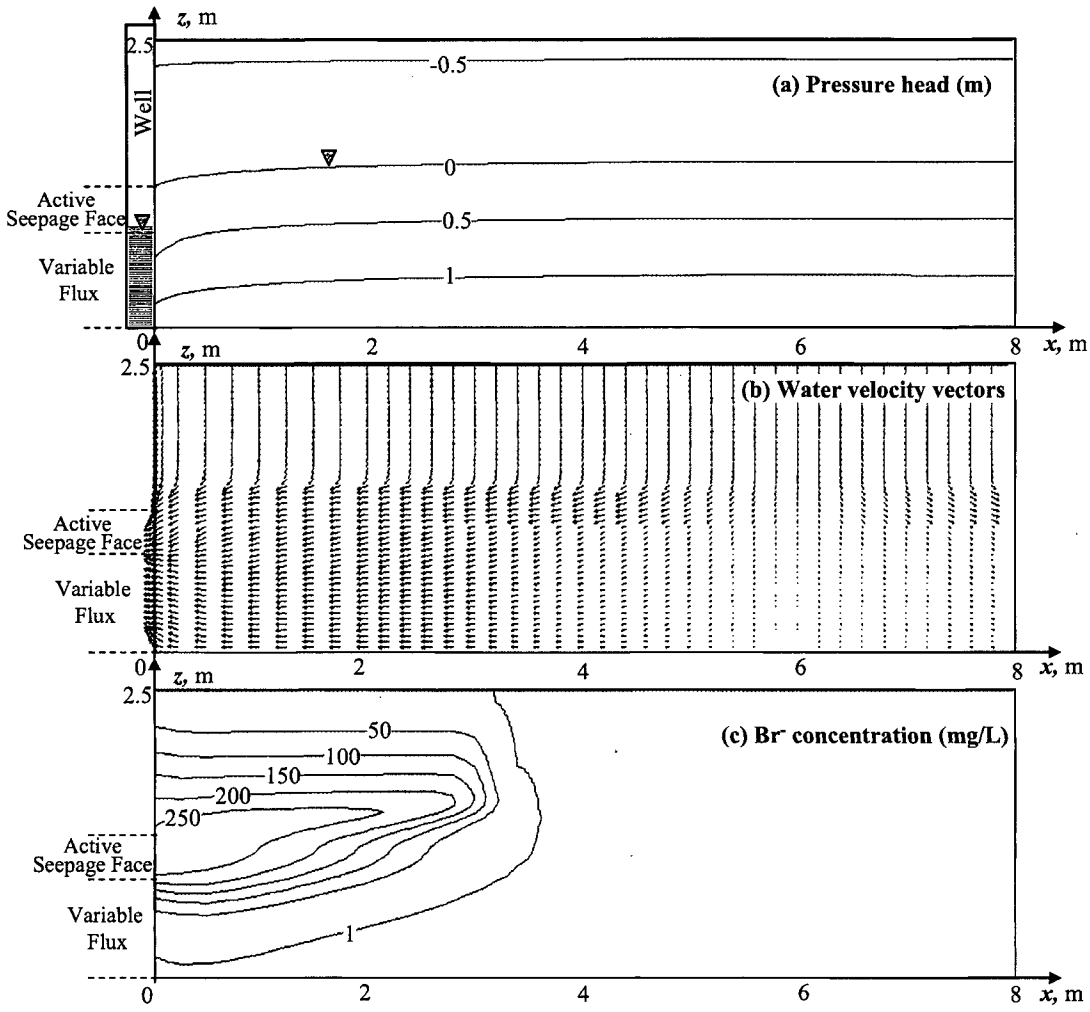

Fig. 4-6. Simulated distributions of (a) pressure head, (b) flow velocity vectors, and (c) Br concentration three days after irrigation started.

4.2 BASE MODEL FOR THE LATERAL FLOW EXPERIMENT

4.2.1 MODEL DESCRIPTION

The HYDRUS-3D software (Šimůnek et al., 2007) was used to simulate three-dimensional subsurface water flow and solute transport in the lateral flow tracer experiment.

4.2.1.1 GEOMETRY OF THE SIMULATION DOMAIN AND SOIL MATERIAL DISTRIBUTION

Based on experimental data that included the location of the tracer application plot, observation (sampling) wells, the topography of the soil surface and of the low permeability bottom (GPR data), we considered a 3D layered domain that extended laterally for 100 m in the x direction and for 70 m in the y direction. The thickness (z direction) of the domain varied from 2.15 m to 5.72 m. The domain was larger than the domain used for the preliminary simulations (50x30 m, see section 3.2.3.7) to diminish the influence of the imposed constant head boundary conditions on flow and transport within the domain. The domain (Fig. 4-7) was composed of 2 major sub-layers: an upper layer representing soil formations characterized by relatively high hydraulic conductivities, and a lower sub-layer composed of materials with predominantly lower permeabilities.

The distribution of soil materials with different texture within the domain was set manually based on logs obtained during installation of observation wells L1-L12. We used a zonation method (Chen et al., 2001, 2004; Hubbard et al., 2003) to assign model parameters within the domain. Six soil materials were considered: Sandy Loam (SL), Sandy Clay Loam (SCL), Loam (L), Silt Loam (SiltL), Silt Clay Loam (SiltCL) and Clay (C). For the SL two different hydraulic conductivities were prescribed: one value for the upper 10 cm soil surface layer (corresponding to the first layer of the finite element mesh in the numerical model), whose conductivity was lower than the conductivity of the rest of the SL domain as a consequence of K_{sat} changes due to soil structural alteration caused by intensive irrigation.

4.2.1.2 FINITE ELEMENT MESH AND OBSERVATION NODES

The unstructured (triangular prisms) finite element mesh consisted of 54, 180 nodes and 100, 156 3D elements (Fig. 4-8). The simulation domain was subdivided into 15 layers (12 layers in the upper sub-layer and 3 layers in the lower sub-layer). The vertical size of the finite element prisms varied depending upon location, with the elements following the surface of the soil surface and the surface of the lower sub-layer. In the upper layer the vertical size of the prisms was 5 cm near the surface, and 15-20 cm near the bottom. In the lower sub-layer the vertical size of the prism varied from 0.3 to 1.5 m (Fig. 4-8, top). The horizontal mesh size decreased from 5 m near the downgradient domain boundary to 0.3 m close to the irrigation plot where most of the transport processes were expected (Fig. 4-8, bottom). Using this geometry and finite element mesh, a 125-day long simulation generally took between 36 to 48 h with a DELL PC Optiplex 755, Intel Core™2 DUO CPU E8400 @3.00 GHz. Further refinement of the finite element mesh required longer simulation times.

Twenty two observation nodes (Fig. 4-9) were assigned to record the simulated breakthrough curves at specific sampling locations in observation wells L1 through L12. Although groundwater was sampled at three depths in all observation wells, only two observation nodes were set for wells L5 and L6 and only one for wells L7 through L12. This because the grid was too coarse in the lower sub-layer.

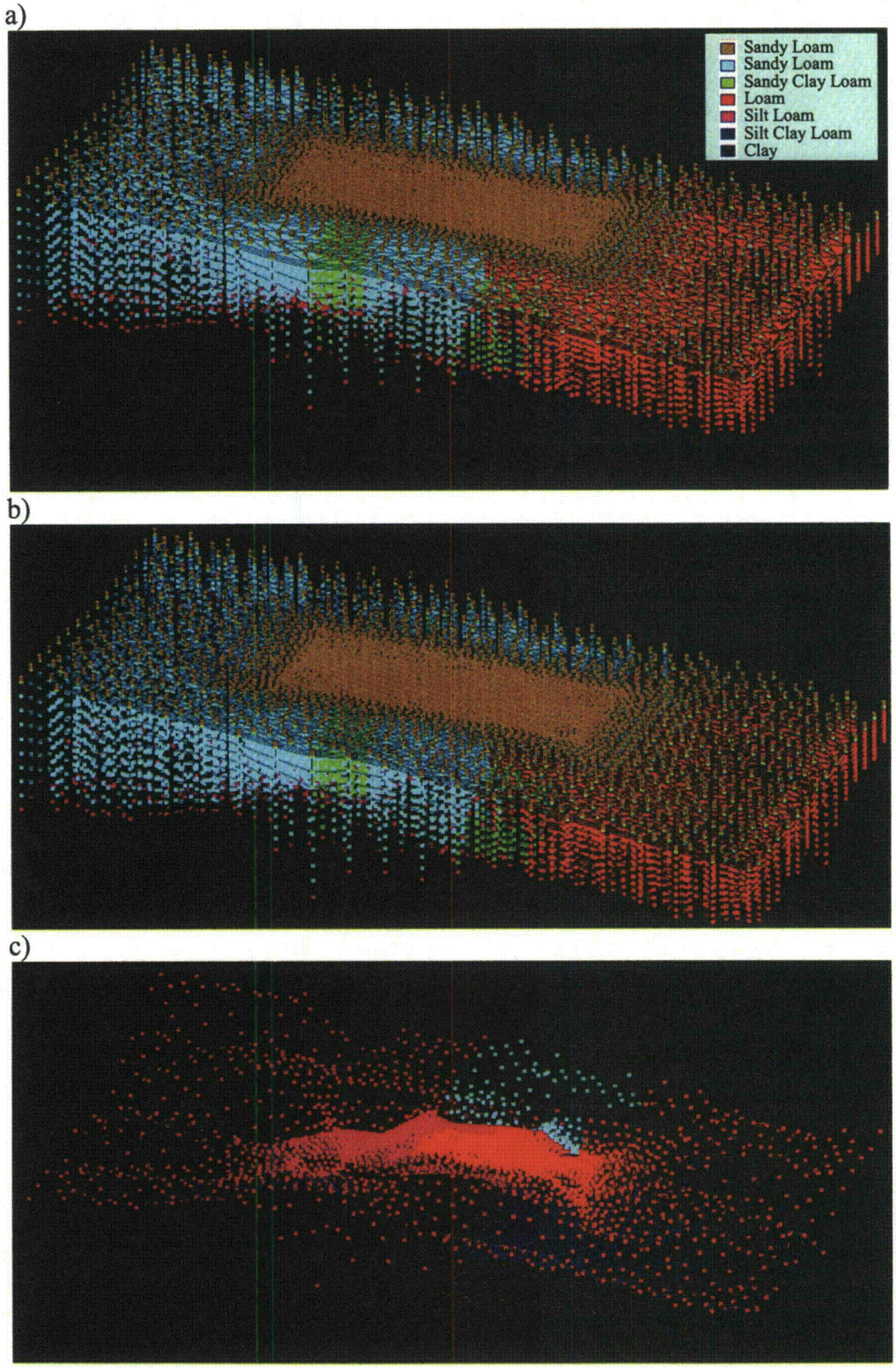

Figure 4-7. Simulation domain used for solving the flow and transport problem with the HYDRUS-3D code: a) whole domain; b) upper sub-layer; c) lower sub-layer.

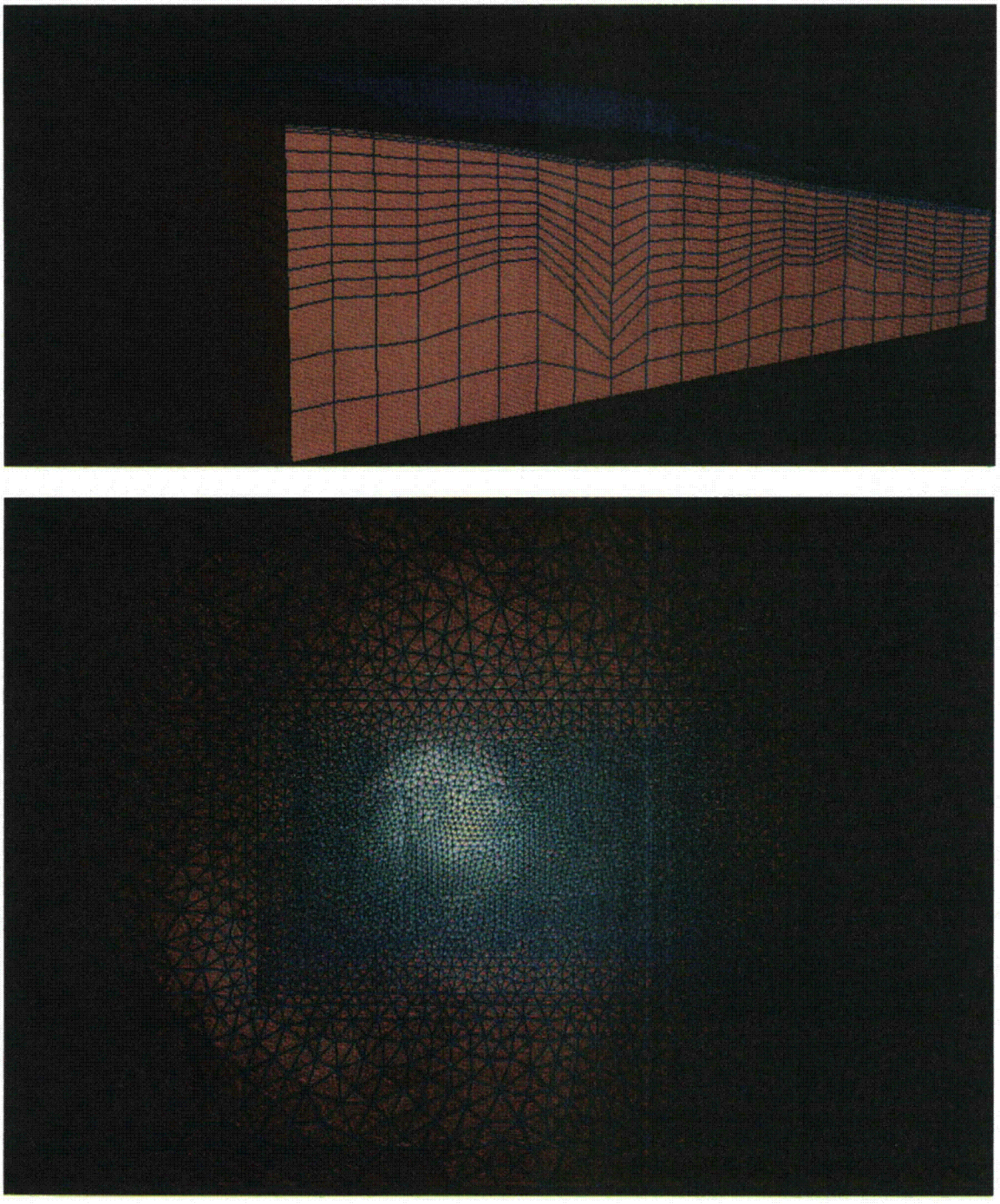

Figure 4-8. Finite element mesh used for the HYDRUS-3D simulations; top –side view, bottom – bird view.

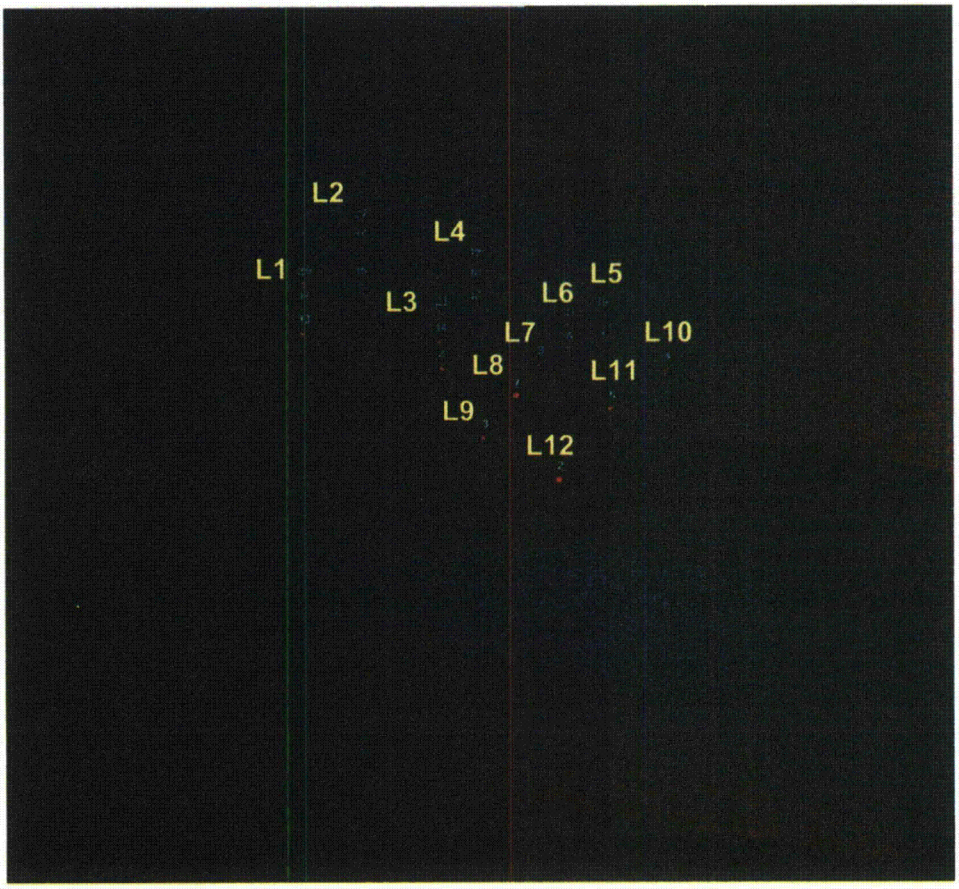

Figure 4-9. Locations of the observation nodes.

4.2.1.3 INITIAL AND BOUNDARY CONDITIONS

As initial condition for the water flow simulations we used an steady-state pressure head distribution. This distribution was obtained by running the flow problem with constant pressure heads along the lateral boundaries (as described below) and zero fluxes along the remaining boundaries of the domain. Simulations ran for about 200 days of elapsed time until steady state flow conditions were reached. The initial Cl^- distribution varied from 10 to 30 mg L^{-1} depending upon location as measured in observation wells prior to the experiment.

The boundary surfaces with the different boundary conditions are shown in Fig. 4-10). Spatially variable, but constant in time pressure head profiles were specified along the lateral boundaries. Atmospheric boundary conditions were used at the soil surface. These conditions simulated a variable flux due to irrigation, precipitation and evapotranspiration within the irrigated plot area, and a variable flux due to precipitation and evapotranspiration along the remaining part of the soil surface. Along the bottom of the domain we used a zero flux boundary condition. The imposed flow rate during each irrigation event was decreased by 28% to account for the amount of water that was lost to overland flow that was collected, and as such had not interacted with the subsurface flow and transport processes.

The distributions of the pressure head along the lateral boundaries were obtained from pressure head values observed during 2006-2007 (Fig. 4-11). Data from wells located in the vicinity and within the simulation domain were used for this purpose. Interpolation was done with the SURFER software. We note that the distributions obtained in this way were very similar for different periods of time.

A third type (Cauchy) boundary condition was used along soil surface to simulate solute transport. Cl concentrations of the water during the tracer application was 4940 mg/l. Cl concentrations of the rainwater and the irrigation water were 8 ppm, while Cl concentrations of groundwater along the lateral boundaries were set to the average observed value of 15 ppm.

Table 4-2 presents hydraulic parameters for different soil materials accepted as initial values for the simulations. These parameters (except for clay) were obtained as an average of those determined with the ROSETTA software using data for soil texture and bulk density. The initial value of the longitudinal dispersivity was 0.5 m, while the ratio of longitudinal to transversal dispersivity was assumed to be 5 in all simulations.

4.2.2 MODEL CALIBRATION AND SIMULATIONS

The HYDRUS-3D software in its current version does not have an option for automatic model calibration. Such an optimization would take an unreasonable amount of time for the fully 3D variably-saturated field scale problem. Therefore, model calibration was performed using a trial-and-error method. Our approach involved the sequential fitting of flow and transport models to available data. At the first step we estimated the velocity field by varying the saturated hydraulic conductivities of the various soil materials. The second step was the calibration of the transport parameters (dispersivities for the conservative tracer) through a series of trial-end-error runs. Much of our attention focused on observation wells L5, L6, and L7 where a well-defined breakthrough curve (BTC) was observed, and where both the arrival front and receding (tailing) part of the breakthrough curve had been recorded.

We started simulations with the hydraulic parameter values listed in Table 4-2. Simulated and observed breakthrough curves for the wells L1 through L9 are compared in Fig. 4-12. We note that the simulated BTCs for L5 through L7 exhibited much later arrival of the tracer than

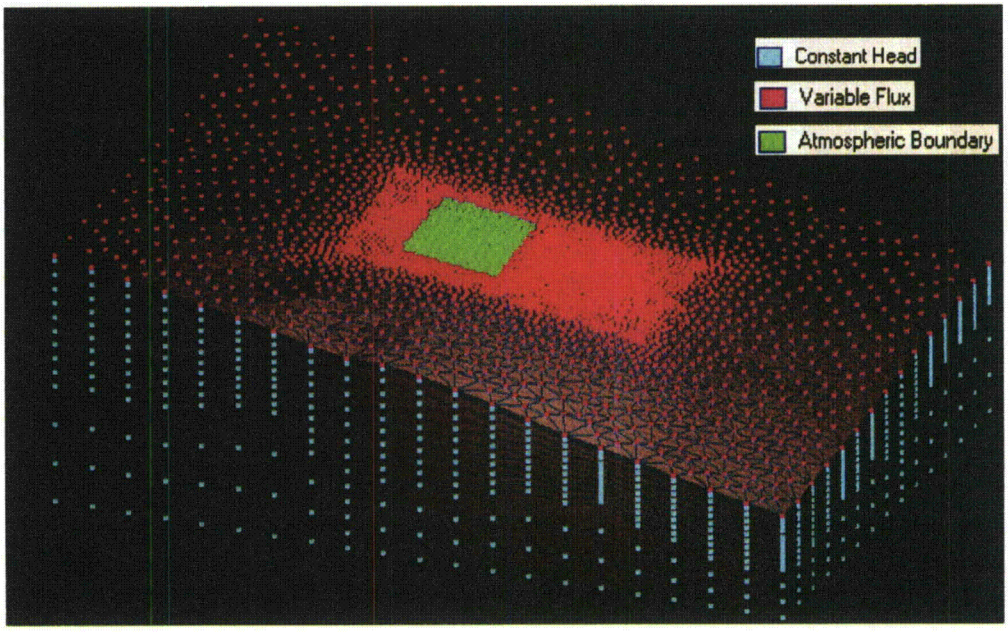

Figure 4-10. Boundary conditions used for the HYDRUS-3D simulations (refer to text for details).

Table 4-2. Initial values of the unsaturated soil hydraulic parameters used in the simulation.

N	Material	Parameters				
	Cm	θ_s	θ_r	α, m^{-1}	n	K_s, m d^{-1}
1	Sandy Loam	0.387	0.053	2.57	1.40	0.26
2	Sandy Clay Loam	0.393	0.066	2.31	1.35	0.13
3	Loam	0.412	0.067	1.20	1.47	0.11
4	Silt Loam	0.450	0.080	0.65	1.56	0.12
5	Silt Clay Loam	0.466	0.087	0.78	1.52	0.12
6	Clay	0.410	0.095	1.90	1.31	0.01

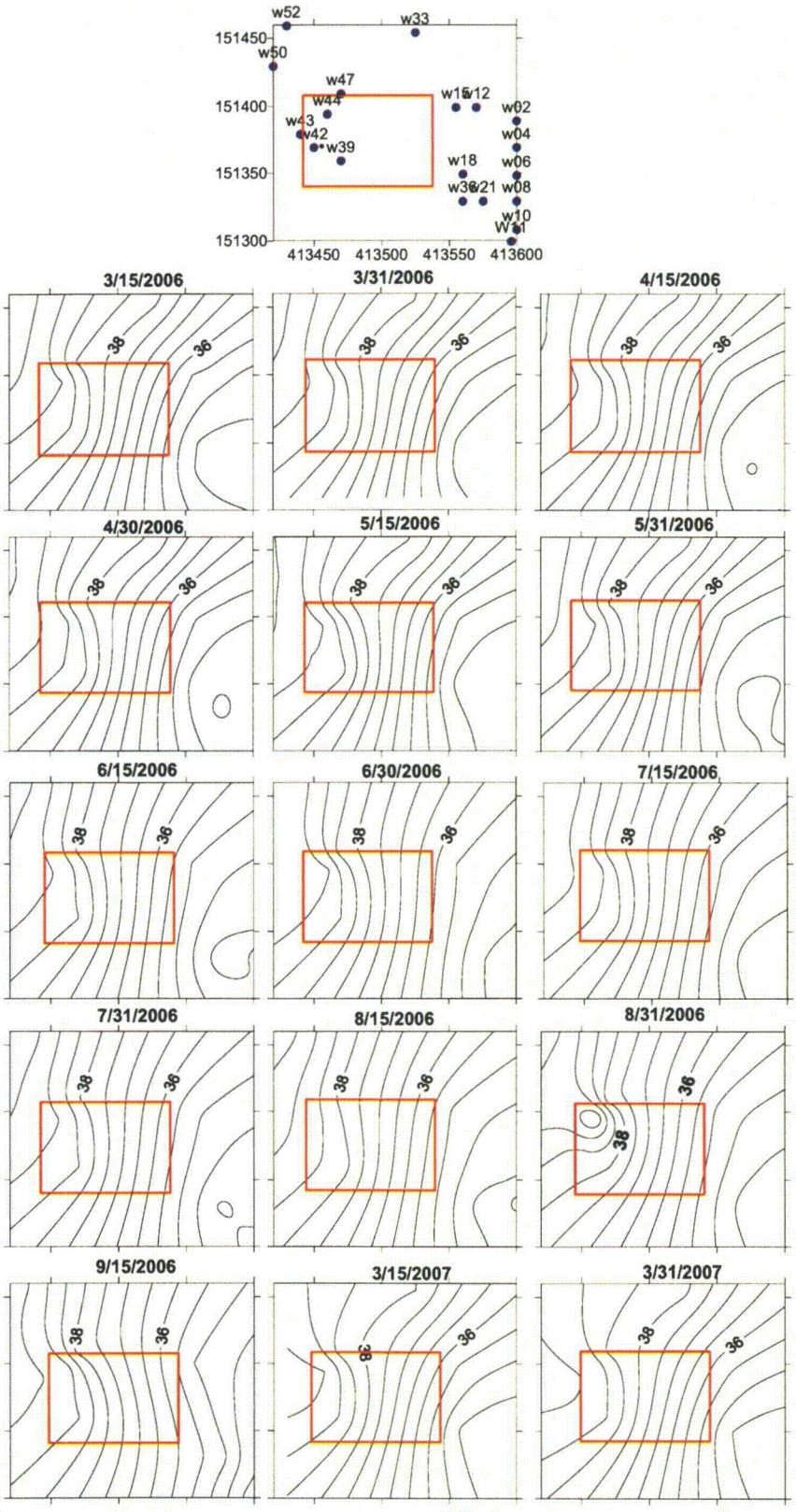

Figure 4-11. Location of observation wells (blue dots) in the vicinity of simulation domain (red rectangle) and hydraulic head distributions at different times in 2006-2007.

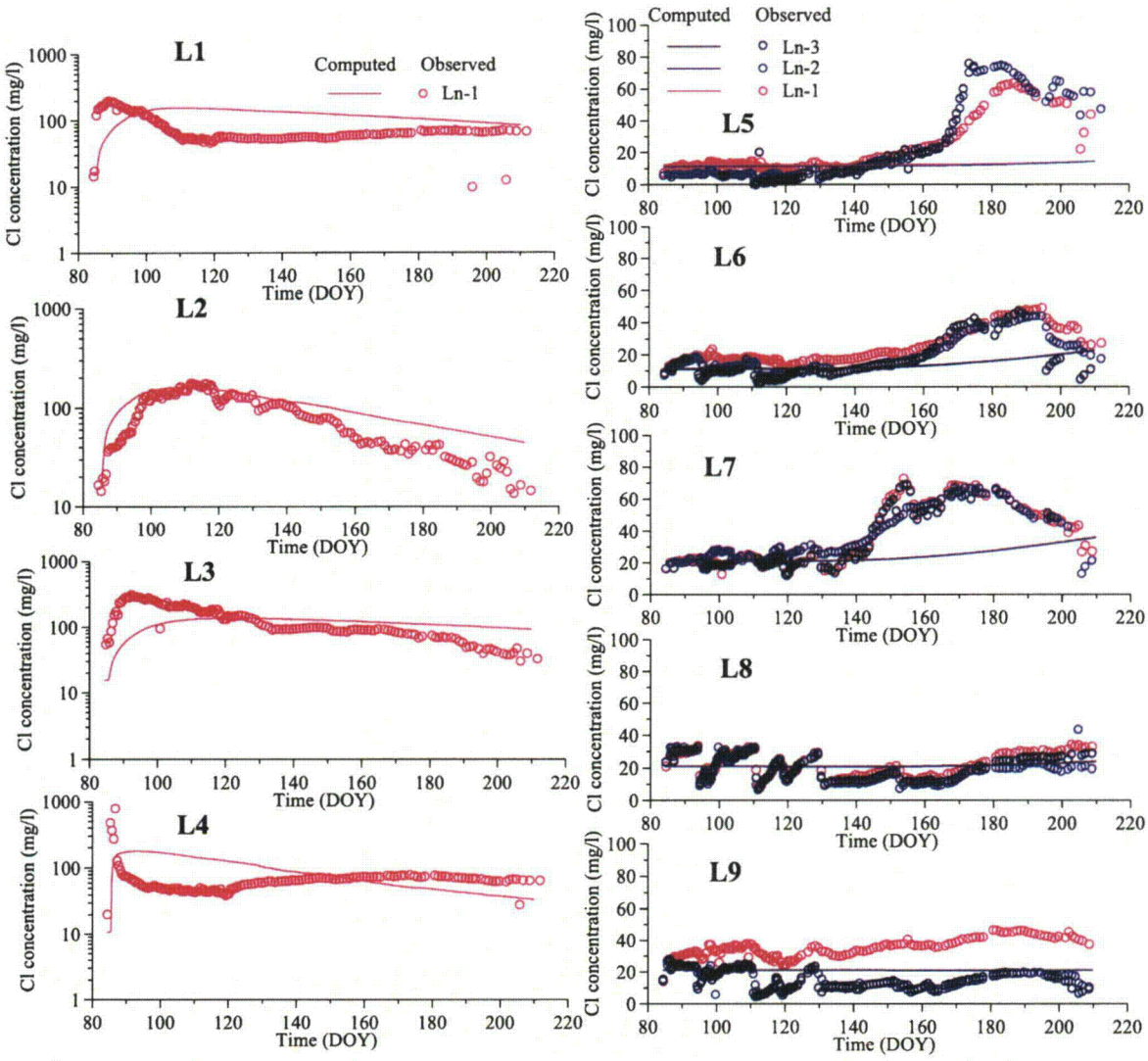

Figure 4-12. Simulated (lines) and observed (circles) chloride breakthrough curves. Simulation results are for the initial set of parameters listed in Table 4-2. L1 through L9 denote observation wells 1-9, ○, ○, and ○ are color codes for L5 through L9 at the depths of 1.65, 1.35 and 1.05 m, respectively; ○ is the color code for the depth of 1.1 m in L1 through L4.

was observed. We assumed that the reason for this was our use of too low hydraulic conductivities of the sandy loam, sandy clay loam and loam materials composing the upper sub-layer of the domain. Hence for the next run we increased the saturated hydraulic conductivity (K_{sat}) values to 2.0, 0.4 and 0.3 m d^{-1} for the sandy loam, sandy clay loam and loam soils, respectively. We further decreased the longitudinal dispersivity (a_L) of these materials from 0.5 to 0.2 m, while the ratio of longitudinal to transversal dispersivity was kept at a_L/a_T=5. The agreement between the simulated and observed BTCs for wells L1through L4 became worse, whereas for L5 through L7 we noted much earlier arrival times of the simulated BTC fronts as compared to the observations. Wells L8-L9 now showed only slight higher concentration. The slope of the simulated BTC increased compared to the case of a_L=0.5 m. Hence more parameter adjustments were clearly needed.

The trial-and-error procedure continued for two months until a better fit for L5 through L8 was obtained. During these runs we also slightly moved the boundaries between the SL, SCL and L soil layers to further improve the fit. The resulting values of K_{sat} were 1.0, 0.6 and 0.2 m d^{-1} for the SL, SCL and L soils, respectively. Results of the simulations for wells L1 through L9 are presented in Fig. 4-13 and 4-14 for the scenarios with a_L=0.5 m and a_L=0.15 m, respectively. The agreement in terms of the magnitude of the concentrations was reasonable. However, the BTC shape was not simulated well. We note that the agreement is better for wells L1-L4 when a_L=0.5 m compared to a dispersivity of 0.15 m, while the opposite is true for wells L5-L8. The receding part of the BTCs in L5 through L7 was not simulated. It seemed that the width of the simulated plume was larger than the actual plume. A quantitative comparison between the latter two scenarios was performed using the coefficient determination (R^2) and the Modified Index of Agreement (MIA) (Table 4-3). Calculated values of these criteria suggest a fair agreement for wells L5, L6, and L7 as well as for L2 and L3 at their lowest sampling depth.

Fig. 4-15 shows the simulated and observed BTCs of wells L10-L12 for the scenarios of a_L=0.5 m and a_L=0.15 m. The results for these two cases are practically identical. The model was not able to simulate the observed oscillations in the measured concentrations at early times and the increase in concentration towards the end of the experiment. According to the model predictions, the plume did not reach wells L10, L11, and L12 by the end of simulation period.

Calculated distributions of the pressure head along the lower (z=0) boundary (which corresponded to an altitude of 35 m above sea) at different times is shown in Fig. 4-16. A groundwater mound was found to develop under the irrigation plot, causing water to spread in all direction. This can be observed in Fig. 4-17 which shows a distribution of the flow velocity at a depth of approximately 1 m. At early times of the experiment between DOY (days of year) 90 and 110) when the groundwater level in the eastern part of the simulation domain was lower than this depth ofl m, preferential flow path may have developed due to particular topography of the restrictive bottom and the distribution of hydraulic properties (Fig. 4-17). Later on (after DOY 130), the flow regime became quasi steady-state and changes were mainly due to variations in precipitation with time.

Fig. 4-18, 4-19, and 4-20 show the simulated tracer plume at different times. The applied tracer initially was pushed to deep soil layers by the incoming fresh water. After some period of time, the plume had a bagel-like shape with concentration in the center of the plume being lower than at the peripheral part (except for concentrations at the lowest depth of 1.4 m). The migration of the plume and its expansion in different directions was controlled by the spatial distribution of the hydraulic properties. By the end of simulation period only the advancing front plume had

reached the observation wells L5-L7. This explains why we were not able to simulate the residing part of BTCs in those two wells.

To assess the effect of the capillary fringe on tracer transport, we performed a simulation with the parameter τ in the van Genuchten-Mualem equation (3-11) set at -3. Changing this parameter from 0.5 (the standard value) to -3 leads to higher unsaturated hydraulic conductivity, and presumably more flow and, consequently, transport in the capillary fringe. Our simulations indicated practically no difference in the BTCs for these two values of τ. The reasons are as follows: 1) after application, the tracer was flushed to the deeper horizons by the infiltrated fresh water (i.e., transport occurred mainly in groundwater); 2) the domain in the vicinity of the plot was close to saturation (i.e., practically no capillary fringe had developed there).

Overall, the calibrated model reproduced the most important features of the lateral flow experiment. The model gave satisfactory levels of peak concentrations and was able to capture arrival times. However, some qualitative differences between simulated and measured concentrations were observed. Because experimentation with the HYDRUS 3D was extremely time-consuming, model abstractions were undertaken as shown in Section 5.2.1 to gain more insight into the effect of subsurface media properties on transport in the soils of this experiment.

Table 4-3. Values of the coefficient of determination (R^2) and the Modified Index of Agreement (MIA) for two simulation scenarios using a_L=0.5 m and a_L=0.15 m

Bore-hole	Obs. Node	R^2	MIA	R^2	MIA
		a_L=0.5 m		a_L=0.15 m	
L1	3	0.198	0.060	0.165	0.032
	2	0.042	0.338	0.001	0.221
	1	0.150	0.433	0.096	0.193
L2	3	0.888	0.431	0.349	0.253
	2	-	-	-	-
	1	0.532	0.730	0.912	0.635
L3	3	0.130	0.440	0.151	0.475
	2	0.558	0.527	0.730	0.748
	1	0.573	0.574	0.003	0.393
L4	3	0.301	0.028	0.256	0.006
	2	0.054	0.081	0.117	0.035
	1	0.000	0.100	0.038	0.052
L5	3	-	-	-	-
	2	0.874	0.703	0.886	0.754
	1	0.842	0.798	0.816	0.853
L6	3	0.505	0.583	0.698	0.742
	2	0.700	0.693	0.494	0.615
	1	-	-	-	-
L7	3	0.821	0.708	0.833	0.803
	2	-	-	-	-
	1	-	-	-	-
L8	3	0.011	0.189	0.071	0.214
	2	-	-	-	-
	1	-	-	-	-
L9	3	0.01	0.327	0.007	0.347
	2	-	-	-	-
	1	-	-	-	-
L10	3	-	-	-	-
	2	0.126	0.379	0.088	0.411
	1	-	-	-	-
L11	3	-	-	-	-
	2	0.078	0.276	0.078	0.272
	1	-	-	-	-
L12	3	-	-	-	-
	2	0.009	0.320	0.011	0.319
	1	-	-	-	-

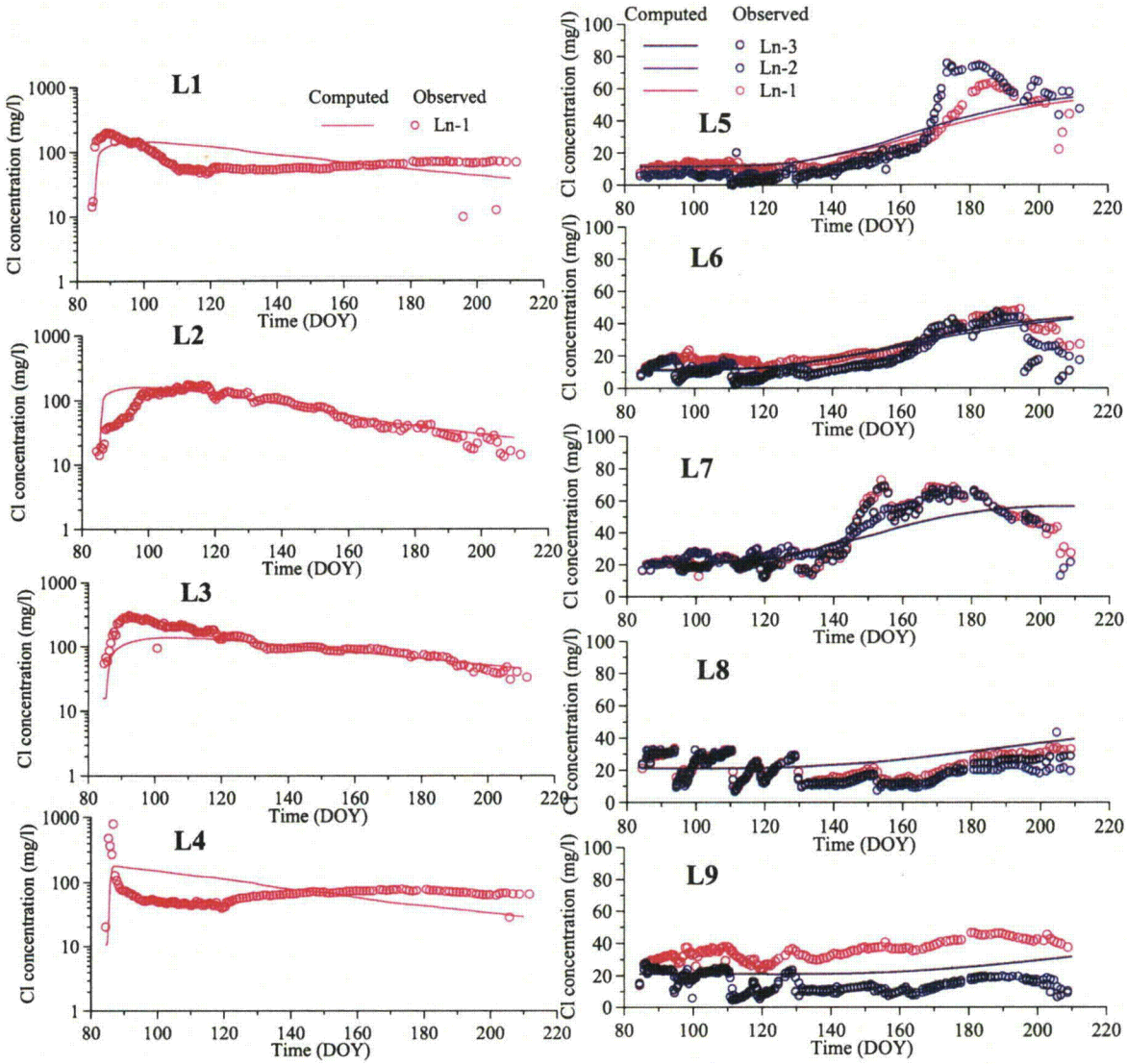

Figure 4-13. Simulated (lines) and observed (circles) chloride breakthrough curves. Simulations are for K_s values of 1.0, 0.6 and 0.2 m d^{-1} for SL, SCL and L, respectively; a_L=0.5 m, a_L/a_T=5. Symbols are the same as in Fig. 4-12.

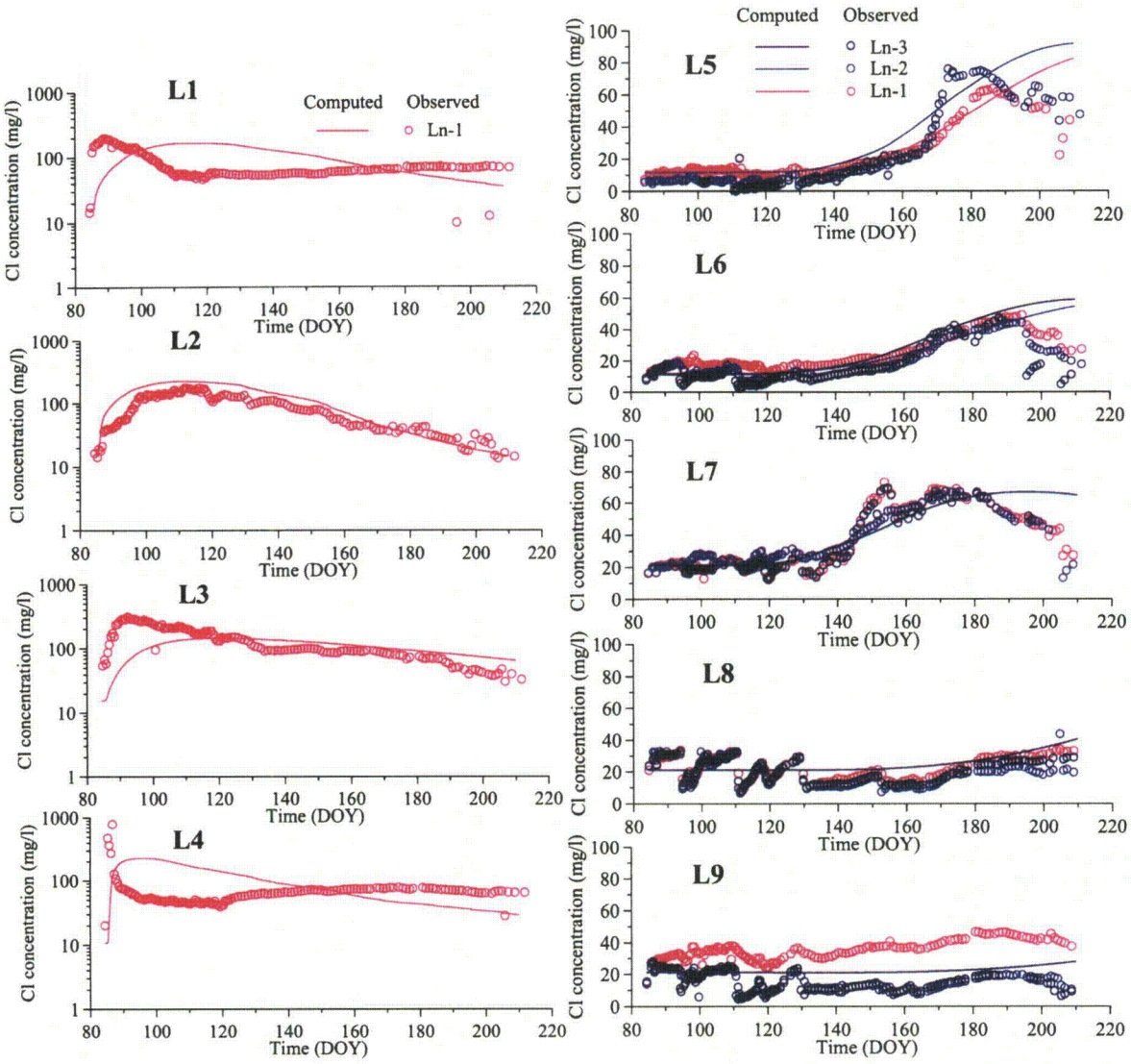

Figure 4-14. Simulated (lines) and observed (circles) chloride breakthrough curves. Simulations are for K_s values of 1.0, 0.6 and 0.2 m d^{-1} for SL, SCL and L, respectively; a_L=0.15 m, a_L/a_T=5. Symbols are the same as in Fig. 4-12.

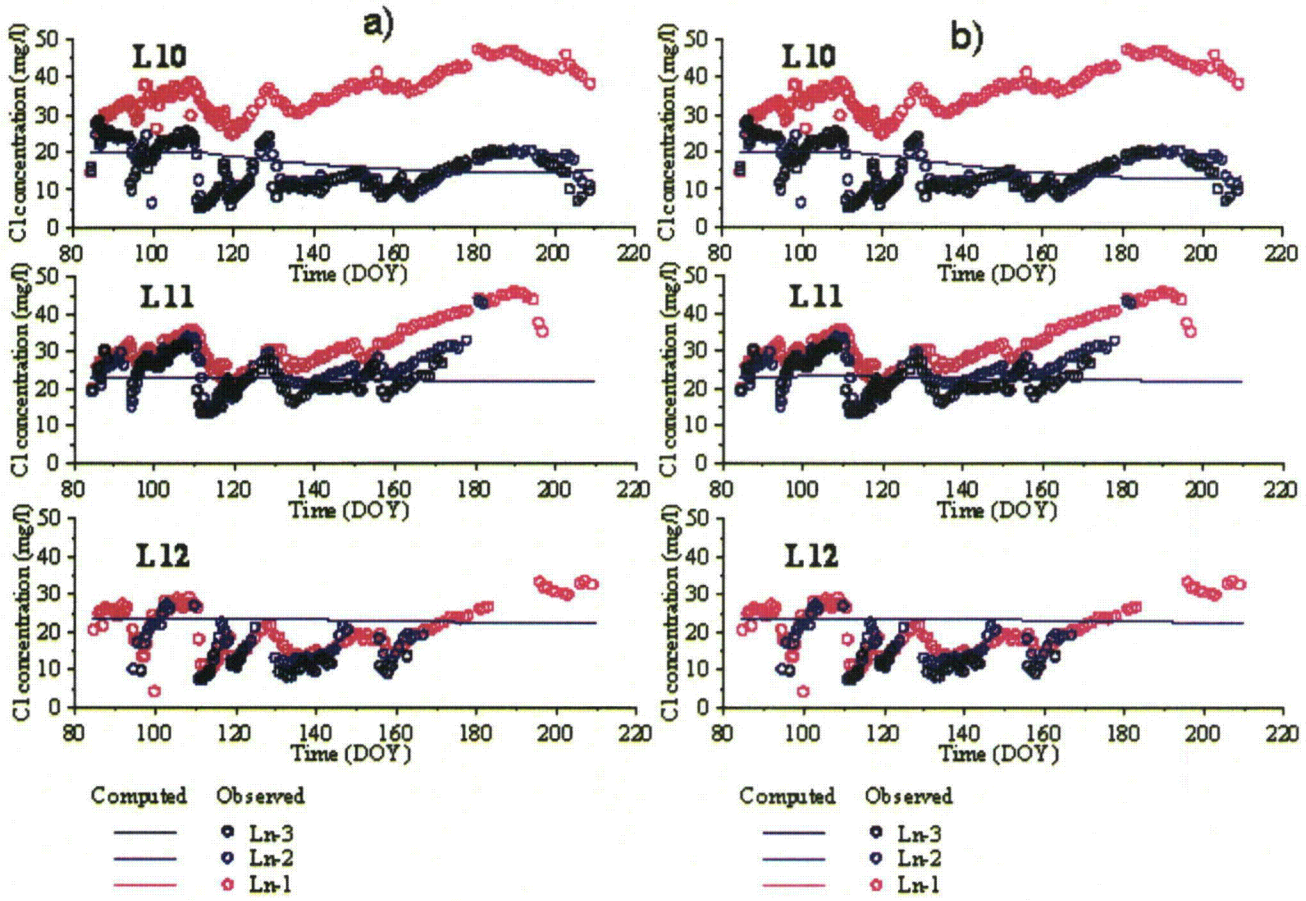

Figure 4-15. Simulated (lines) and observed (circles) chloride breakthrough curves. Simulations for for K_s values of 1.0, 0.6 and 0.2 m d^{-1} for SL, SCL and L, respectively; a) a_L=0.5 m and b) a_L=0.15 m. Symbols are the same as in Fig. 4-12.

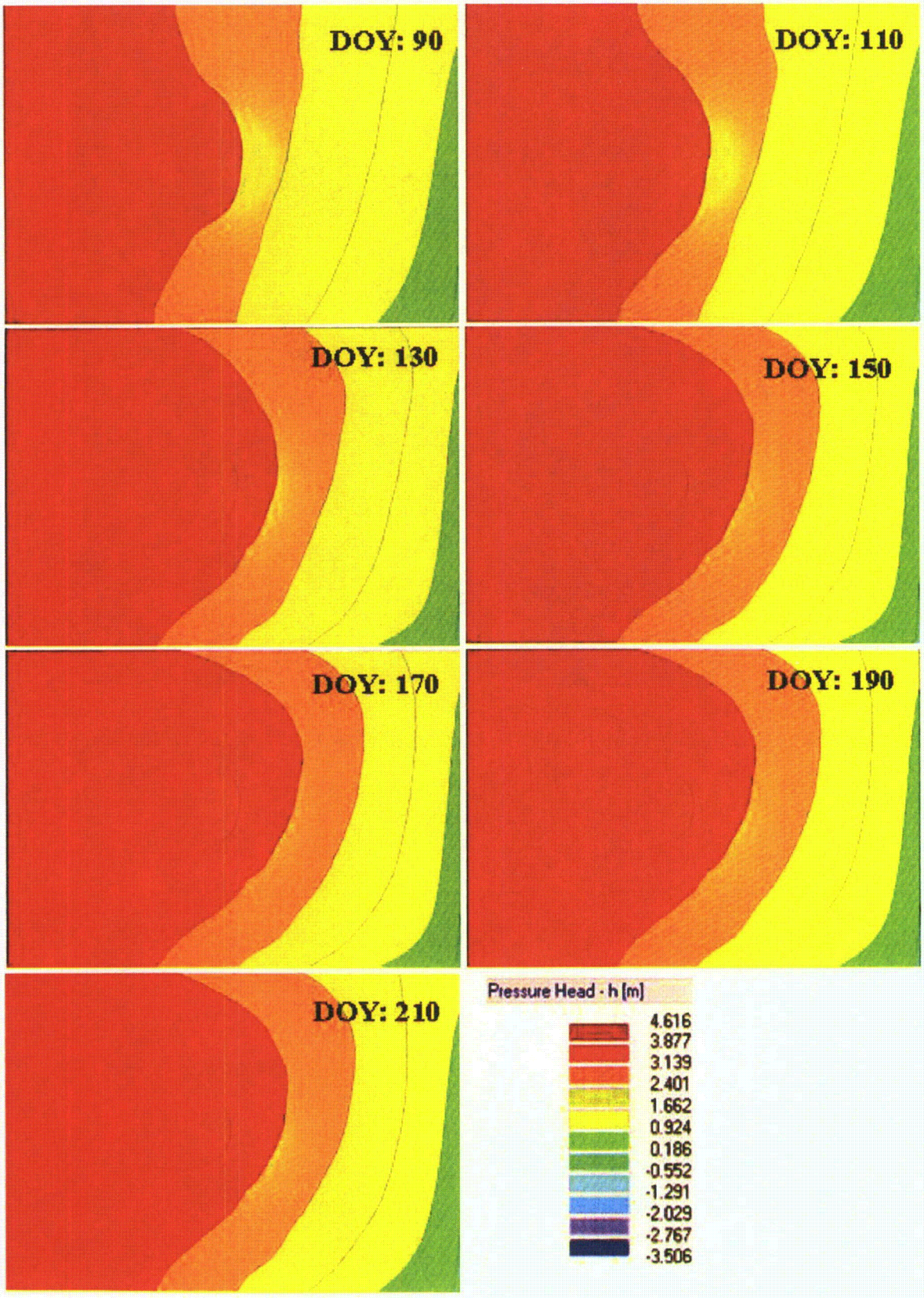

Figure 4-16. Simulated distributions of the pressure head at the bottom of the simulated flow domain (z=0), corresponding to an altitude of 35 m above sea level); DOY is the day of the year.

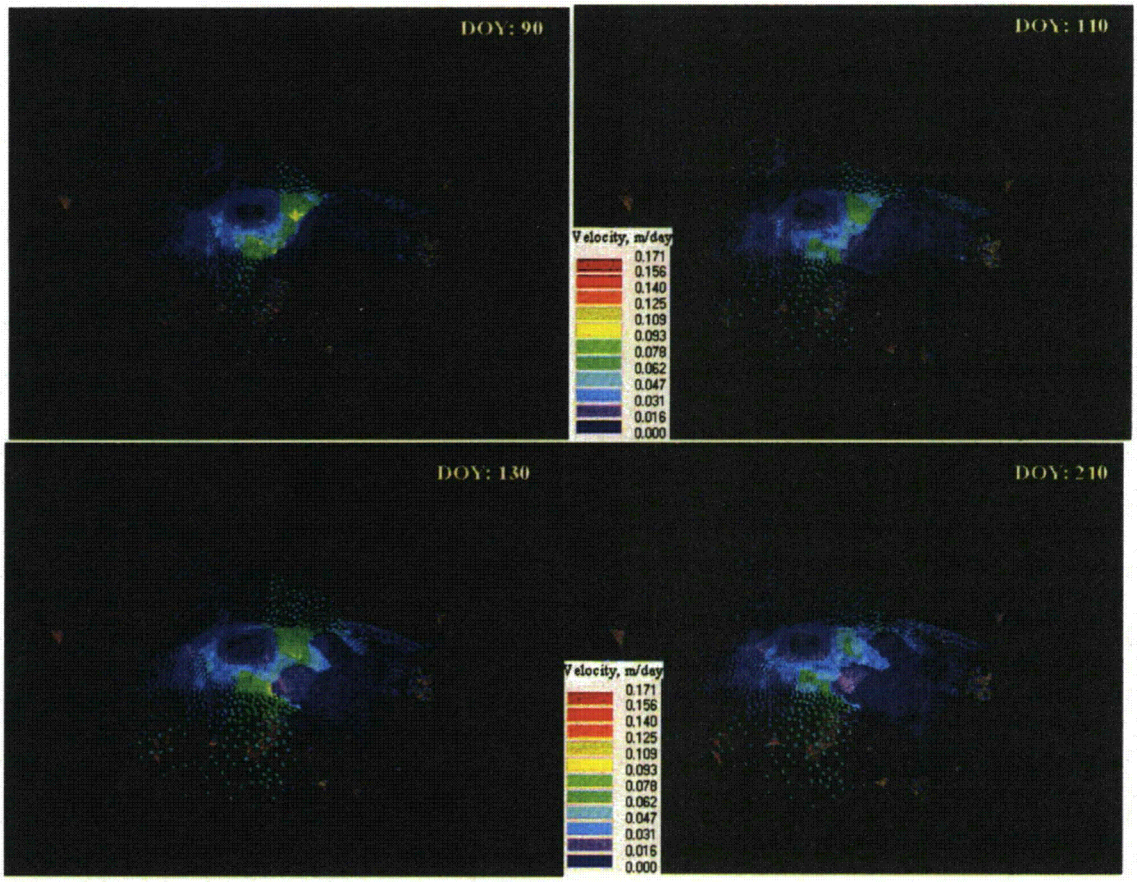

Figure 4-17. Simulated Darcy velocity vectors at a depth of around 1 m below the soil surface; DOY is the day of year.

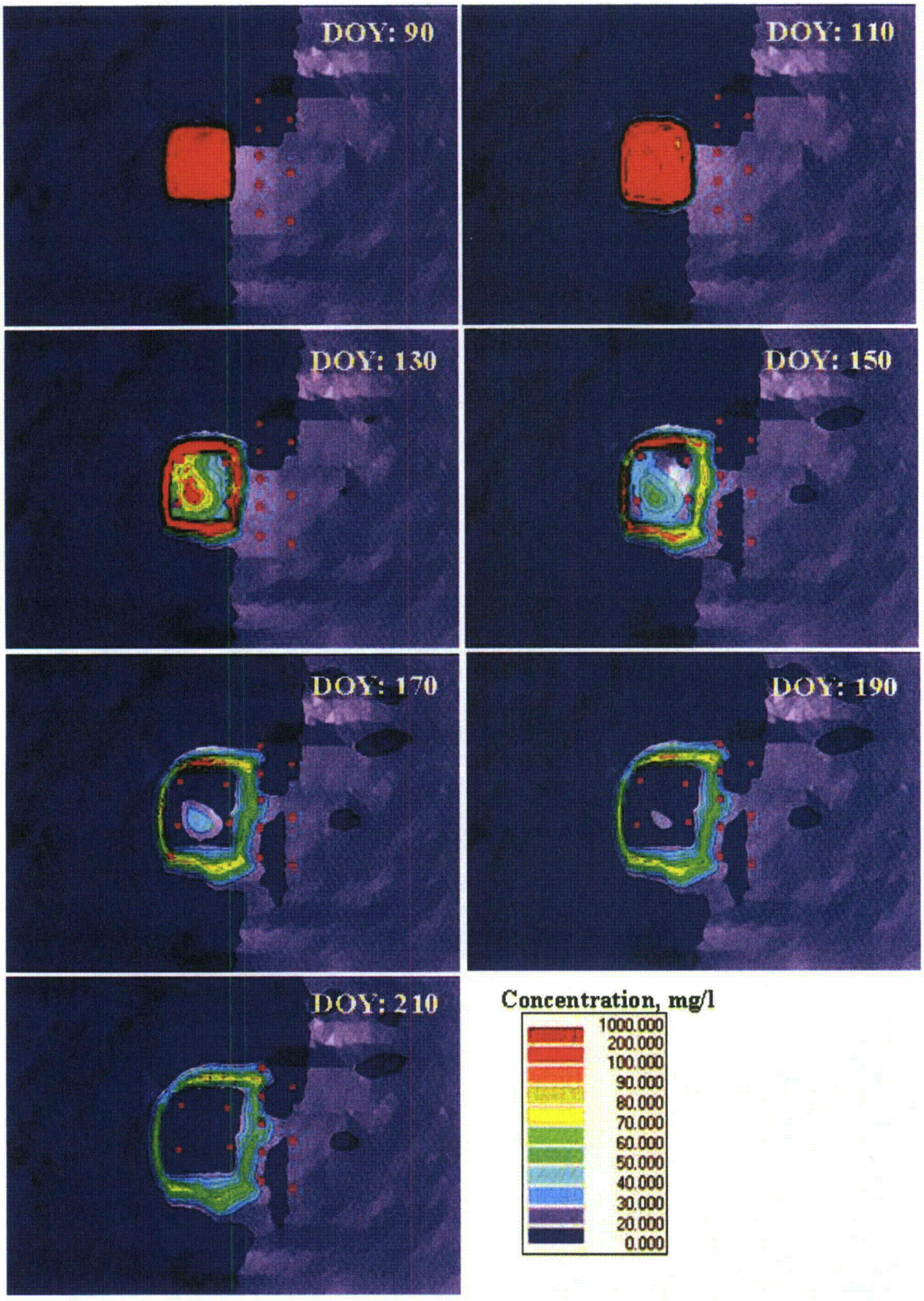

Figure 4-18. Simulated Cl concentration distributions at a depth of 0.5 m below the surface; DOY is the day of year, pink dots represent the locations of the observation boreholes.

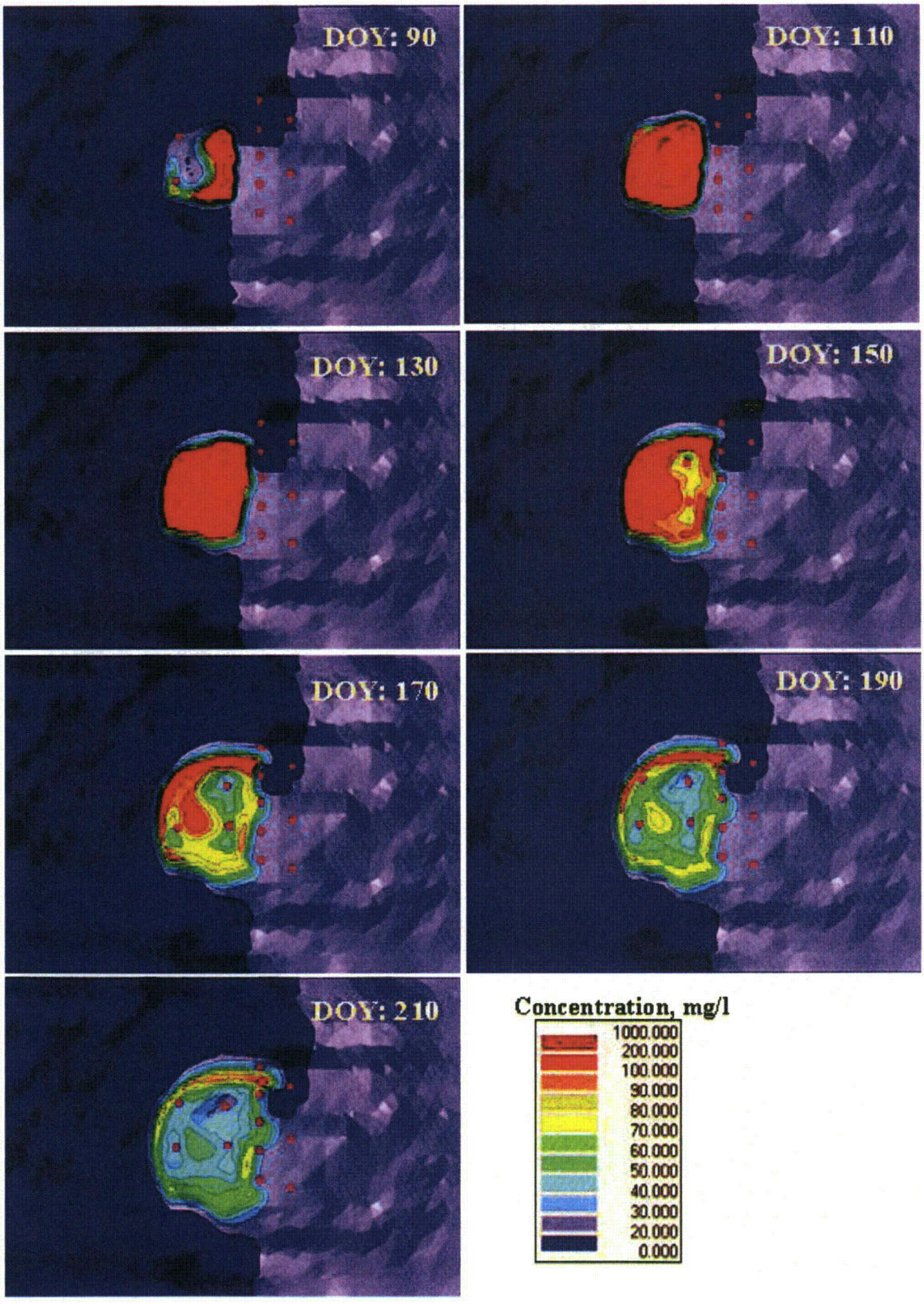

Figure 4-19. Simulated distribution of Cl concentration at a depth of 1 m below the surface; DOY is the day of year, pink dots represent the locations of the observation wells.

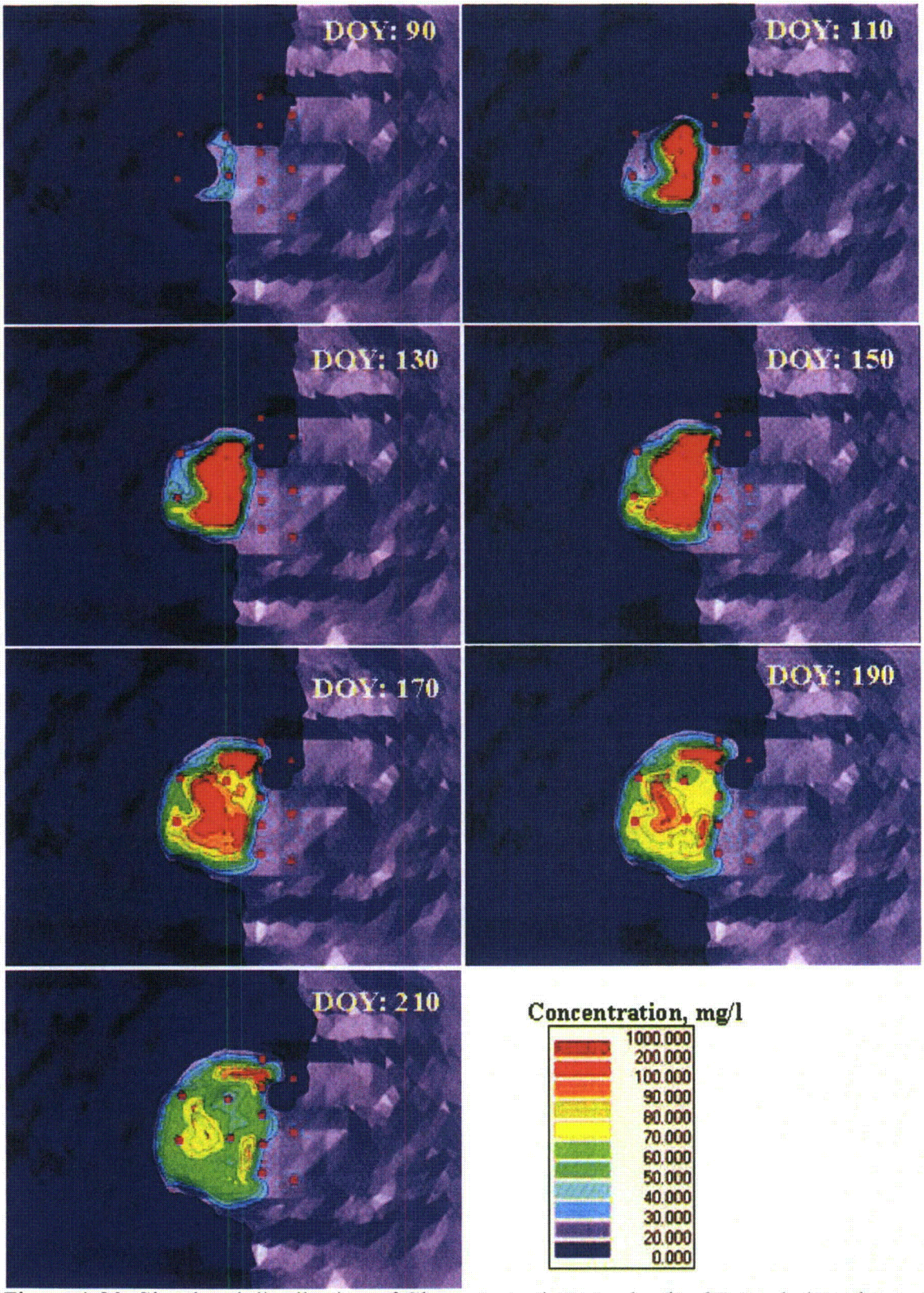

Figure 4-20. Simulated distribution of Cl concentration at a depth of 1.4 m below the surface; DOY is the day of year, pink dots represent the location of the observation wells.

5 MODEL ABSTRACTION APPLICATIONS

5.1 FLUX MEASUREMENT EXPERIMENT

5.1.1 ABSTRACTION BY REDUCING THE DIMENSION OF THE FLOW DOMAIN

A 1D simulation of water flow and Br transport in the unsaturated zone was carried out to assess the effect of reducing the dimension of the flow domain on tracer transport to the well. We calculated the breakthrough curve (BTC) of Br at a depth of 1.68 m, which corresponds to the initial groundwater level and as such could be considered a well (a sink) in the 1D approximation. The simulations were performed with two transport models: 1) a 1D equilibrium model; and 2) a dual-porosity (mobile-immobile water) transport model assuming physical non-equilibrium. In both cases the longitudinal dispersivity (a_L) was fixed at 15 cm, while the immobile water content (θ_m) for the nonequilibrium model was assumed to be 0.09 (fitted such that the simulated and observed peak concentration arrival times at the well were the same).

Results are presented in Fig. 5-1. The equilibrium transport model exhibited relatively late arrival of both the BTC front and the maximum concentration at the groundwater level. The non-equilibrium model, which simulates preferential flow, correctly predicted the arrival of the maximum concentration; however, the simulated BTC front arrived much earlier than the observed front. Thus, we can conclude that this abstraction would lead to the wrong conclusion about the existence of preferential flow in the soil, and that the arrival of the solute at the well may well have been controlled by lateral (multi-dimensional) flow in the subsurface and the presence of a seepage face.

5.1.2 ABSTRACTION BY USING AN APPROXIMATE ANALYTICAL FLOW MODEL

Narrowing the purpose of a modeling project sometimes allows one to considerably simplify the model, including making a change in the key output variables. We consider here the case where modeling may be used to estimate the radius of the tracer application area beyond which no losses would occur because of lateral subsurface flow away from the well. The recovery of an applied tracer is an important factor in a field tracer experiment to assess the solute mass balance.

In a radially convergent saturated flow field the recovery depends on the tracer application radius and the capture well zone. To avoid losses of the tracer with lateral flow, the application radius must be less than the radius of the water table divide where the radial flow velocity is zero (Fig. 5-2). The radius of the water table divide can be estimated in an approximate manner from a solution of the Boussinesq equation for steady-state radial unconfined flow towards a well, subject to Dirichlet boundary conditions as follows

$$\frac{1}{r}\frac{\partial}{\partial r}\left(K_s r h \frac{\partial h}{\partial r}\right) = -iH(a-r)\ ,\ r_0 \le a \le R \qquad (5\text{-}1)$$

$$r = r_0:\quad h = h_0 \qquad (5\text{-}2)$$

$$r = R:\quad h = h_R \qquad (5\text{-}3)$$

where h is the water table height above the impermeable layer (L), r is the radial coordinate (L), K_{sat} is the hydraulic conductivity of the aquifer, i is the recharge rate (L/T), $H(r)$ is the Heaviside step function, a is the radius of the infiltration area ($r_0 \le a \le R$), r_0 and R are the radii of the well and the outer boundary (L), respectively, and h_0 and h_R are the water table heights at $r=r_0$ and $r=R$, respectively.

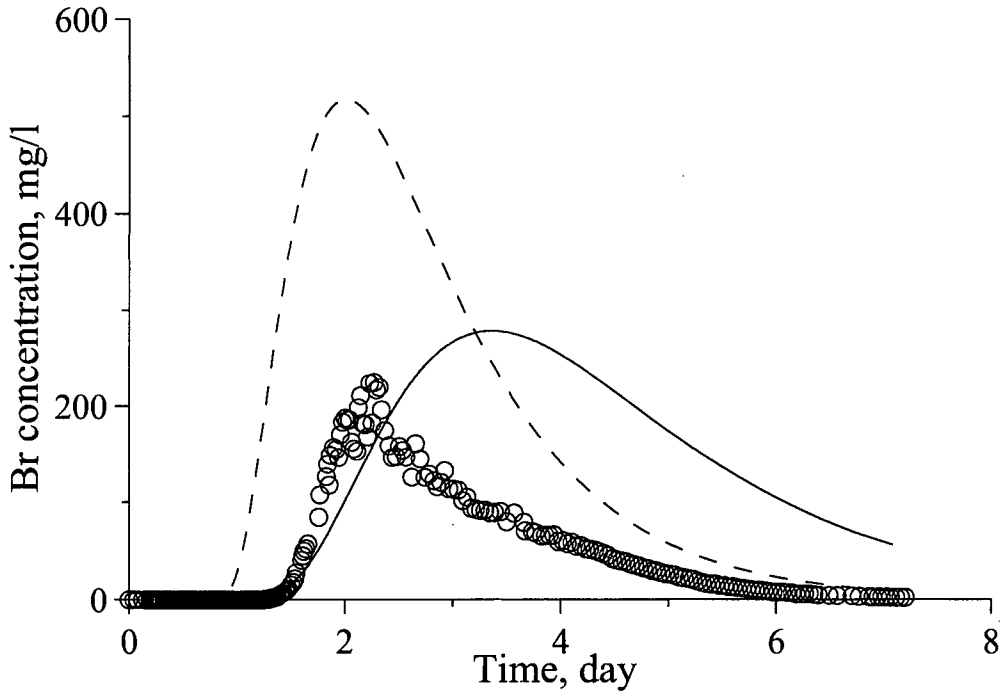

Figure 5-1. Breakthrough curves of Br observed in the pumping well (open circles) and simulated at the groundwater level with two 1D models; solid line - equilibrium model, dashed line – non-equilibrium model.

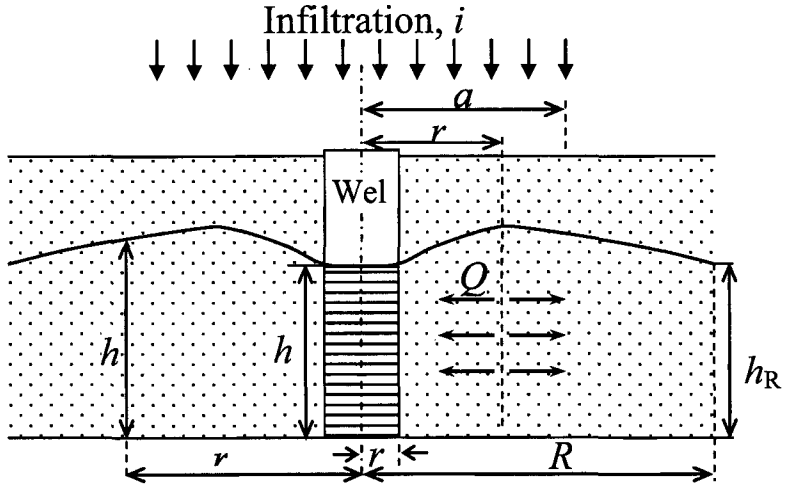

Figure 5-2. Schematic of unconfined radial flow with infiltration.

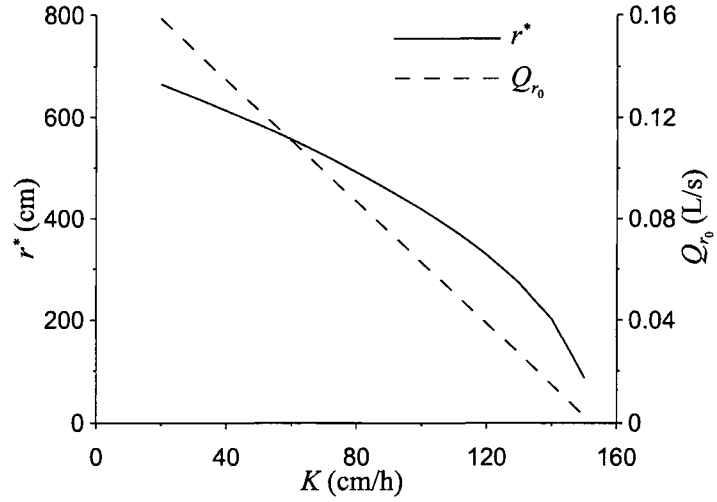

Figure 5-3. Well capture radius (r^*) and pumping discharge (Q_{r0}) as a function of the saturated hydraulic conductivity (K_{sat}) for a given set of parameters (r_0=2.5 cm, R=3000 cm, a=2000 cm, i=0.41 cm/h, h_0=90 cm, h_R=82 cm).

Assuming a constant hydraulic conductivity, K_{sat}, and integrating Eq. (5-1), we obtained an analytical expression for the radial water flux, Q (LT^{-3}), towards the well as a function of the radial position, r, as follows

$$Q = -2\pi K_{sat} r h \frac{\partial h}{\partial r} =$$

$$\pi\left\{ir^2 H(a-r) - ia^2 H(r-a) - \left[\left(h_R{}^2 - h_0{}^2\right)K_{sat} + i\left(\frac{a^2 - r_0{}^2}{2} + a^2 \ln\frac{R}{a}\right)\right] \Big/ \ln\frac{R}{r_0}\right\} \quad (5\text{-}4)$$

For the limiting case when $a=R$ (application radius equals the radius of the outer boundary), this solution coincides with an equation derived previously by Aravin and Numerov (1965).

An equation for the radius of the water table divide (r^*) may be obtained by solving the equation for $Q=0$ to obtain for the case when $r^*<a$

$$r^* = \sqrt{\left[\left(h_R{}^2 - h_0{}^2\right)\frac{K_{sat}}{i} + \left(\frac{a^2 - r_0{}^2}{2} + a^2 \ln\frac{R}{a}\right)\right] \Big/ \ln\frac{R}{r_0}}. \quad (5\text{-}5)$$

The discharge rate from the pumping well is now given by

$$Q_{r_0} = -2\pi r_0 K_{sat} h_0 \frac{\partial h}{\partial r}\Big|_{r=r_0}$$

$$= \pi\left\{ir_0{}^2 - \left[\left(h_R{}^2 - h_0{}^2\right)K_s + i\left(\frac{a^2 - r_0{}^2}{2} + a^2 \ln\frac{R}{a}\right)\right] \Big/ \ln\frac{R}{r_0}\right\} \quad (5\text{-}6)$$

Results of simulations with the HYDRUS-2D code indicated that the water table divide was located at about 660 cm from the well. An approximate estimate of the well capture radius can be obtained also with Eq. (5-5), which assumes steady-state flow conditions. Such conditions likely occurred during days 3 to 5 of the experiment when the pumping rate varied very little around a mean value of 0.12 L/s. The assumption of steady-state flow was further confirmed by the HYDRUS-2D simulations. Using Eqs. (5-5) and (5-6), we estimated the well capture radius (r^*) of our field tracer experiment to be 580 cm, and the pumping discharge rate (Q_{r0}) to be 0.12 L/s for our field experiment. For the calculations we used r_0=2.5 cm, R=3000 cm, a=2000 cm, K=52 cm/h, i=0.41 cm/h, h_0=90 cm, and h_R=82 cm. The values of both r^* and Q_{r0} decreased with increasing values of the hydraulic conductivity (Fig. 5-3).

The analytical solutions for r^* (Eq. 5-5) and Q_{r0} (Eq. 5-6) were obtained with several simplifying assumptions such as having steady flow, a homogeneous aquifer, and no seepage face. This caused Eq. (5-5) to underestimate the well capture radius as compare to the more comprehensive HYDRUS-2D variably-saturated flow simulations. Nevertheless, this example demonstrates that for practical purposes the analytical solution can provide a useful first approximation of system parameters needed for the design of these type of tracer experiments.

5.2 LATERAL FLOW EXPERIMENT

5.2.1 ABSTRACTION BY IGNORING VADOSE ZONE

5.2.1.1 2D FLOW AND TRANSPORT IN GROUNDWATER

A first abstraction step considered here is a reduction in the dimension of the problem from three to two dimensions. Specifically, the fully 3D saturated-unsaturated flow and transport

problem as described in the Section 4.2 was replaced by a 2D problem in which flow and transport occur only in groundwater. The effect of the vadose zone on retention and transport hence was ignored in this abstraction. The MODFLOW and the MT3D models were used consecutively for the approximate flow and solute transport simulations, respectively, while data preprocessing and postprocessing were implemented using the GMS software.

For the simulations we used a rectangular flow domain of 10,000 x 7,000 cm. The lower boundary of the simulated domain was a horizontal plane at an elevation of 35 m. The upper boundary was the soil surface with elevations as shown in Fig. 3-36. The domain used previously for the HYDRUS-3D simulations was discretized laterally using a telescopic refinement grid with the center coinciding with the center of the irrigated area. The base size of the finite elements was 50 cm, and increased with a bias of 1.05 to the maximum size of 500 cm as the distance to the irrigated area increased. Each one-layer spatial grid had 4940 nodes.

The automated interpolation and material distribution in GMS created a stratigraphy that was substantially different from the stratigraphy used in the base 3D model using HYDRUS 3D. Therefore a special effort had to be made to obtain a material distribution that was as close as possible to the distribution used in the HYDRUS 3D base model. The procedure consisted of the following steps:

- the lateral material distribution was imaged for each of 14 layers of the HYDRUS 3D grid;
- a 3D grid was built in GMS that had the same geometry as the layers in HYDRUS 3D;
- the "Boreholes" module of GMS was used to introduce 87 boreholes (Fig. 5-4, top left);
- vertical coordinates of all 14 layers were defined as in the HYDRUS 3D base model;
- a table of material distributions was built for each borehole (Fig. 5-4, top right);
- locations of material boundaries were defined using the "Auto assign horizons" option of the ":Boreholes" module;
- The MODFLOW HUF (Hydrological Unit Flow) module was used to define hydraulic properties of each cell of the 3D grid, while the "horizons to HUF" option was used to interpolate the borehole data to the grid nodes (inverse distance weighting was used for this interpolation).

The above procedure resulted in 14 hydrologic units within the simulation domain. Examples of material distributions along various domain cross-sections are shown in Fig. 5-4, bottom.

Dirichlet boundary conditions were defined along the vertical boundaries of the simulation domain. The initial distribution of groundwater levels in the domain was obtained by fitting the solution of the stationary flow problem to initial groundwater levels in the observation wells. The fitting was accomplished by varying the groundwater recharge separately within the irrigation area and outside this area. The model performance indicators obtained for this solution were: a Root Mean Square Error of 26 cm, a Mean Absolute Error of 21 cm and a Mean Error of 3 cm.

Groundwater recharge during the experiment was computed from a surface water balance using available rainfall data, evapotranspiration rates calculated with the Penman-Monteith equation, measured runoff data, and the applied irrigations and their schedule.

The following setup was adopted for the numerical solution procedure. All cells were convertible, and the option "prevent cell drying and assign bottom elevation to dry cells" was used. The simulated experimental period of 112 days was divided into 481 stress period of varying durations depending upon the rainfall and irrigation rates. A minimum time step of 0.1 d

was used. This time step was not allowed to exceed any of the stress period durations. The PCG2 (Pre-condition Conjunctive Gradient module with Modified Incomplete Cholesky matrix preconditioning methods) module was used as the matrix solver. As convergence criteria we used a head change of 1 cm and a residual of 1 m^3. Cells along the irrigated area periodically flooded, which caused some oscillations during the numerical solutions. Using the "Cell wetting parameter" module did not improve the convergence (i.e., less oscillations or a computationally more efficient solution). The overall global mass balance error for the cumulative volume was a modest 0.47%, which further caused up to believe that the solution was reasonable.

The MODFLOW calibration was carried out using the PEST software package. The MODFLOW solution for this purpose was fitted to the observed groundwater depths. Estimated hydraulic conductivity and specific yield values are shown in Fig. 5-4. The model performance indicators with the calibrated parameters were: a Root Mean Square Error of 44 cm, a Mean Absolute Error of 32cm, and a Mean Error of 3 cm. The accuracy the transient flow calibration was lower than the accuracy of initial ground water calibration. A likely reason for this is the difficulty of handling fully saturated soil layers in MODFLOW. The Fig. 5-5 illustrates this with a comparison of simulated and measured groundwater levels during a period with complete saturation. Simulated groundwater values appear to be higher than 1 m above the soil surface, which caused large model errors.

The MODFLOW calibration was evaluated using criteria outlined by Reilly and Hardbaugh (2004). The conceptual model of the system under investigation corresponded to our preliminary survey and monitoring data, and hence seemed to be reasonable. The mathematical representation of the boundaries were also reasonable since the flow domain boundaries were relatively far from the irrigation area, as was confirmed by preliminary simulations (data not shown). Simulated head and flow distribution were found to mimic important aspects of the flow system, such as magnitude and direction of the head contours. Except for periods of full soil profile saturation, quantitative measures of head differences between the simulated and observed values seemed acceptable in view of the objectives of our study. Noting that MODFLOW was not fully capable of simulating flow in the system under study, we nevertheless, proceeded with simulating transport in the lateral flow experiment using the MT3D model. The average of concentrations at three observation depths was used for our comparisons of simulated and measured values.

The first set of simulations was carried out assuming the same values of the dispersivity and the effective porosity for all materials. An example of the type of results we obtained is shown in Fig. 5-6. The field data and simulations indicate that tracer concentrations at different wells reflected different subsurface transport conditions. For example, wells 5 and 7 seem to receive the tracer from a subsurface channel having the lowest dispersivity and the lowest effective porosity compared with other wells. Well 6 reflected transport conditions with a low effective porosity but a relatively high dispersivity. Wells 8 and 9, on the other hand, are most probably within a subdomain having a relatively high effective porosity. To confirm these conjectures, the simulation domain was separated into three subdomains, each one having its unique transport parameters as shown in Fig. 5-7. Simulated results using this approach provided a better match with the well tracer data.

Overall, the abstraction of the full 3D model to a 2D groundwater flow and transport model provided important insights into the subsurface transport properties. Values of the effective porosity (n_e) generally increased with clay content (e.g., Fig. 5-4, top right). However, the values were substantially smaller than the porosity of the soil materials. This indicates that field scale

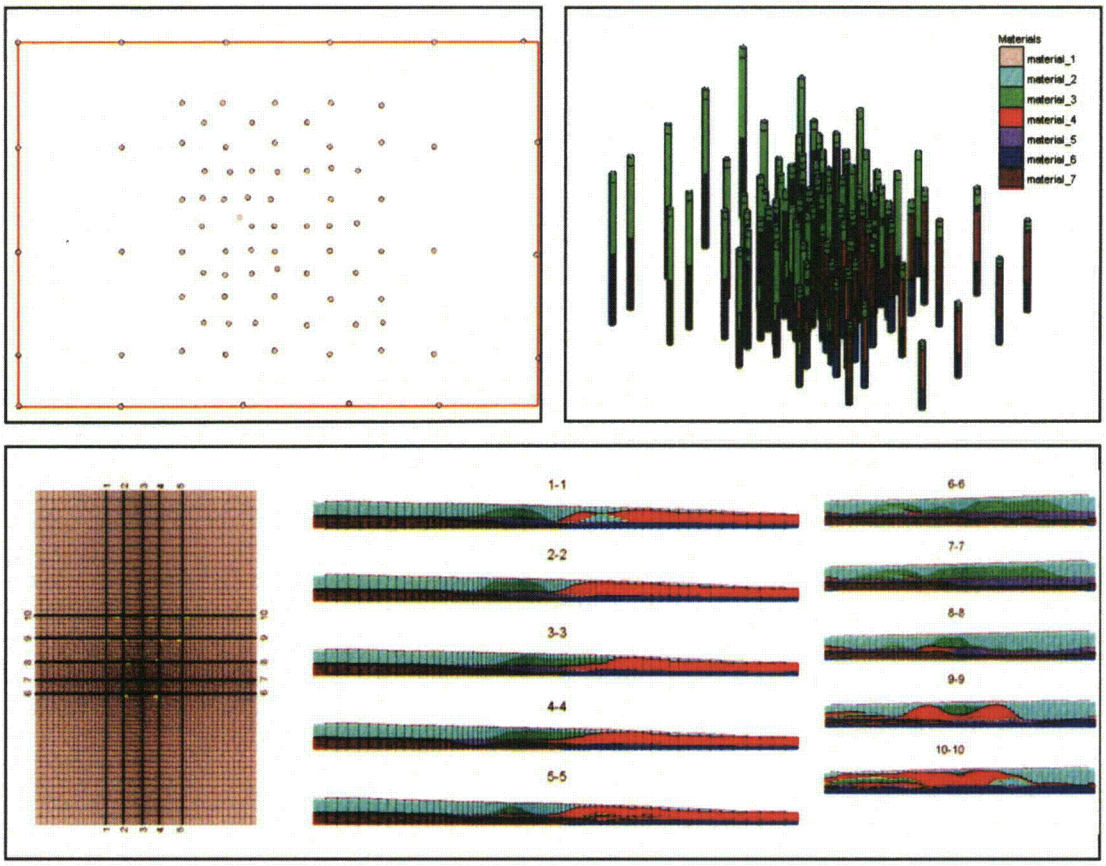

Figure 5-4. Conversion of the subsurface material distributions from the HYDRUS 3D model grid to the MODFLOW model grid. Top left – locations of artificial boreholes with properties defined in HYDRUS3D, top right – material distribution in artificial boreholes, bottom – cross-sections of material distributions in MODFLOW.

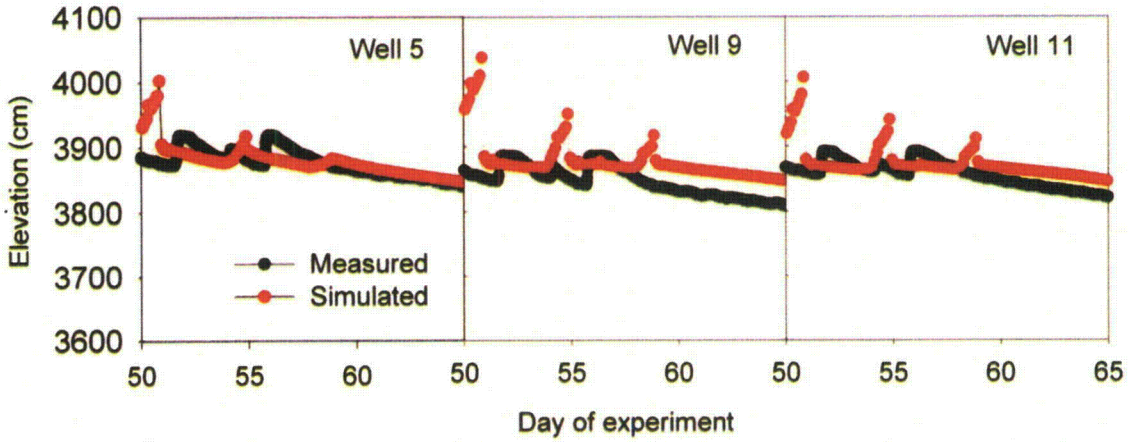

Figure 5-5. Measured and simulated groundwater levels during a period of full soil saturation with water.

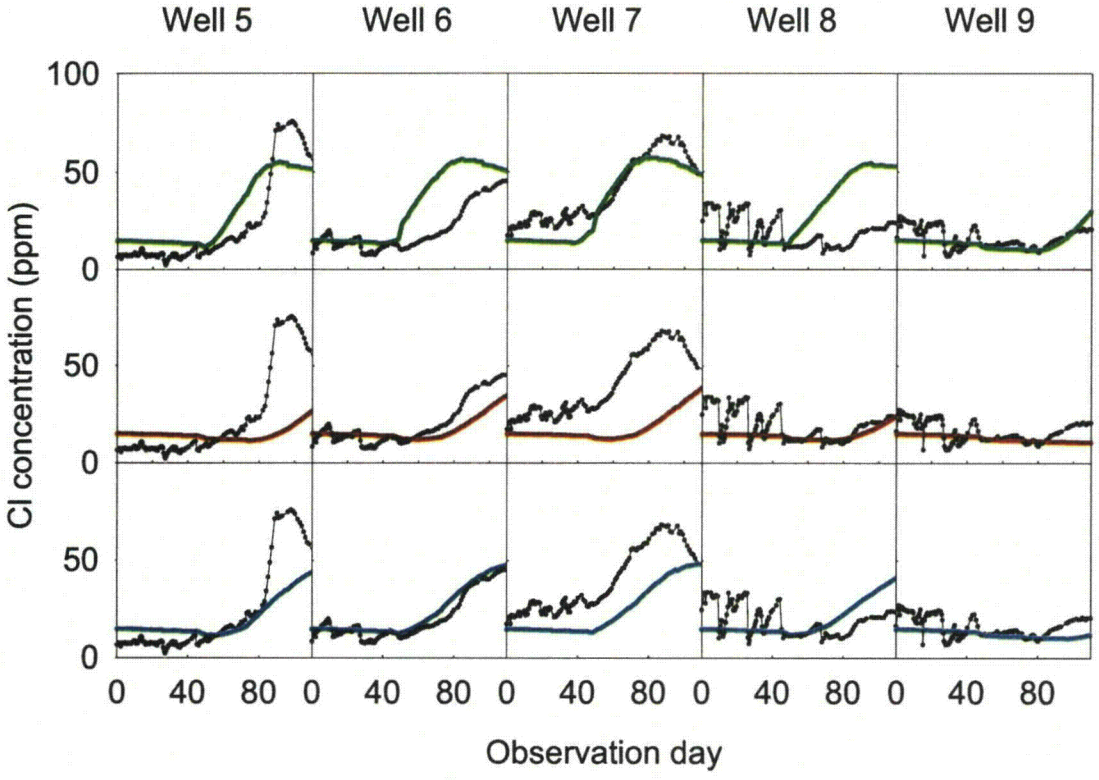

Figure 5-6. Measured (▬) and simulated tracer breakthrough in observation wells with the same values of dispersivity a_L and effective porosity n_e across the simulated transport domain; ▬ a_L=1 cm, n_e=0.2 cm^3cm^{-3}; ▬ a_L =1 cm, n_e=0.3 cm^3cm^{-3}; ▬ a_L =10 cm, n_e=0.2 cm^3cm^{-3}

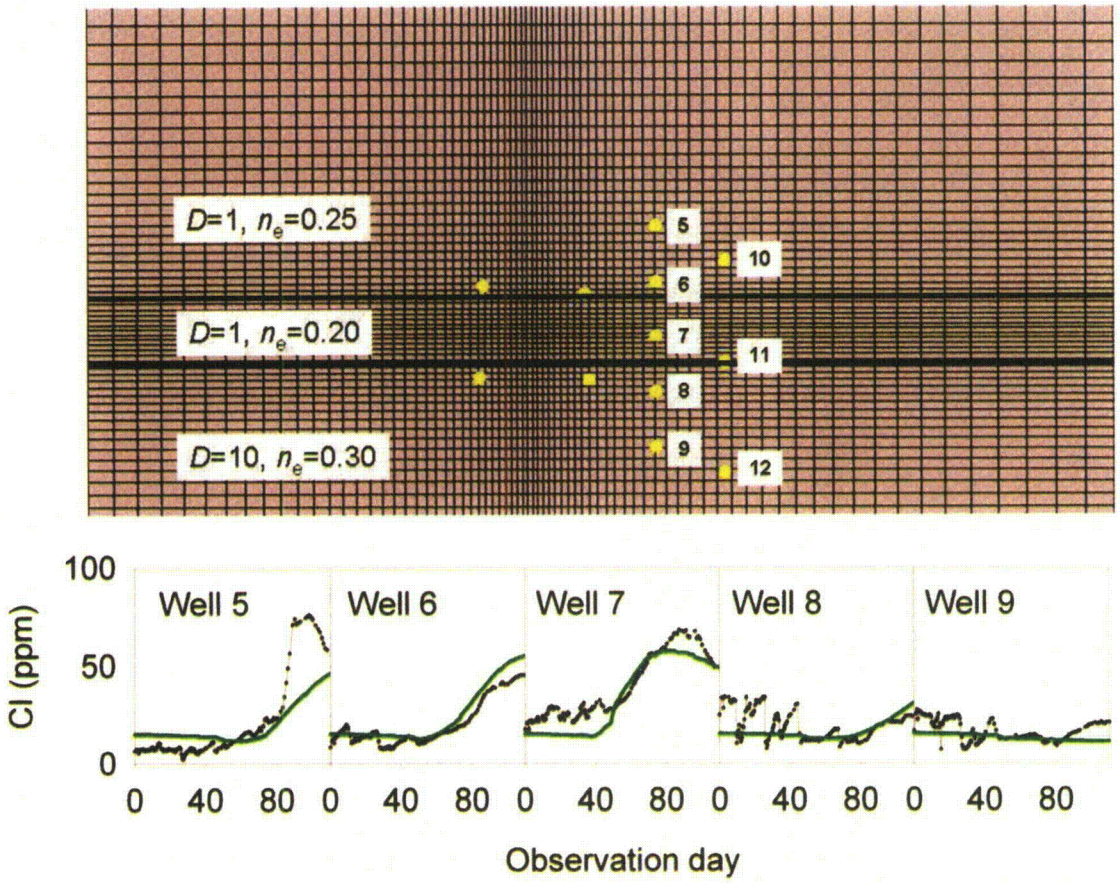

Figure 5-7. Tracer transport simulations with three subdomains (top) having different parameters for the dispersivity a_L (cm) and effective porosity n_e. Measured (▬) and simulated (▬) Cl breakthrough curves are shown for five different observation wells (bottom).

transport at the study site occurred preferentially and that a substantial part of the soil profile conducted very little water and solute. The field heterogeneity as described in Sections 3.2.3.3, 3.2.3.4, 3.2.3.5, and 3.2.3.8 created the essential prerequisites for such preferential transport to occur.

5.2.1.2 1D TRANSPORT IN GROUNDWATER

Simulations of 1D transport in groundwater were carried outusing the windows-based STANMOD software package (Šimůnek et al., 1999). Specifically, we solved the inverse problem to determine transport parameters using the CXTFIT code, which is a part of the STANMOD software. As input for the simulations we used the observed breakthrough curves at wells L1 through L12. The conceptual scheme is presented in Fig. 5-8. We started simulations at the time the tracer was applied to the soil surface. Subseqent leaching to groundwater by fresh irrigation and rain water created a toroid- (or donut-) like concentration distribution in the horizontal plane around the pumping well. For the 1D transport problem we assumed a stepwise initial distribution along the flow direction as shown in Fig. 5-8.

The maximum concentration C^* of the initial step function resulting from leaching of the applied tracer and subsequent mixing with groundwater was estimated from the observed concentrations in wells L3 and L4 at the edge of the tracer application area. A least-squares optimization with CXTIFT allowed us to estimate the flow velocity (v) and the dispersion coefficient (D) from the breakthrough curves. In addition, to obtain a better fit between the observed and simulated BTCs, the length of the concentration step Δx and concentration C^* (Fig. 5-9) were adjusted by trial and error. Despite the fact that this affected the uniqueness of the optimization, we used this procedure to solve the inverse problem. The estimated parameters are presented in Table 5-2, while the observed and fitted BTCs are shown in Fig. 5-9.

Fair agreement between simulated and observed concentrations was obtained for wells L5 through L7, whereas a worse fit was obtained for wells L9 through L12 because of oscillations versus time. These oscillations were especially pronounced for L8. We believe that this behavior is a result of fast vertical preferential flow during infiltration following high-intensity precipitation events, which cannot be modeled by CXTFIT.

The groundwater flow velocity between the tracer application plot and first line of the wells (L5 through L9) was found to vary from 0.030 to 0.077 m d^{-1}. Dispersivity (a_L) values were in the range of 0.30-1.16 m, which are reasonable values for a field-scale tracer simulation in which a highly heterogeneous medium is represented by an equivalent homogeneous porous medium. Estimated flow velocities obtained for the second line of wells (L10, L1, and L12) were larger than those of L5 though L9, whereas the dispersivities had the same order of magnitude.

A noticeable increase in Cl^- concentration was observed at the deepest sampling points (1.65 m depth) of wells L10 through L12 of the second row of observation wells, starting at approximately day 60, while the concentrations in wells L5, L6, L7 and L9 of the first row of wells started to increase somewhere between 40 and 60 days after the experiment started. If we assume that the increase of concentrations of wells L10 through L12 was associated with the same source as for L5, L6, and L9, then the obtained results suggest a much higher flow velocity between the first and the second rows of the wells. This could be due to preferential flow through a thin conductive layer in the lower soil horizons. Another possible cause could be the presence some unknown source of high salinity in the study area, something that may need further testing.

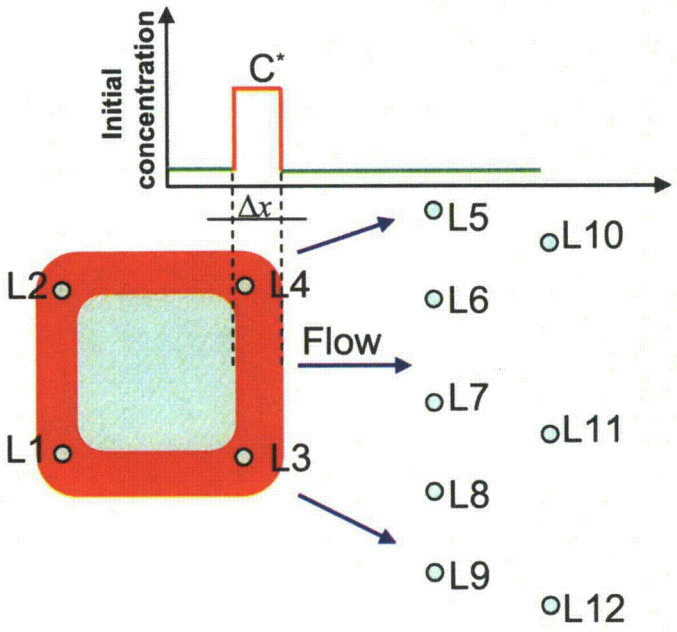

Figure 5-8. A conceptual scheme for simulating 1D transport in groundwater during tracer transport experiment.

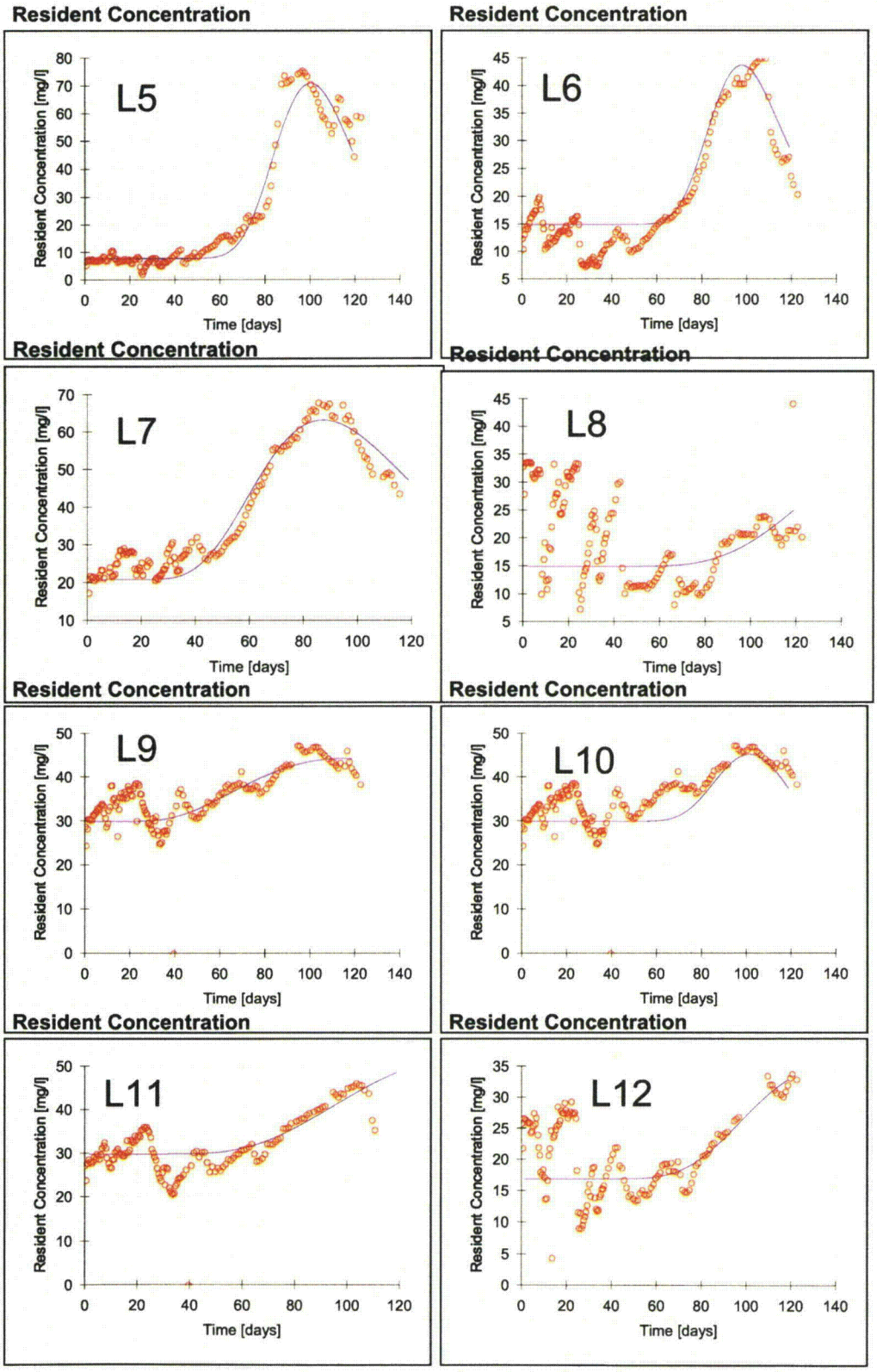

Figure 5-9. Observed (red circles) and fitted (blue lines) breakthrough curves in wells 1 through 12.

Table 5-1. Calibrated aquifer parameters

Material	Parameter	Value	Relative sensitivity	95% confidence interval
Sandy Loam	Horizontal conductivity (cm d^{-1})	101	0.00009	36.7
	Specific yield	0.11	0.021	0.0027
Sandy Loam	Horizontal conductivity (cm d^{-1})	138	0.0016	3.86
	Specific yield	0.11	0.021	0.0027
Sandy Clay Loam	Horizontal conductivity (cm d^{-1})	53	0.00052	5.15
	Specific yield	0.05	0.0047	0.000265
Loam	Horizontal conductivity (cm d^{-1})	4	0.000093	1.8
	Specific yield	0.14	0.085	0.0011
Silt Loam	Horizontal conductivity (cm d^{-1})	18	0.00018	5.35
	Specific yield	0.14	0.00011	3.3
Silty Clay Loam	Horizontal conductivity (cm d^{-1})	102	0.0029	1.5
	Specific yield	0.1	NA[§]	-
Clay Loam	Horizontal conductivity (cm d^{-1})	11	0.00016	5.7
	Specific yield	0.1	NA	-

[§]Was not estimated

Table 5-2. Parameters found by solving the inverse of 1D transport in groundwater using CXTFIT.

Borehole	v, m d^{-1}	D, m^2 d^{-1}	a_L, m	Δx, m	C^*, mg l^{-1}	R^2
L5	0.077	0.079	0.97	1.5	150	0.954
L6	0.058	0.042	0.72	0.5	150	0.707
L7	0.077	0.023	0.30	3.0	100	0.931
L8	0.030	0.011	0.37	0.5-4.0	150	0.331
L9	0.054	0.063	1.16	3.0	100	0.528
L10	0.121	0.025	0.21	1.0	150	0.384
L11	0.081	0.093	0.87	3.0	150	0.560
L12	0.111	0.079	0.71	3.0	150	0.221

($a_L=D/v$ is the dispersivity, R^2 is determination coefficient)

5.2.2 ABSTRACTION WITH A CHANGE IN SCALE: PROFILE AGGREGATION

To assess the effect of the soil profile aggregation on the simulation results, we abstracted the model and converted the heterogeneous profile of the upper sub-layer to into an equivalent homogeneous medium. Two scenarios were considered: a profile composed of sandy loam (SL), and a profile consisting of a silt loam (SiltL). The saturated hydraulic conductivities were set according to Rawls et al. (1998) as 1.360 and 0.346 m/day, for SL and SiltL textural classes, respectively. The longitudinal dispersivity was assumed to be 0.2 m in both simulations. Results are presented in Fig. 5-10 to 5-12. Profile homogenization had only a minor effect on the simulated BTCs of wells L1 through L4 where vertical transport prevailed; however, the influence was very significant for wells L5 through L9 (Fig. 5-10 and 5-11).

Introducing a homogeneous SL profile did lead to a delay of the tracer arrival time at well L5, and in early appearance in wells L6-L9 (Fig. 5-10). The simulated maximum concentrations in L6-L9 were at the same time were also significantly higher than the observed concentrations. Assuming a homogeneous SiltL profile with much lower hydraulic conductivity caused a delay in the tracer arrival times at wells L5-L7 compare to the calibrated model (Fig. 5-11). The effect of profile homogenization using SiltL on the BTCs of wells L8 and L9 was relatively minor. This was expected since the logs of these wells indicated the presence of low-permeability layers in this part of the study area. A comparison of simulations obtained with the homogeneous SL and SiltL profiles is shown in Fig. 5-13a and b, respectively, for wells L10-L12. Notice that the homogeneous SL simulations produced increases in the tracer concentration of wells L10, L11, and L12, but not for the other observation wells.

5.2.3 ABSTRACTION OF REQUIRED PARAMETERS: USING PEDOTRANSFER FUNCTIONS

In this section we present the results of model abstraction scenario where we used pedotransfer functions (Rawls et al., 1998) to estimate the saturated hydraulic conductivities of the various soil materials from soil texture. The following K_{sat} values were used in the simulations: 1.36, 0.18, 0.094, 0.346, 0.09 and 0.048 m/day for SL, SCL, L, SiltL, SiltCL and C, respectively. Results are presented in Fig.5-14.

Substituting the calibrated K_{sat} with values determined using pedotransfer functions had minor effect on the BTCs of wells L1-L4 and L10-L12. The flow paths between the tracer application plot and L5 followed mainly a layer having a SL texture whose PTF K_{sat} value was very close to the calibrated value. Hence, the influence of the PTF abstraction was not significant for L5 either. However, for wells L6 through L9 we observed a delay in the simulated BTCs since the PTF estimated K_{sat} values of SCL and L were more than two times lower than the values obtained by the trial-and error.

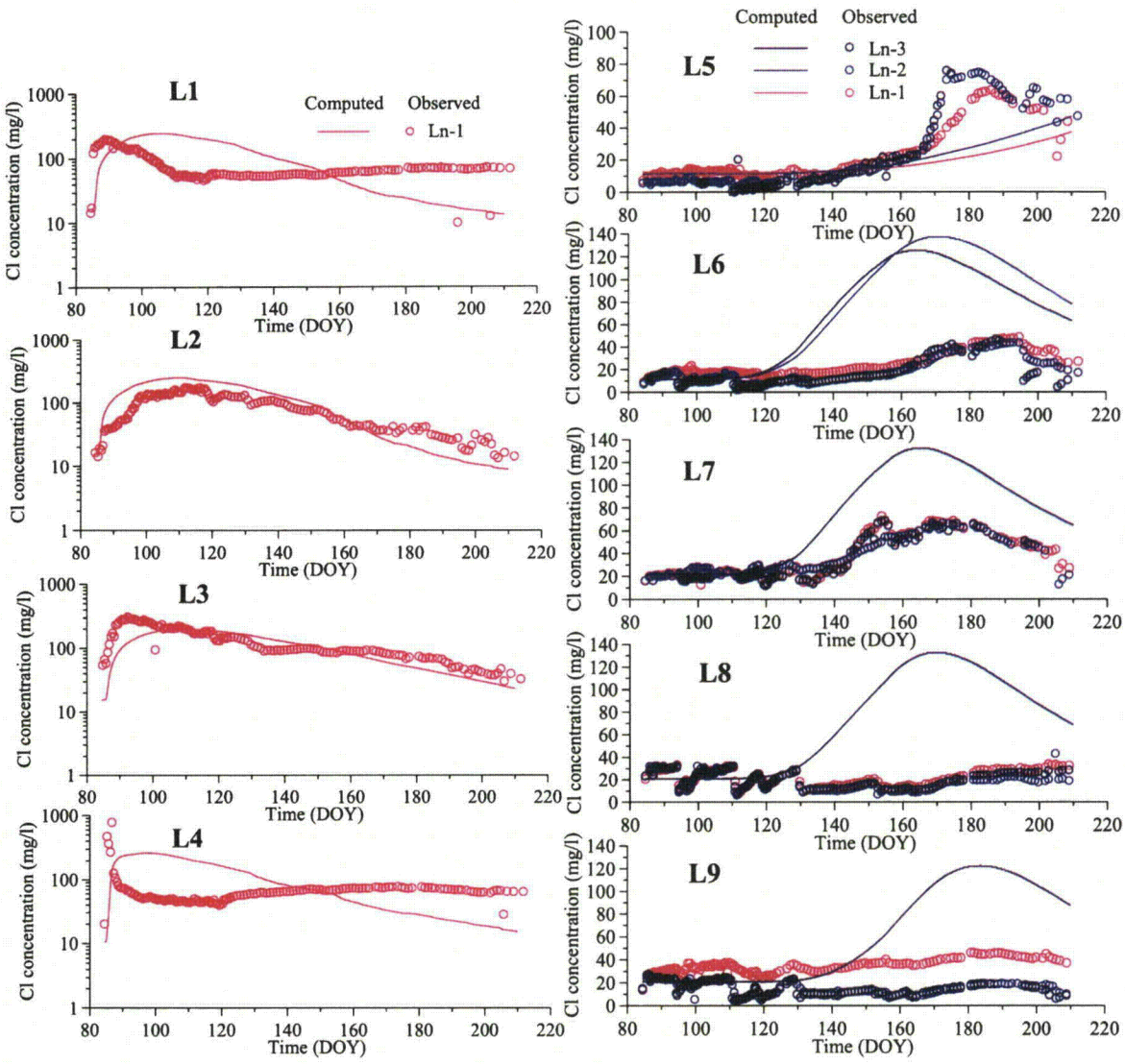

Figure 5-10. Observed and simulated chloride breakthrough curves for the homogeneous sandy loam (SL) profile. Symbols are the same as in Fig. 4-12.

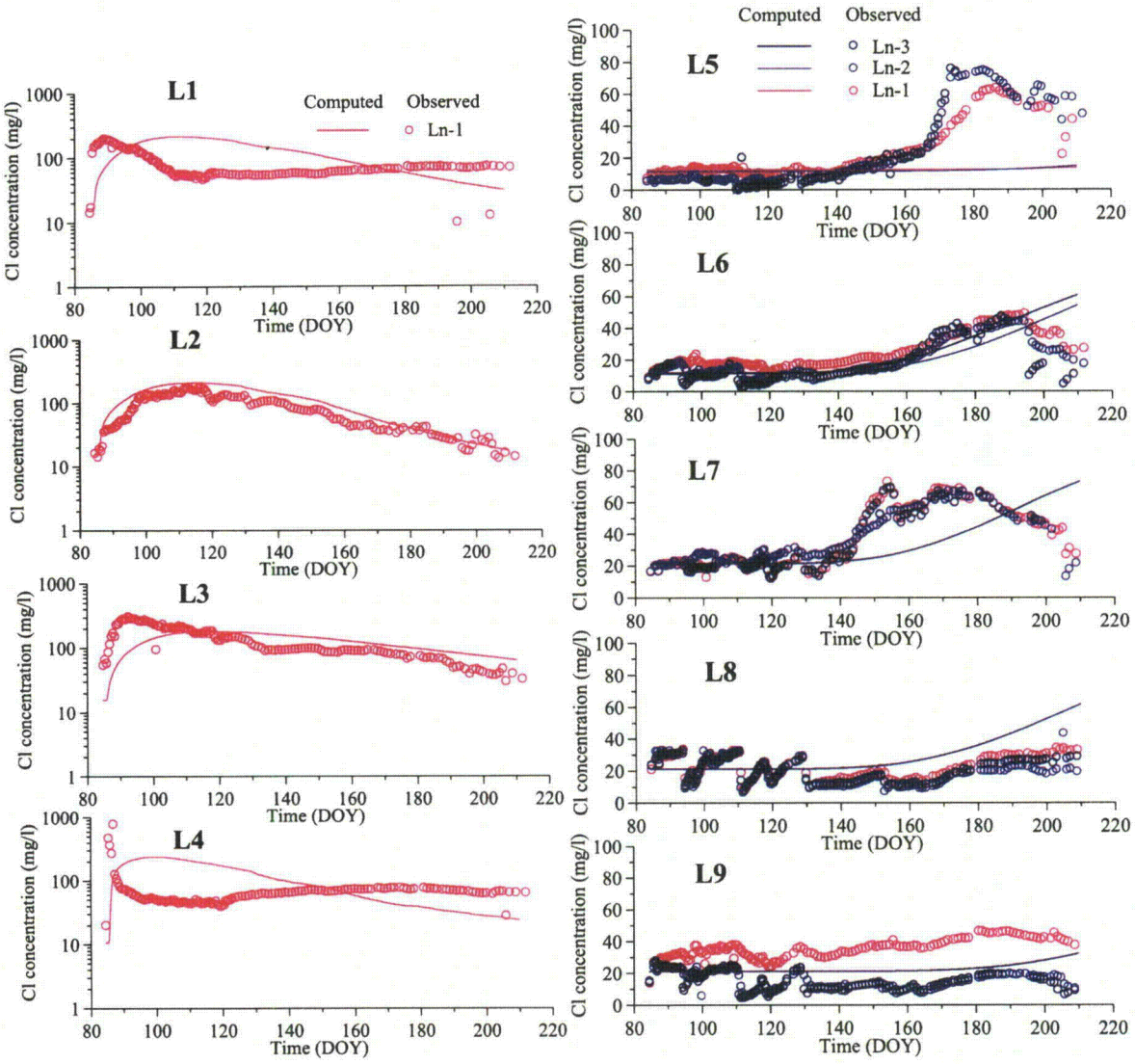

Figure 5-11. Observed and simulated chloride breakthrough curves for the homogeneous silt loam (SiltL) profile. Symbols are the same as in Fig. 4-12.

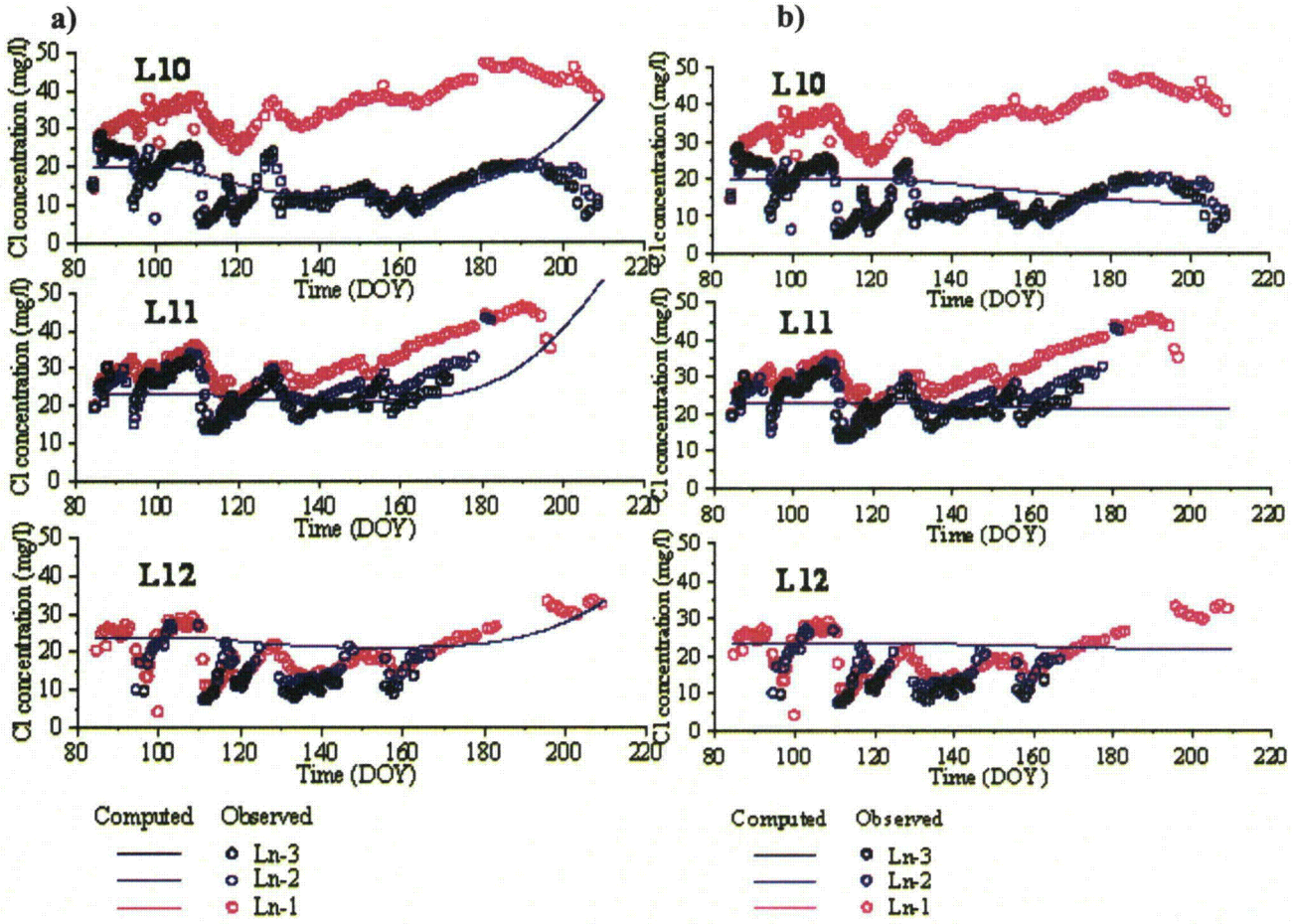

Figure 5-12. Observed and simulated chloride breakthrough curves for homogeneous profiles: a) sandy loam, and b) silt loam. Symbols are the same as in Fig. 4-12.

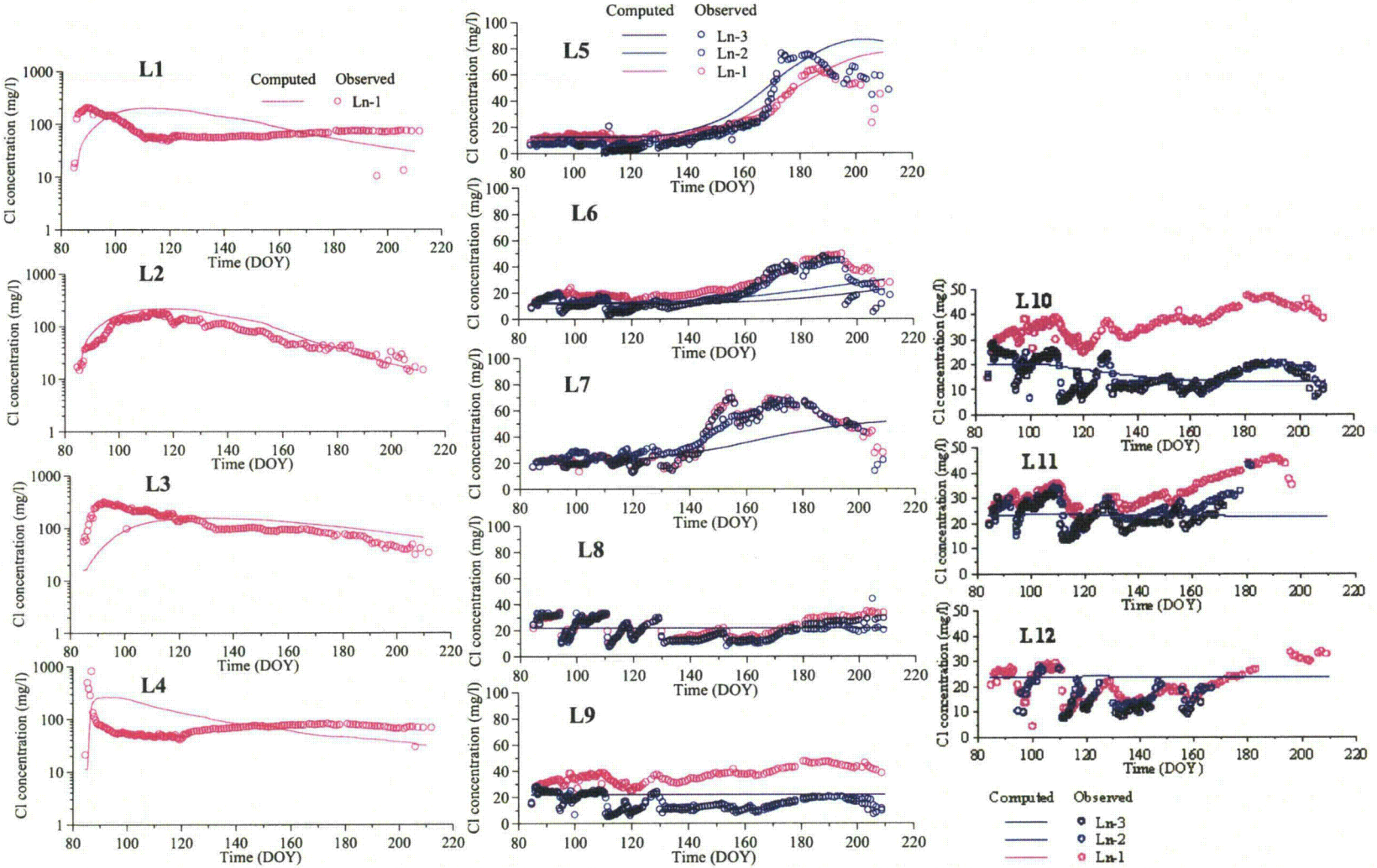

Figure 5-13. The observed and simulated chloride BTCs curves for the abstracted model in which K_{sat} values were determined using pedotransfer functions developed by Rawls et al., (1998). Symbols are the same as in Fig. 4-12.

5.3 SUMMARY AND CONCLUSION

This study was designed and performed to demonstrate the applicability of model abstraction techniques to subsurface flow and contaminant transport problems. The study focused on future applications of modeling to contingency planning and management of potential and actual contaminant release sites within the scope of the US NRC operations.

Subsurface flow and transport modeling may have various purposes including site characterization, explaining the existing subsurface contamination pattern, and projecting the contaminant release results under various environmental and management scenarios. Contributing to the characterization the subsurface flow and transport domain was the purpose of modeling in this work.

Modeling was only one component of characterization of the subsurface in this work that also included using the borehole data, laboratory studies of soil hydraulic properties, applying geophysical methods, monitoring soil moisture and soil pressure head, groundwater monitoring, field hydrogeological tests, and tracer studies. The important role of modeling in characterizing the subsurface was to describe the transport conditions. Given the non-uniqueness of interpretations of geophysical data, the small scale of borehole and laboratory data as well as of most groundwater samples and tests, and the limitation of soil moisture monitoring in revealing the hydraulic conductivity of soils, development of alternative conceptual subsurface transport models, and distinguishing between these models, was the essential part of the modeling effort.

The OPE3 experimental field site near Beltsville, MD, has been extensively studied for more than 10 years using geophysical, biophysical, remote sensing, and soil and groundwater monitoring methods. Available data are analyzed using a systematic procedure based on a broad vadose zone modeling context developed in this study. A major focus was on the existence of subsurface structural units and features that may drastically change the fate and transport of contaminants in the vadose zone, as well as of projected trajectories of the contaminant plume in groundwater. We found that solute transport in soils and shallow groundwater at the site is potentially affected by such features as the presence of a restrictive fine-textured layer that is not fully continuous laterally, the complex topography of the restrictive layer favoring preferential flow and transport along preferred pathways along its surface relief, the presence of natural capillary barriers, possible funnel flow in a coarse-textural layer between more fine-textured layers, and local high-conductivity parts of the soil pore space.

An extensive field survey and monitoring program had to be initiated as part of this work in spite of the existence of a large database of soil and groundwater properties at the site. The main reason for this was the difference in scale at which the site was characterized previously, and the scale at which flow and transport processes are of a concern in contaminant release applications. Specifically, our 20 x 20 m research site required additional characterization since the site presented only a single pixel in the characterization of the entire 300 x 300 m OPE3 site

The employed geophysical methods provided essential information about transport-controlling subsurface features. A 2x2 m ground penetrating radar survey showed the existence of a mostly continuous restrictive layer with complex topography. Soil electric resistivity monitoring furthermore revealed the existence of narrow hydrologically active vertical zones. The obtained data indicate that large parts of subsurface soils may not fully participate in the prevailing flow and transport processes. Biophysical monitoring of the research area allowed delineation of relatively large structural units in the soil cover that provided distinctly different

conditions for plant growth. The size of those units exceeded the scale of investigation in this work.

The borehole log data showed surprisingly high spatial variability for the relatively small sites. For example, soil texture was represented by six textural classes in the range from sandy loam to silty clay loam. This underscored the possibility of the existence of the subsurface preferential solute transport, and at the same time indicated that the defining a representative elementary volume for the subsurface may be difficult if at all possible.

Laboratory water retention data clearly indicated the presence of macroporosity in soils that potentially could case the fine-scale high-conductivity part of the soil pore space. Hydraulic conductivity measurements at the same scale showed that, in actuality, such high conductivity would require not only the presence of macropores but also the connectivity between these pores, could be found only in a relatively small percentage of locations.

Soil moisture and soil pressure head monitoring data provided the information about field hydraulic properties of unsaturated soils. The field water retention was well defined by those measurements. This indicated that the Richards model could be an appropriate conceptualization of the flow processes in soils under study. It appeared necessary to develop a site-specific calibration of capacitance probes, and the method was developed for that purpose in this work.

Two field experimental studies, both of original design, were carried out and analyzed using model abstraction. One study, referred as the solute flux experiment, was meant to imitate a soil column experiment at the plot scale. The experiment involved the application of a conservative tracer around a well and subsequent irrigation with simultaneous pumping of ground water. This experiment should provide insight into the significance of zones in the soils having a high vertical conductivity. A second study was designed to observe the lateral transport of a surface-applied conservative tracer pulse when transport was controlled by regular irrigation pulses and natural precipitation. This second experiment should demonstrate the effect of the topography and continuity of the restrictive layer, as well as the significance of funnel flow due to the presence of a coarse layer between the finer-textured layers. The vadose zone during both experiments was monitored for soil water content and pressure heads, while groundwater levels and the groundwater chemical composition were also recorded. Groundwater compositions were monitored at three different depths.

Two preliminary modeling projects preceded the lateral transport experiment. One was undertaken to estimate the potential importance of runoff and the need to intercept this runoff. This study required developing a new model and software to simulate coupled surface-subsurface flow and transport at the plot scale for the 30x30 m study area. The software coupled the FEMWATER and 2DSOIL codes, the former simulating subsurface flow and the latter overland flow using a diffusive flow approximation. For the second modeling project we used the new software, HYDRUS-3D, to simulate flow and transport in the three-dimensional subsurface domain at the site. The purpose was to estimate the required duration of the experiment and the frequency of sampling needed to capture in detail the solute breakthrough curves in a number of observation wells. Both preliminary modeling studies were found useful in terms of improving the experiment setup and the schedule of the experiment.

The solute flux experiment comprised approximately 7 days, whereas the lateral flow experiment continued for four months. About 10,000 analyses were made of the tracer concentration in order to develop the breakthrough curves. A preliminary analysis of the experimental results was used to obtain a conceptual representation of the prevailing subsurface transport processes. We hypothesized that preferential transport of solutes occurred in both

experiments. Vertical transport in the unsaturated zone seemed to occur much faster than suggested by the observed water fluxes. The tracer breakthroughs in the lateral transport experiment occurred at substantially different times in the wells at similar distances from the application area. The differences in times to some extent corresponded to soil textural differences.

There were no indications in the solute flux experiment results that the Buckingham-Darcy flow model and the corresponding Richards equation were not applicable to the data. Therefore, water flow in both the unsaturated zone and in groundwater was simulated with the Richards equation using the HYDRUS2D software package.

The seepage face along the observation well was found to be an important feature of the experimental setup of the solute flux experiment. Transport occurred both in groundwater as well as in the capillary fringe. The Richards equation for flow and the convection-dispersion model for transport were both successfully calibrated and provided good representations of the experimental results. No assumption about preferential solute transport in highly conductive parts of the soil pore space was needed.

The 2D model for flow and transport in the variably saturated zone was abstracted to a 1D model for vertical water flow and solute transport to groundwater. While ignoring the presence of a seepage face, the 1D model allowed preferential transport of solutes to occur. It appeared that this model was able to provide only approximate qualitative and quantitative predictions of solute breakthrough. The invoked abstraction demonstrated that ignoring the actual geometry of the flow and transport domain and the essential features of the flow process in the field can create a distorted conceptualization of transport in the subsurface.

One more abstraction step was considered for 2D solute transport to demonstrate that a simple analytical model sometimes may be sufficient for certain modeling application. This abstraction was used to investigate the ability of the pumping well to intercept all of the surface-applied tracer, which is a critical aspect of the solute transport experimental setup. For this to occur, the tracer application zone must remain within the groundwater depression cone around the well. We showed that a simple analytical model evaluated the depression cone size with the same degree of accuracy as the more refined 2D saturated-unsaturated flow model.

Results of the lateral flow experiment were relatively more complex than results of the solute flux experiment. Some small temporal scale (1 – 2 days) phenomena were observed in some wells that could not be explained. We ignored these fine scale phenomena and concentrated on conceptualization of the flow and transport at larger temporal scale.

The fine-textured low-permeability layer was found to divert the tracer according to the topography of the layer. There were no indications that the Buckingham-Darcy flow model and corresponding Richards equations were inapplicable at the larger scale, likely because flow and transport at that scale seemed to be driven mostly by the hydraulic gradients in groundwater. The complexity of the flow and transport domain required the use of a full 3D representation. For this reason we used the HYDRUS3D software to simulate flow and transport in the lateral flow experiment.

Since HYDRUS3D does not have a calibration option, only trial and error calibration could be applied. Given that 2 days of computation were needed for each simulation run with this code, we streamlined the calibration procedure by calibrating the model directly to the breakthrough curves, and not to groundwater levels. This created a dilemma in terms of selecting an appropriate conceptual model for transport. Solutes could be delivered to a well via two different transport mechanisms: (a) transport via a network of well-connected pathways that comprise

only part of the bulk soil porosity at the field scale, thus assuming that part of the domain does not participate in the transport process, or (b) transport through all of the domain. To deliver solute to a well at approximately the same time, average water fluxes should be smaller in case (a) as compared to the case (b). We selected case (b) and used several model abstractions to justify this selection

The trial-and-error calibration based on zonation of the flow and transport domain was reasonably successful. The maximum concentration levels and the 50% concentration arrival times were described satisfactory. However, we could not accurately reproduce the shape of the breakthrough curves.

A dimension reduction abstraction considered only 2D flow in groundwater. MODFLOW and MT3D were used for this purpose. A special effort was undertaken to use in this abstraction the same zonation and layering as in the complete 3D representation. MODFLOW calibration capabilities were used successfully to reproduce the groundwater levels, while dispersivity and effective porosity values were estimated by trial and error from the breakthrough curves.

The 2D abstraction process showed that the assumption of part of the soil not significantly participating in the solute transport process created a better representation of the breakthrough curves. A reasonable representation of solute transport was achieved with an effective porosity of 60-70% of total soil porosity. Thus, the model abstraction step helped to substantially improve the conceptualizaton of the subsurface transport conditions.

A 1D abstraction step allowed efficient assessment of intrinsic groundwater velocities and the hydrodynamic dispersion parameters in different directions. The results also suggested the location of preferential flow pathways.

Using pedotransfer functions to estimate saturated hydraulic conductivities and/or to substitute the heterogeneous soil profile by an equivalent homogeneous medium indicated that this kind of model abstraction may lead to incorrect estimates of tracer front arrival times at some locations. Actually, results depended on the complexity of the heterogeneity being abstracted. Since small-scale heterogeneities may control flow and transport at the larger scale, a careful profile aggregation and analysis of the results is required.

Several observations have been made during the data analysis in this work.

First, our detailed studies revealed considerable soil heterogeneity at a very small site. We do not know how common such a degree of heterogeneity is since studies at this level of detail are relatively rare. It is important to recognize that the scale of our experiment was comparable the scale of solute release. Exclusion of a substantial part of the soil from the active solute transport process appears to be an important consequence of soil heterogeneity at the field scale.

Second, calibration of vadose zone models is much more trying than calibration of groundwater models. This is because of the nonlinearity of the governing flow processes and the large number of parameters involved. Substantial changes in soil water contents and flow rates must occur to reliably calibrate a vadose zone model.

Third, the use of models that assume the presence of mobile and immobile zones was avoided in this work. Such models are undoubtedly important when breakthrough tails are of interest. However, measuring tails takes time that is often impractical for field scale tracer studies where transport is controlled by weather conditions rather than by regional groundwater flow rates. And even when the tail is known, severe correlations are usually observed between the many parameters needed in this type of modeling. Assuming an effective porosity allowed us to characterize the subsurface so as to obtain the correct arrival times, and to obtain a reasonable approximation of the concentration maximum and the center of the mass position.

Fourth, the available software was generally adequate for simulations. However, both HYDRUS3D and MODFLOW packages encountered difficulties when soil became fully saturated during the intensive rainfall.

Fifth, results of this study have implications for solute monitoring transport in heterogeneous formations. Well data generally represent a fairly small scale. In our experiments we encountered distinctly different breakthrough curves in wells that were approximately in similar positions relative to the source along the tracer plume propagation direction. A more general representation of solute transport in terms of integrated properties may be needed in order to provide a more reliable and accurate representation with models.

This work demonstrated the usefulness of model abstraction in simulations of flow and transport in variably-saturated subsurface. Whereas multidimensional and multi-process representations leaves room for several competing conceptual models for flow and transport, simpler models that retain the most essential features of those representations could provide meaningful alternatives.

6 REFERENCES

Abit, S.M., A. Amoozegar, M.J. Vepraskas and C.P. Niewoehner, "Solute Transport in the Capillary Fringe and Shallow Groundwater: Field Evaluation," *Vadose Zone Journal*, 7:890-898, 2008.

Allen, G., L.S. Pereira, D. Raes, and M Smith. 1998. "Crop Evapotranspiration - Guidelines for Computing Crop Water Requirements, FAO Irrigation and Drainage Paper 56, 1998. Available at http://www.fao.org/docrep/X0490E/x0490e00.htm (contents accessed on August 20, 2009).

Altman, S.J., B.W. Arnold, R.W. Barnard, G.E. Barr, C.K. Ho, S.A. McKenna, and R.R. Eaton, "Flow Calculation for Yucca Mountain Groundwater Travel Time,"(*GWTT-95*). *SAND96-0819*, Sandia National Laboratories, Albuquerque, NM, 212pp., 1996.

Anderson, M.P., "Using Models to Simulate the Movement of Contaminants through Groundwater Flow Systems," *Critical Reviews in Environmental Controls,* 9(2):97–156, 1979.

Angier, J.T., G.W. McCarty, and K.L. Prestegaard, "Hydrology of a First-Order Riparian Zone and Stream, Mid-Atlantic Coastal Plain, Maryland," *Journal of Hydrology*, 309(1-4): 149-166, 2005.

Baliga, B.R., and S.V. Patankar, "A Control Volume Finite-element Method for Two-dimensional Fluid Flow and Heat," *Numerical Heat Transfer*, 6:245-261, 1983.

Baliga, B.R., and S.V. Patankar, "A New Finite-Element Formulation for Convective-diffusion Problems," *Numerical Heat Transfer*, 3:393-409, 1980.

Bandurraga, T.M., and G.S. Bodvarsson, "Calibrating Hydrogeologic Parameters for the 3-D Site-scale Unsaturated Zone Model of Yucca Mountain, Nevada," *Journal of Contaminant Hydrology*, 38(1-3): 25-46, 1999.

Barnston, A.G., S. Mason, L. Goddard, D.G. Dewitt, and S.E. Zebiak, "Multimodel Ensembling in Seasonal Climate Forecasting at IRI," *Bulletin of the American Meteorological Society,* 84:1783–1796, 2003.

Baumhardt, R.L., R.J. Lascano, S.R. Evett, "Soil Material, Temperature, and Salinity Effects on Calibration of Multisensor Capacitance Probes," *Soil Science Society of America Journal,* 64:1940-1946, 2000.

Bidaux, P., and C-F. Tsang, "Fluid Flow Patterns Around a Well Bore or an Underground Drift With Complex Skin Effects," Water Resources Research, 27(11): 2993-3008, 1991.

Bigelow, J.H., and P.K. Davis, *Implications for Model Validation of Multiresolution, Multiperspective Modeling (MRMPM) and Exploratory Analysis*, MR-1750, RAND, 2138, Santa Monica, CA, 2003

Blöschl, G., and Sivapalan, M., "Scale Issues in Hydrological Modeling", *Hydrological Processes*, 9: 251-290, 1995.

Boyle, D.P., Gupta, H.V., Soroshian, J., Koren, V., Zhang, Z., M. Smith, "Toward Improved Streamflow Forecasts: Value of Semidistributed Modeling," *Water Resources Research*, 37: 2749-2759, 2001.

Buczko, U. and H.H. Gerke, "Modeling Two-Dimensional Water Flow and Bromide Transport in a Heterogeneous Lignitic Mine Soil," *Vadose Zone Journal*, 5:14–26, 2006.

Chen, J., S. Hubbard, and Y. Rubin, "Estimating The Hydraulic Conductivity at the South Oyster Site From Geophysical Tomographic Data Using Bayesian Techniques Based on the Normal Linear Regression Model," *Water Resources Research*, 37(6): 1603–1613, 2001.

Chen, J., S. Hubbard, Y. Rubin, C. Murray, E. Roden, and E. Majer, "Geochemical Characterization Using Geophysical Data and Markov Chain Monte Carlo Methods: a Case Study at the South Oyster Bacterial Transport Site in Virginia," *Water Resources Research*, 40(12), W12412, doi:10.1029/2003WR002883, 2004.

Dane, J.H. and J.W. Hopmans, "Pressure cell," *In* Dane, J.H., and G.C. Topp - ed., *Methods of Soil Analysis. Part 4. Physical Methods*, pp. 684-688, ASA and SSSA, Madison, WI, 2002.

Davis, J.A., S.B. Yabusaki, C.I. Steefel, J.M. Zachara, G.P. Curtis, G.D. Redden, L.J. Criscenti, B.D. Honeyman, "Assessing Conceptual models for Subsurface Reactive Transport of Inorganic Contaminants" *EOS*, 85(44): 449-455, 2004.

Davis, P.K., and Bigelow, J.H., "*Motivated Metamodels: Synthesis of Cause-effect Reasoning and Statistical Metamodeling*. MR-1570," RAND, 2138, Santa Monica, CA, 2003.

Deiana, R., G. Cassiani, A. Villa, A. Bagliani, and V. Bruno, "Calibration of a Vadose Zone Model Using Water Injection Monitored by GPR and Electrical Resistance Tomography," *Vadose Zone Journal*, 7(1): 215 – 226, 2008.

Domenico, P.A. and F.W. Schwartz, *Physical and Chemical Hydrogeology, second ed.* John Wiley and Sons, Inc., New York, p. 506, 1998.

Doolittle, J.A., K.A. Sudduth, N.R. Kitchen, and S.J. Indorante, "Estimating Depths to Claypans Using Electromagnetic Induction in a Sand Aquifer: Spatial Variability of Hydraulic Properties and its Methods," *Journal of Soil and Water Conservation*, 6:572–575, 1994.

Drost, W., D. Klotz, A. Koch, H. Moser, F. Neumaier, and W. Rauert, "Point Dilution Methods of Investigating Ground Water Flow by Means of Radioisotopes," Water Resources Research, 4(1): 125-146, 1968.

Evett, S.R., B.B. Ruthardt, S.T. Kottkamp, T.A. Howell, A.D. Schneider, and J.A. Tolk "Accuracy and Precision of Soil Water Measurements by Neutron, Capacitance, and TDR Methods" *17th World Congress of Soil Science, August 14-21, 2002, Bangkok, Thailand, Transactions,* pp. 318-1 - 318-8. (CD-ROM), 2002.

Fares, A., P. Buss, M. Dalton, A.I. El-Kadi, and Parson, L.R., "Dual Field Calibration of Capacitance and Neutron Soil Water Sensors in a Shrinking-swelling Clay Soil," *Vadose Zone Journal*, 3:1390-1399, 2004.

Freeze, R.A. and J.A, Cherry. Groundwater. Prentice-Hall, Engelwood Cliffs, N.J. USA. 604pp., 1979

Gardner, C.M.K., T.J. Dean, and J.D. Cooper, "Soil Water Content measurement with a High-frequency Capacitance Sensor," *Journal of Agricultural Engineering Research*, 71: 395–403, 1998.

Gee, G.W. and Or, D.,*Particle-Size Analysis. In* Dane, J.H. and G.C. Topp (ed.) Methods of soil analysis. Part 4. Physical Methods. ASA and SSSA, Madison WI:278-282, 2002.

Gerke, H.H., and M.Th. van Genuchten, "A Dual-Porosity Model for Simulating the Preferential Movement of Water and Solutes in Structured Porous Media," *Water Resources Research*, 29: 305-319, 1993.

Gish, T.J. and K.-J.S. Kung, "Procedure for Quantifying a Solute Flux to a Shallow Perched Water Table," *Geoderma*, 138:57–64, 2007.

Gish, T.J., C.L. Walthall, C.S.T. Daughtry, and K.-J.S. Kung. "Using Soil Moisture and Spatial Yield Patterns to Identify Subsurface Flow Pathways," *Journal of Environmental Quality*, 34:274-286, 2005.

Gish, T.J., W.P. Dulaney, C.S.T. Daughtry, and K-J.S. Kung, "Use of Ground-penetrating Radar to Identify Ground Water Pathways at the Watershed Scale," *Soil Science Society of America Journal*, 66: 1620-1629, 2002.

Gish, T.J., Walthall, C.L., Daughtry, C.S.T., Dulaney, W.P., McCarty, G.W., "Watershed-scale sensing of subsurface flow pathways at OPE3 site", In: *Proceedings of the First Interagency Conference on Research in the Watersheds, October 27-30, 2003, Benson, Arizona.* p. 192-197, 2003.

Guber, A.K., Ya.A. Pachepsky, M.Th. van Genuchten, J. Simunek, D. Jacques, A. Nemes, T.J. Nicholson, R.E. Cady, "Multimodel Simulation of Water Flow in a Field Soil Using Pedotransfer Functions," *Vadose Zone Journal*, 8:1–10, 2008.

Guber, A.K., Gish, T.J., Pachepsky, Y.A., van Genuchten, M.T., Daughtry, C.S.T., Nicholson, T.J., Cady, R.E., Temporal Stability of Soil Water Content Patterns Across Agricultural Fields. *Catena,* 73: 125-133, 2007.

Guber, A.K., Ya.A. Pachepsky, M.Th. van Genuchten, W.J. Rawls, D. Jacques, J. Simunek, R.E. Cady, and T.J. Nicholson, "Field-Scale Water Flow Simulations Using Ensembles of Pedotransfer Functions for Soil Water Retention," *Vadose Zone Journal*, 5:234–247, 2006.

Guswa, A.J. and D.L. Freuberg, "On Using the Equivalent Conductivity to Characterize Solute Spreading in Environments with Low-Permeability Lenses," W*ater Resources Research*, 38(8): 1132 (DOI 10.1029/2001WR000528), 2002.

Halevy, E., H. Moser, O. Zellhofer, and A. Zuber,"Borehole Dilution Techniques: A Critical Review," In: Isotopes in Hydrology, Proceeding of a symposium, Vienna, 1967

Hassan, A. and K. Hamed, "Prediction of Plume Migration in Heterogeneous Media Using Artificial Neural Networks," *Water Resources Research*, 37(3): 605-624, 2001.

Hecht-Nielsen, R. "Neurocomputing," Addison-Wesley Publishing Company, Reading, MA, pp. 433 pp., 1990.

Hill, M.C., "The Practical Use of Simplicity in Developing Ground Water Models," *Ground Water*, 44(6): 775-781, 2006.

Hill, M.C., and C.R. Tiedeman, *Effective Groundwater Model Calibration: With Analysis of Data, Sensitivities, Predictions, and Uncertainty*, Wiley and Sons, 464 p. 2007

Hubbard, S., J. Chen, J. Peterson, K. Williams, D. Watson, P. Jardine, and M. Fienen. "Characterization & Monitoring at FRC Area 3 using Geophysical Data Conditioned to Hydrogeological Data", 2003. Available at http://public.ornl.gov/orifc/update_aug03.pdf (contents accessed on August 20, 2009).

Jacques, D., Simunek, J., Timmerman, A., and J. Feyen, "Calibration of Richards and Convection–Dispersion Equations To Field-Scale Water Flow And Solute Transport Under Rainfall Conditions," *Journal of Hydrology*, 259: 15-31, 2002.

Jarvis, N.J. "Modeling the Impact of Preferential Flow on Nonpoint Source Pollution," pp. 195-221 in: H.M. Selim and L. Ma (eds.*), Physical Nonequilibrium in Soils: Modeling and Applications*, Ann Arbor Press, Chelsea, MI. 1999.

Kelleners, T.J., R.W.O. Soppe, J.E. Ayars, J. Simunek, and T.H. Skaggs, "Inverse Analysis of Upward Water Flow in a Groundwater Table Lysimeter," *Vadose Zone Journal*, 4:558-572, 2005.

Köhne, S., B. Lennartz, J.M. Köhne, and J. Šimůnek, "Bromide Transport at a Tile-Drained Field Site: Experiment and One- and Two-Dimensional Equilibrium and Non-Equilibrium Numerical Modeling," *Journal of Hydrology*, 321:390–408, 2006.

Kron T.D. and D. Rosberg. "An Artificial Neural Network Based Groundwater Flow and Transport Simulator," http://www.isva.dtu.dk/staff/tdk/nn.2.pdf ,1998.

Kung, K. -J.S., E.J. Kladivko, T.J. Gish, T.S. Steenhuis, G. Bubenzer, and C.S. Helling, "Quantifying Preferential Flow by Breakthrough of Sequentially Applied Tracers: Silt Loam Soil," *Soil Science Society of America Journal,* 64:1296–1304, 2000.

Legates, D.R., and G.J. McCabe, Jr. "Evaluating the Use of "Goodness-Of-Fit" Measures in Hydrologic and Hydroclimatic Model Validation," *Water Resources Research*, 35:233–241, 1999.

Li, Y, W. Chao, L.-Z. Yang and Y.P. Li, " Influence of Seepage Face Obliquity on Discharge of Groundwater and its Pollutant into Lake from A Typical Unconfined Aquifer," *Journal of Hydrodynamics, Ser. B*, 19:756-761, 2007.

Looms, M.C., K.H. Jensen, A. Binley, and L. Nielsen, "Monitoring Unsaturated Flow and Transport Using Cross-Borehole Geophysical Methods," *Vadose Zone Journal*, 7(1): 227 – 237, 2008.

Masket, S, Dibike, Y.B, Jonoski, A and D.P. Solomatine, "Groundwater Model Approximation With ANN for Selecting Optimum Pumping Strategy for Plume Removal," pp. 67-80 in O. Schleider and A. Zijderveld, (eds.), *AI Methods in Civil Engineering Applications, 2nd Joint Workshop on AI Methods in Civil Engineering Applications*, Cottbus, 2000.

McLaren, R.G., Forsyth, P.A., Sudicky, E.A., Vanderkwaak, J.E., Schwartz, F.W., Kessler, J.H., "Flow and Transport in Fractured Tuff at Yucca Mountain : Numerical Experiments on Fast Preferential Flow Mechanisms," *Journal of Contaminant Hydrology,* 43(3-4): 211-238, 2000.

McLaughlin D. "Recent Developments in Hydrologic Data Assimilation" *Reviews of Geophysics. Supplement*: 977-984, US National report to International Union of Geodesy and Geophysics, Paper 95RG00740, American Geophysical Union. Washington, D.C., 1995.

Meisel, W.S. and D.C. Collins, " Repromodeling: An Approach to Efficient Model Utilization and Interpretation'" *IEEE Transactions on Systems, Man, and Cybernetics SMC-3*: 349-358, 1973.

Meyer, P.D., M.L. Rockhold, G.W. Gee, and T.J. Nicholson, *Uncertainty Analyses of Infiltration and Subsurface Flow and Transport for SDMP Sites*, NUREG/CR-6565, PNNL-11705. U.S. Nuclear Regulatory Commission. Washington, DC 20555-0001, 1997.

Mohanty, B.P., Bowman R.S., Hendrickx J.M.H., and M.Th. van Genuchten, "New Piecewise-Continuous Hydraulic Functions for Modeling Preferential Flow in an Intermittent Flood-Irrigated Field," *Water Resources Research*, 33: 2049-2063, 1997.

Morgan, K.T., L.R. Parsons, T.A. Wheaton, D.J. Pitts, and T.A. Obreza, "Field Calibration of a-Capacitance Water Content Probe in Fine Sand Soils," *Soil Science Society of America Journal,* 63:987-989, 1999.

Nelson, D.W., and L.E. Sommers, "Total Carbon, Organic Carbon, and Organic Matter". *In* Sparks, D.L. - ed., *Methods of Soil Analysis. Part 3. Chemical Methods*, pp. 961-1011, ASA and SSSA, Madison, WI, 1996.

Neuman, S.P., P.J. Wierenga, and T.J. Nicholson. *A Comprehensive Strategy of Hydrogeologic Modeling and Uncertainty Analysis for Nuclear Facilities and Sites*, NUREG/CR 6805. U.S. Nuclear Regulatory Commission. Washington, D.C. 20555-0001, 2003.

Pachepsky, Y.A., A.K. Guber, M.T. Van Genuchten, T.J. Nicholson , R.E. Cady, J. Simunek, M.G. Schaap, "Model Abstraction Techniques for Soil-Water Flow and Transport",

NUREG/CR-6884, U.S. Nuclear Regulatory Commission, Washington, DC 20555-0001, 2006.

Pachepsky, Y.A., and Rawls, W.J. (eds.), "Development of Pedotransfer Functions in Soil Hydrology," *Developments in Soil Science*, 30, Amsterdam, Elsevier, 2004.

Pachepsky, Y.A., Timlin, D.J., and W.J. Rawls, "Soil Water Retention as Related to Topographic Variables," *Soil Science Society of America Journal*, 65: 1787-1795, 2001.

Pachepsky, Ya.A., Timlin, D.J., Acock, B., Lemmon, H., and Trent, A. *2DSOIL - A New Simulator of Soil and Root Processes. Release 02.* USDA-ARS Systems Research Laboratory Beltsville, MD. 142 pp. 1993.

Page, A.L., R.H. Miller, and D.R. Keeney (Eds.), *Methods of soil analysis. Part 2. Chemical and microbiological properties.* American Society of Agronomy, Inc. and Soil Science Society of America, Inc., Madison, Wis., 1982.

Palmer, C.D., " Borehole Dilution Tests in the Vicinity of an Extraction Well," *Journal of Hydrology*, 146: 245-266. 1993.

Palmer, T.N., A. Alessandri, U. Andersen, P. Cantelaube, M. Davey, P. Délécluse, et al., "Development of a European Multimodel Ensemble System for Seasonal-to-interannual Prediction (DEMETER)," *Bulletin of the American Meteorological Society,* 85:853–872, 2004.

Palmer, T.N., C. Brankovic, and D.S. Richardson, "A Probability and Decision-model Analysis of PROVOST Seasonal Multi-model Ensemble Integrations," *Quarterly Journal of the Royal Meteorological Society*, 126:2013–2035, 2000.

Paltineanu, I.C., and J.L. Starr, "Real-Time Soil Water Dynamics Using Multisensor Capacitance Probes: Laboratory Calibration," *Soil Science Society of America Journal,* 61:1576-1585, 1997.

Poeter, E., and D. Anderson, "Multimodel Ranking and Inference in Ground Water Modeling," *Ground Water*, 43:597–605, 2005.

Polyakov V., A. Fares, and M.H. Ryder, "Calibration of a Capacitance System for Measuring Water Content of Tropical Soil," *Vadose Zone Journal*, 4:1004-1010, 2005.

Pruess, K. "A General-Purpose Numerical Simulator for Multiphase Fluid and Heat Flow," *Report LBL-29400*, Lawrence Berkeley Laboratory, Berkeley, CA, 103 p., 1991.

Rawls, W.J., and Y.A. Pachepsky, "Soil Consistence and Structure as Predictors of Water Retention," *Soil Science Society of America Journal,* 66:1115-1126, 2002.

Rawls, W.J., and Ya.A. Pachepsky, "Using Field Topographic Descriptors to Estimate Soil Water Retention," *Soil Science*, 167: 423-235, 2002.

Rawls, W.J., Brakensiek, D.L., and K.E. Saxton, "Estimation of Soil Water Properties," *Trans. ASAE* 25: 1316-1320, 1982.

Reilly, T.E, and A.W. Harbaugh, A.W., *Guidelines for Evaluating Ground-Water Flow Models.* Scientific Investigation Report. 2004-5038, 30 pp., US Geological Survey, 2004

Reynolds, W.D. and D.E. Elrick, "Constant Head Soil Core Method", *In*: Dane, J.H. and G.C. Topp - ed.), *Methods of Soil Analysis. Part 4. Physical Methods*, pp. 802-808, ASA and SSSA, Madison, WI, 2002.

Richards, D.R., H.J. Lin, G. Yeh, H. Cheng, J. Cheng, "*FEMWATER: a Three-Dimensional Finite Element Computer Model for Simulating Density-Dependent Flow and Transport in Variably Saturated Media,*" Report A769723. Army Engineer Waterways Experiment Station, Vicksburg MS, 1997.

Romano, N., and M. Palladino, "Prediction of Soil Water Retention Using Soil Physical Data and Terrain Attributes," *Journal of Hydrology.*, 265: 56-75, 2002.

Rubin, Y., and S.S. Hubbard (eds.), *"Hydrogeophysics,"* Springer, 2005.

Samoue¨lian, A., I. Cousin, A. Tabbagh, A. Bruand, and G. Richard. 2005. Electrical Resistivity Survey in Soil Science: A Review. *Soil and Tillage Research* 83:173–193.

SENTEK. 1995. *Factory Literature for the EnviroSCAN.* Sentek Pty. Ltd., Kent Town, South Australia.

Shukla, S., and F. Jaber, "Estimation of Groundwater Recharge in South Florida Using Drainage Lysimeters," *ASAE Paper* 072036, 2007.

Silliman, S.E., B. Berkowitz, J. Šimůnek, and M.Th. van Genuchten, "Fluid Flow and Solute Migration Within the Capillary Fringe," *Ground Water* 40(1):76-84, 2002.

Šimůnek, J., M. Sejna, and M.Th. van Genuchten, *"The HYDRUS-2D Software Package for Simulating the Two-Dimensional Movement of Water, Heat, and Multiple Solutes in Variably-Saturated Media. Version 2.0,"* IGWMC-TPS-53. Int. Ground Water Modeling Center, Colorado School of Mines, Golden, CO, 1999.

Šimůnek, J., M.Th. van Genuchten, M. Šejna, N. Toride, and F.J. Leij, *"The STANMOD Computer Software for Evaluating Solute Transport in Porous Media Using Analytical Solutions of Convection-Dispersion Equation"*, Version 1.0. *IGWMC-TPS-71*, Int. Ground Water Modeling Center, Colorado School of Mines, Golden, CO, 32 p.

Šimůnek, J., M.Th. van Genuchten and M. Sejna, *"The HYDRUS-1D Software Package for Simulating the One-Dimensional Movement of Water, Heat, and Multiple Solutes in Variably-Saturated Media,"* Version 3.0., Department of Environmental Science, University of California, Riverside, CA, 2005.

Šimůnek, J., Šejna, M., and M.Th. van Genuchten. 2007. "The HYDRUS Software Package for Simulating the Two- and Three-Dimensional Movement of Water, Heat and Multiple Solutes in Variably-Saturated Media," User Manual, Version 1.02, PC-Progress, Prague, Czech Republic. 203 p.

Šimůnek, J., Vogel, T., and van Genuchten, M.Th., *The SWMS2D Code for Simulating Water Flow and Solute Transport in Two-dimensional Variably Saturated Media, Version 1.21.* Research Report No. 132, 197 p., U.S. Salinity Laboratory, USDA, ARS, Riverside, California. 1994.

Smettem, K.R.J., Oliver, Y.M., Pracilio, G., and R.J. Harper, "Data Availability and Scale in Hydrologic Applications," pp. 253-272, in: Pachepsky, Y. and Rawls, W.J. (eds.), *Development of Pedotransfer Functions in Soil Hydrology.* Amsterdam, Elsevier, 2004.

Therrien, R., and E.A. Sudicky, "Three-Dimensional Analysis of Variably-Saturated Flow and Solute Transport in Discretely-Fractured Porous Media," *Journal of Contaminant Hydrology*, 23: 1-44, 1996.

Thomas, G.W., "Soil pH and Soil Acidity," *In* Sparks, D.L. - ed., *Methods of soil analysis. Part 3. Chemical methods,* pp. 475-490, ASA and SSSA, Madison, WI, 1996.

Timlin, D.J., Y.A. Pachepsky, and C.L. Walthall. "A Mix of Scales: Topography, Point scales, and Yield Maps," pp. 227-242, in Y.A. Pachepsky, D.E. Radcliffe, and H.M. Selim (eds.), *Scaling Methods in Soil Physics,* CRC Press, Boca Raton, FL, 2003.

Tsai, F.T-C., N-Z. Sun, and W.W-G. Yeh, "Global-Local Optimization Methods for the Identification of Three-Dimensional Parameter Structure in Groundwater Modeling," *Water Resources Research*, 39, 1043, doi:10.1029/2001WR001135, 2003.

Tseng, M.H., "Explicit Finite Volume Non-oscillatory Schemes for 2D Free-surface Flows," *International Journal for Numerical Methods in Fluids*, 30:831-843, 1999.

U.S.NRC, "Branch Technical Position on Site Characterization for Decommissioning," U.S.Nuclear Regulatory Commission, Washington, DC, 1994.

U.S.NRC, "Site Decommissioning Management Plan," *NUREG-1444,* U.S. Nuclear Regulatory Commission, Washington, DC, 1993.

Van Genuchten, M.T., Leij, F.J., and Lund, L.J. (eds.), "Proceedings of the International Workshop on Indirect methods for Estimating the Hydraulic Properties of Unsaturated Soils", University of California, Riverside, CA, 1992.

Van Genuchten, M.Th., F.J. Leij, and L.Wu (Eds.). "Characterization and Measurement of the Hydraulic Properties of Unsaturated Porous Media," *Proceedings of the International Workshop*, Riverside, California, October, 22-24, 1997, University of California, Riverside, 1997.

Van Genuchten, M.Th., "A Closed-form Equation for Predicting the Hydraulic Conductivity of Unsaturated Soils," *Soil Science Society of America Journal,* 44:892–898, 1980.

Van Ness, E.H., and M. Scheffer, "A Strategy to Improve the Contribution of Complex Simulation Models to Ecological Theory", *Ecological Modelling*, 185: 153-164, 2005.

Ventrella, D., Mohanty, B.P., Simunek, J. Losavio, N., and M.Th. van Genuchten, "Water and Chloride Transport in a Fine-Textured Soil: Field Experiments and Modeling," *Soil Science*, 165(8): 624-631, 2000.

Wang, C.G., and D.G. Jamieson, "An Objective Approach to Regional Wastewater Treatment Planning," *Water Resource Research*, 38(3): 1022, (DOI 10.1029/2000WR000062), 2002.

Weill, S., E. Mouche, and J. Patin, "A generalized Richards equation for surface/subsurface flow modeling," *Journal of Hydrology*, 366:9-20, 2009.

Wilson, G.V., Gwo, J.P., Jardine, P.M., and R.J. Luxmoore, "Hydraulic and Nonequilibrium Effects on Multiregion Flow," pp. 37-61 in: H.M. Selim and L.Ma (eds.), *Physical Nonequilibrium in Soils; Modeling and Application*, Ann Arbor Press, Chelsea, MI, 1998.

Ye, M., S.P. Neuman, and P.D. Meyer, "Maximum Likelihood Bayesian Averaging of Spatial Variability Models in Unsaturated Fractured Tuff", *Water Resources Research*, VOL. 40, W05113, doi:10.1029/2003WR002557, 2004.

Zhu, J. and B.P. Mohanty, "Spatial Averaging of Van Genuchten Hydraulic Parameters for Steady State Flow in Heterogeneous Soils: A Numerical Study," *Vadose Zone Journal*, 1: 261-272, 2002.

Zurmühl, T. "Capability Of Convection-Dispersion Transport Models To Predict Transient Water and Solute Movement in Undisturbed Soil Columns," *Journal of Contaminant Hydrology*, 30: 101-110, 1998.

Zurmühl, T., and W. Durner, "Modeling Transient Water and Solute Transport in a Biporous Soil," *Water Resources Research*, 32: 819-829, 1996.

APPENDIX A. REVIEWING THE MODELING PROBLEM CONTEXT

The decision to perform model abstraction is made from considerations of the base model and the key output (see section 2.2). Therefore, reviewing the base model and the key output is the first step of any model abstraction.

A1.1 REVIEWING KEY OUTPUT

Subsurface hydrologic models simulate complex systems and as such may generate a large number of output variables describing such systems. Which part of the model-generated information presents key output depends upon the purposes of the modeling project.

A1.1.1 Key output use

The purpose of subsurface flow and transport modeling may include:

- Improve the understanding of the vadose zone to optimize future monitoring or for planning a specific experiment
- Evaluating the effects of past management practices or previous events on vadose zone chemistry and hydrology
- Understanding the current state of the vadose zone to define possible sources of contamination and their interaction with groundwater systems
- Predicting changes in the vadose zone resulting from existing or alternative management scenarios, and quantifying the role of the vadose zone in determining groundwater recharge rates and contaminating groundwater.

Each of these purposes involves different key output that could be used to resolve specific regulatory, budgetary, societal or other issues. A single model could be used for several purposes, but the key output and boundary and initial conditions appear to be specific for a particular modeling project.

A1.1.2 Key output type and scale

Various types of transformation or parts of the modeling results may be used to derive the key output. Specifically,

- data filtering, e.g. concentrations and fluxes at specific times and/or locations
- boundary water fluxes such as
  - ground water recharge rates
  - runoff losses
  - losses to the lateral through boundaries
- boundary contaminant fluxes such as
  - fluxes to the water table
  - projection of the known source area to the water table
  - lateral fluxes in the capillary fringe to susceptible water sources and wetlands
- maximum contaminant concentrations across various boundaries of the simulation domain

- average concentrations of solute fluxes across various boundaries
- contaminant arrival times to various boundaries
- cumulative masses of contaminant transported through or stored in the vadose zone

The key output scale defines the temporal and spatial intervals over which the model output can be averaged to address the questions being asked. Daily, monthly, seasonal and yearly averages may be of interest depending upon the regulatory practices regarding the specific contaminant. Both a single maximum or total cumulative amounts may be used depending upon the contaminant involved and the accepted dose model. Similarly, spatial averaging of the pollution footprint in the vadose zone may yield sources as small as a borehole sample or as large as an agricultural field or an entire hydrologic response unit. Whatever the adopted scales, a review of output type and scale has to articulate and document the procedures used to derive the key output from the modeling results.

A1.1.3 Accuracy of the key output

The acceptable accuracy and uncertainty of the key output has to be requested from the end users. The acceptable accuracy relates to the performance of the model with respect to existing observations. The uncertainty relates to variations in the key output due to quantifiable variations in model parameters, external forcing, and scenarios.

In some cases, mandatory regulations are in place that articulate the statistics to be used for evaluating model performance. Sometimes the regulatory criteria list threshold values that are established in certain risk assessment guidelines. It is necessary to verify whether these threshold values appear within or outside realistic ranges of the predicted key output variables, given their uncertainty.

If the requirements for model accuracy are not established, characterizing the uncertainty in the key output becomes a part of the revew of the base model. As the model abstraction is applied, changes in the accuracy and uncertainty of the key output may be used to decide upon the applicability of a particular model abstraction technique.

A1.1.4 Evaluating model performance

One is generally not able to directly estimate the accuracy of the key output since output is a derived value and simply cannot be measured. The performance of the model per se must then be evaluated. A large number of statistical tests has been proposed and may be used for this purpose (e.g. Belocchi et al., 2004; Hill and Tiedeman, 2007). It is preferable to use statistical tools that evaluate simple and clear ideas about the correspondence between data and the simulations, e.g.,

- how variability in model errors compares with variability in the data?
- do model residuals have spatial or temporal trends?
- is there a systematic relative or absolute error in the predictions?
- how reliable are parameters derived from calibrations?
- how realistic are parameter derived values from calibrations?
- does the model tend to magnify errors in the inputs?

The performance of a model in terms of the adopted statistics must be compared with the performance of other models developed for similar purposes and having a similar complexity. Also, small model error measures usually do not guarantee that the model will perform well also when used for predictions. Simpler models with larger errors against observations can be more robust and perform better for some forecasts. Therefore, correct assumptions about the vadose zone, the boundaries of the simulation domain, and possible sources, sinks, and chemical and biological transformations within the simulation domain are often more important than the model error.

A1.2 REVIEWING ASSUMPTIONS MADE DURING DEVELOPMENT OF THE BASE MODEL AND JUSTIFICATIONS FOR THOSE ASSUMPTIONS

A1.2.1 Subsurface structural units

The vadose zone typically consist of various horizons and connected or disconnected lenses. The profile may contain massive, cross-bedded, and horizontally-bedded units, both poorly and well sorted. All of these structural units may conduct water differently, with chemical transport and transformation similarly varying among the different units. Even with significant advances recently in hydrogeophysical techniques, precise delineation of the various units remains a challenge in many practical situations. Borehole-based stratification often cannot provide the type of exhaustive coverage generally needed for the simulation domain. Measurements of pollutant concentrations are point based and depend upon the interaction of the measurement device (e.g. suction lysimeters) with the soil at different levels of water contents.

Because of the great uncertainty in characterization, many often question the feasibility of performing vadose zone flow and transport simulations. While uncertainty definitely is an issue, such simulations are likely to become increasingly more popular, and essential, because of the importance of the vadose zone in terms of storing, transforming and redirecting pollutants entering this zone from the soil surface. In such simulations, the pertinent challenge is not to obtain a full-fledged three-dimensional description of the locations and properties of structural units. The relevant challenges are answers to such questions as

- Does a specific site have subsurface structural units and features that may drastically change the fate and transport of pollutants in the vadose zone along the projected trajectory of a contaminant plume?
- If a restrictive fine-material layer is expected, does it have dikes or faults; can the layer have gaps?
- If a restrictive layer is expected, can it have a topography causing flow and transport via preferential pathways along it upper surface?
- Are there natural capillary barriers (i.e., boundaries between finer material overlaying the coarse sediments)? If yes, are gaps in these barriers expected?
- Can funnel flow in coarse-textural soils develop due to presence of a layer of coarse materials between two fine-textured layers?
- Can geochemical conditions of saturated or perched zones in the vadose zone cause changes in pollutant transformations or retention?
- Can well-conducting layers contain fine-scale high-conductivity parts of the pore space that will facilitate transport through large pores during episodic infiltration events?
- Is the lateral conductivity of the capillary fringe large enough to allow substantial contribution of the capillary fringe to lateral transport above the water table?

An essential condition here is to obtain answers to these questions from an available database that is as broad as possible. The database has to include information from public and private sources, cover both quantitative and qualitative (expert) information, and encompass both site-specific and generic information. The geological, hydrogeologic, and hydrogeophysical assessment can gain benefit greatly from complementary sources as types of stream hydrographs, the presence and hydrology of springs, the presence of paleosoils, documented fragipans, experience during well construction, occurrence and concentrations of agricultural chemicals in well water, and crop yield variability in dry years.

A1.2.2 Dimension of the problem

Most vadose zone flow and transport simulations are currently carried out in only one dimension (i.e., only vertical transport is considered). This is not sufficient for sites where unsaturated flow and transport pathways may be altered substantially due to presence of redirecting structural units mentioned in the previous section. A two dimensional representation is needed when

- lateral transport can be substantial,
- restrictive layers, if present, are well defined,
- flow in the vadose zone is controlled by infiltration.

A three-dimensional representation is needed when

- the contaminant release source is providing also a substantial amount of infiltration,
- substantial lateral transport in the vadose zone is expected, both along and across the main groundwater flow direction.

A1.2.3 Simulation domain, initial and boundary conditions

The simulation domain must be selected such that it reflects the dimension of the problem and allows one to set justifiable boundary conditions along all boundaries. One-dimensional (1D) problems require boundary conditions along the soil surface and the bottom of the vadose zone. Either a free drainage condition, or a zero pressure head condition at the ground water level (if the latter is monitored in time), is generally sufficient to simulate flow in this case.

1D simulations likely will not provide correct simulations if substantial transport in the capillary fringe is expected, or if a restrictive layer exist that not only can cause perched water to develop but also may contain gaps that allows rising groundwater to move upward through gaps in the restrictive layer. In such cases 2D or 3D simulations are necessary. Multi-dimensional vadose zone flow and transport simulations are best simulated when

- the simulation domain includes both a vadose zone and an aquifer, and
- flow and transport need to be considered jointly, without assuming some rule of fluid and mass exchange between the vadose zone and groundwater.

Boundary conditions in the groundwater subdomain have to be established according to existing guidelines for groundwater modeling. Boundary conditions for flow in the vadose zone must be established either from vadose zone monitoring data, or from preliminary 1D simulations of the vadose zone at the lateral boundaries of the flow domain. Alternatively, they can be defined in a more arbitrary fashion to provide continuity in the pressure head along a vertical direction from the water table to the soil surface. In the latter case, however, the boundaries should be placed far enough from the contaminant plume, so that the boundary conditions would not affect flow and transport within the domain of interest. This has to be verified by preliminary simulations using realistic values for the flow and transport parameters.

Daylight surface boundary conditions have to be

- harmonized with the time step accepted in the model.
- set with proper attention to runoff from and run-on to the soil surface simulation domain;
- reflect water and chemical uptake.

The representation of initial conditions depends on the purpose of the modeling. For exploratory and forecast purposes it is customary to run the model with realistic boundary conditions for relatively simulated periods (up to one year), and to use the results of this run as initial conditions for the flow model. For parameter estimation and understanding the current situation at the field site, measured initial values of the vadose zone state variables should be used.

A1.2.4 Estimated model parameters

The estimated parameter values must be obtained and reviewed irrespective if calibration applied or not. The estimated parameters for flow and transport either

- are used directly in the simulations;
- serve as initial estimates for model calibration;
- used in evaluations of the results of a calibration

A list of estimated flow and transport parameters for each subsurface structural unit typically includes

- soil water retention parameters
- uunsaturated soil hydraulic conductivity parameters
- molecular diffusion coefficient of the contaminant
- dispersivity
- dual-porosity parameters
- chemical transformation parameters
- biological transformation parameters

Additional parameters are used if the pollutant experiences colloid-facilitated transport, volatilization, or is represented by nanoparticles.

General requirements of the parameter estimation include

- using several sources,
- matching scales

- correcting for field conditions
- defining uncertainty

Using several sources is recommended since a similarity in soil type (e.g., soil texture) by no means guarantees a comparable similarity in the flow and transport parameters. For example, soils of similar texture may exhibit up to two orders of magnitude differences in hydraulic conductivity. A compendium of literature flow and transport parameters in soils is given by Pachepsky and Rawls (2004).

A match in the scale of an experimentI is important when selecting literature values of hydraulic conductivity and dispersivity parameters since they are known to depend on the support or extent of the experiment in which they have been measured. A rule of thumb recommendation is to use parameters from experiments in which the support or extent is close to the vertical size of the cell used in numerical simulations.

A correction is often needed when relying on laboratory-measurements of the hydraulic conductivity, the dispersivity, and dual-porosity parameters since they depend on the spatial scale of an experiment. Methods to account for this change in scale can be found in both the soils (Pachepsky et al., 2003) and groundwater (Neuman, 1990, 1995) literature. Corrections to field conditions are more difficult for chemical and biological transformation because they are specific to the type of pollutant. However, the anticipated differences in adsorption, dissolution, and transformation rates have to be articulated and taken into account in uncertainty-based modeling projects.

Defining uncertainty in the estimated parameters is necessary for

- performing multiple simulations to evaluate the prediction uncertainty if no calibration is envisaged;
- determining the prior distributions of parameters to determine the posterior distributions of calibrated parameters if Bayesian methods are used in the calibrations;
- evaluating the calibration results.

Obtaining parameter estimates from multiple sources provides the necessary information for uncertainty characterization. It is imperative to use estimates not only of average values found in the literature, but also of the uncertainty in the average values that are reported in many (but not all) literature sources. An alternative method is to use probability distributions developed for soils from a large international database (Meyer et al., 1997).

A1.2.5 Data available for calibration

Data needed for calibration of a vadose zone flow and transport model may include, in particular, monitoring data of

- the soil water content,
- the soil pressure head,
- soil water fluxes,
- concentrations of pollutants in soils,
- tracer concentrations if a tracer test has been run,
- hydrogeophysical data from cross-borehole monitoring of infiltration events, hydrogeophysical data from surface monitoring of soil water contents,
- groundwater levels,

- concentrations of pollutant or tracers in groundwater.

In spite of the fact that flow and transport processes in the vadose zone are slow, tracer tests are desirable for evaluating the possibility of rapid pollutant transport in dual-porosity soils. Calibration data must be available if the purpose of modeling is to analyze results of current or future management scenarios of contingencies. One may argue that running a model with all parameters within their variability ranges may provide an exhaustive characterization of the uncertainty in predictions. This is true provided the structural units are conceptualized in a correct way, but that cannot be guaranteed in absolute terms. The credibility of a model increases if the calibration returns physically meaningful parameter values.

All vadose zone measurements are to some extent indirect, and are affected by interactions between the measuring device and the medium being studied. Therefore, all data used for calibration have to be reported with expertly or directly estimated errors. This is needed to evaluate the calibration results in terms of their accuracy.

The type of data, number of data points, and the frequency of data collection for reliable calibration is site-specific and depends on the method of calibration (see below). An optimal methodology of defining the best monitoring strategy for calibrating a vadose zone model presents an avenue of future research.

A1.2.6 Calibration procedure and results

Two calibration methods are used most often in vadose zone flow and transport modeling: trial-and-error (manual) calibration and automated calibration. Automated calibration does not change locations and dimensions of structural units; it only varies material properties within these units to match simulated and measured values. Trial-and-error calibrations usually change both the locations and the dimensions of the structural units until a better fit is obtained.

An advantage of automated calibration is the objectivity in which the parameters are obtained. A disadvantage is that it may end up supporting an incorrect conceptualization of the flow and transport processes embedded in the model. Trial-and-error methods mirror automated calibration in terms of these advantages and disadvantages. If automated calibration is used, the statistics of parameters should be analyzed in the same way as recommended in groundwater modeling projects (Hill and Tiedeman, 2007).

Vadose zone simulations are notoriously slow because of the nonlinearity in the governing flow equations. Therefore, automated calibration is usually implemented only for one-dimensional simulations. Calibration in two- and three-dimensional simulations is usually achieved using trial-and-error process.

The calibration process should include

- normalization of measurements to exclude the effect of the measurement unit on the calibration results,
- justified removal of non-sensitive parameters from calibration,
- assignment of different and explicable weights to measurements of different types.

A1.2.7 Software properties

Because of the nonlinearities involved, numerical solutions of coupled vadose zone and groundwater problems often show unstable behavior, or produce unacceptable errors in the mass balances for water and solutes. This behavior, including the software used for the simulations, has to be documented and reported.

A1.2.8 Model documentation

Reviewing the documentation of a model is an essential component of the base model review. Reily and Harbaugh (2004) indicate in their guidelines for evaluation of groundwater models that "because models are embodiments of scientific hypotheses, a clear and complete documentation of the model development is required for individuals to understand the hypotheses, to understand the methods used to represent the actual system with a mathematical counterpart, and to determine if the model is sufficiently accurate for the objectives of the investigation". The same is true for vadose zone modeling. Clarifications on all of the topics addressed in appendices A1 and A1.2.1 through A1.2.7 have to be included in the documentation.

APPENDIX B. FIELD CALIBRATION OF MULTISENSOR CAPACITANCE PROBES

Multisensor capacitance probes (MCPs) are used in field soil water content monitoring for various applications, such as for irrigation scheduling, estimating soil hydraulic properties, and evaluating water uptake by plants. It is desirable to know how representative data are from multisensor capacitance probes for a small plot surrounding the sensor. For example, such information may be needed if a plot is used for an infiltration experiment and soil water is monitored with the sensor to characterize the infiltration rate (Shukla and Jaber, 2007). Such upscaling may result in both random and systematic errors. Random errors may arise from small-scale variations in soil water contents and from variability of soil properties since capacitance probes are sensitive to soil bulk electrical conductivity (Baumhardt et al., 2000; Evett et al., 2006; Kelleners et al., 2004) and soil mineralogy (Fares et al., 2004). Systematic upscaling errors may results from deficiencies in the calibration. In most cases, MCPs have been calibrated in the laboratory (Paltineanu and Starr, 1997; Baumhardt et al., 2000; Polyakov et al., 2005). Baumhardt et al. (2000) reported that the manufacturer-supplied MCP calibration equations were applicable to estimate soil water contents in Ap and calcic horizons of an Olton soil when the soil was air dried, but not when near saturation. They concluded that MCP calibration should be soil-specific. Morgan et al. (1999) came to the same conclusion when they tested manufacturer and laboratory (Paltineanu and Starr, 1997) calibrations on three fine sandy soils of Florida, while Evett et al. (2006) concluded the same for three other soils.

Since MCP sensors provided a very important stream of information for both site characterization and monitoring during the experiment, we assessed the magnitude and variations in the difference between MCP-measured and plot-averaged gravimetrically measured water contents across 1 m^2 plots at the site , and searched for ways to modify the MCP calibration to better represent plot-averaged water contents. Multisensor capacitance probes (EnviroSCAN, SENTEK Pty Ltd., South Australia) were installed for this purpose in the spring of 2006 to monitor the soil water content and provide data for validation of a water flow model. Four plots (each 1 m^2 and 10 m apart) were instrumented with MCPs located at 10 cm depth increments from 10 to 60 cm. Reference readings were taken for each sensor in air and water before installation. Undisturbed soil cores were taken with a 100 cm^3 soil auger at 50 cm distance from the MCPs at the vertices of an equilateral triangle in triplicate at three dates with distinctly different water contents at depths corresponding to the MCPs installation. The triangle was rotated by 40° before the second and third samplings. Soil water contents and soil bulk densities were measured gravimetrically. Soil texture was measured with the pipette method (Gee and Or, 2002) after dispersion with sodium pyrophosphate $Na_4P_2O_7$ of soil samples taken when the MCP access tubes were installed.

To compare the MCP measurements with observed water content, the sensor scaled frequency (SF) was converted to volumetric water content using the SENTEK (1995) factory calibration equation:

$$\theta = (0.792SF - 0.0226)^{2.4752} \qquad \text{(B-1)}$$

as well a laboratory calibration for a mesic Aquic Hapludult silt loam soil as obtained by Paltineanu and Starr (1997):

$$\theta = 0.490SF^{2.1674} \qquad \text{(B-2)}$$

The root-mean-square difference RMSD between plot-averaged $\theta_{a,i}$ and MCP-estimated water contents $\theta_{MCP,i}$

$$\mathrm{RMSD} = \sqrt{\sum_{i=1}^{n} (\theta_{a,i} - \theta_{MCP,i})/n} \qquad \text{(B-3)}$$

was used to characterize the MCP measurements. Here n is the total number of compared water contents.

Substantial variability in soil texture and soil bulk density with depth was observed at the four locations (Tables B-1 and B-2). Clay content was generally less in the topsoil (0-25 cm) than in the subsoil (25-65 cm) layer. Silt content was relatively constant (17-25%) at all depths, while sand content was less in the subsoil compared to the topsoil. Soil bulk density was less in the topsoil (1.34-1.69 g cm^{-3}) than in the subsoil (1.69-1.95 g cm^{-3}). The variation coefficient of soil bulk density ranged from 1 % to 14 %.

Soil samples were taken at three dates when the soil was not excessively hard or soft for sampling, resulting in different soil water content ranges at different soil depths. Generally the water content range was wider in the top layer compared to that in the subsurface layers. Soil water contents were in the range from 0.10 to 0.51 $m^3 m^{-3}$ in the topsoil, from 0.10 to 0.42 $m^3 m^{-3}$ at depths of 25-55 cm, and from 0.09 to 0.38 $m^3 m^{-3}$ in the 55-65 cm soil layer of four plots (Fig. B-1). Spatial variability in the soil water content measured at each of the four plots changed with soil depth. The standard deviations of the water content ranged from 0.02 to 0.12 $cm^3 cm^{-3}$, while the average water content ranged from 0.16 to 0.39 $cm^3 cm^{-3}$ in topsoil (data not provided here). The variability in soil water contents was in the range from 0.02 to 0.07 $cm^3 cm^{-3}$ and did not correlate with the soil water content in the subsoil. Deviations of MCP data from the measured water contents were observed at all depths in the four plots (Fig. B-1).

The MCP data obtained with the SENTEK factory and laboratory calibrations are compared with plot-averaged soil water content measurements in Fig. B-2. Both random and systematic errors can be observed, resulting in root-mean-squared differences (RSMDs) in the range from 0.037 to 0.058 $cm^3 cm^{-3}$ for the SENTEK factory, and from 0.036 to 0.063 $cm^3 cm^{-3}$ for the laboratory calibrations, respectively. Both MCP calibrations overestimated soil water contents at the low water contents and underestimate at the high water contents (Fig. B-2). We concluded that a calibration correction was needed to minimize the MCP errors of plot-averaged water content measurements.

To correct the MCP performance, the coefficients a and b of linear regression between MCP-measured and plot-averaged water contents:

$$\theta_{a,i} = a\theta_{MCP,i} + b \qquad \text{(B-4)}$$

were calculated for data from all depths pooled together, for the topsoil (0-25 cm) data, the subsoil (25-65 cm) data, and for each observation depth separately. The calibration equations were transformed by combining equations (B-1), (B-2) with equation (B-3). The corrected equations are shown in Table B-3. Differences in coefficients of the MCP calibration equations indicate that the correction is depth-specific for both the SENTEC factory and the laboratory calibrations.

Although the correction obtained with all pooled data reduced RMSD values for the entire depth range of 0-65 cm, smaller RMSDs were observed when corrections were applied to each depth or each soil horizon separately (Table B-4). This implies that depth or horizon specific corrections may be helpful to further reduce errors in the MCP measurements.

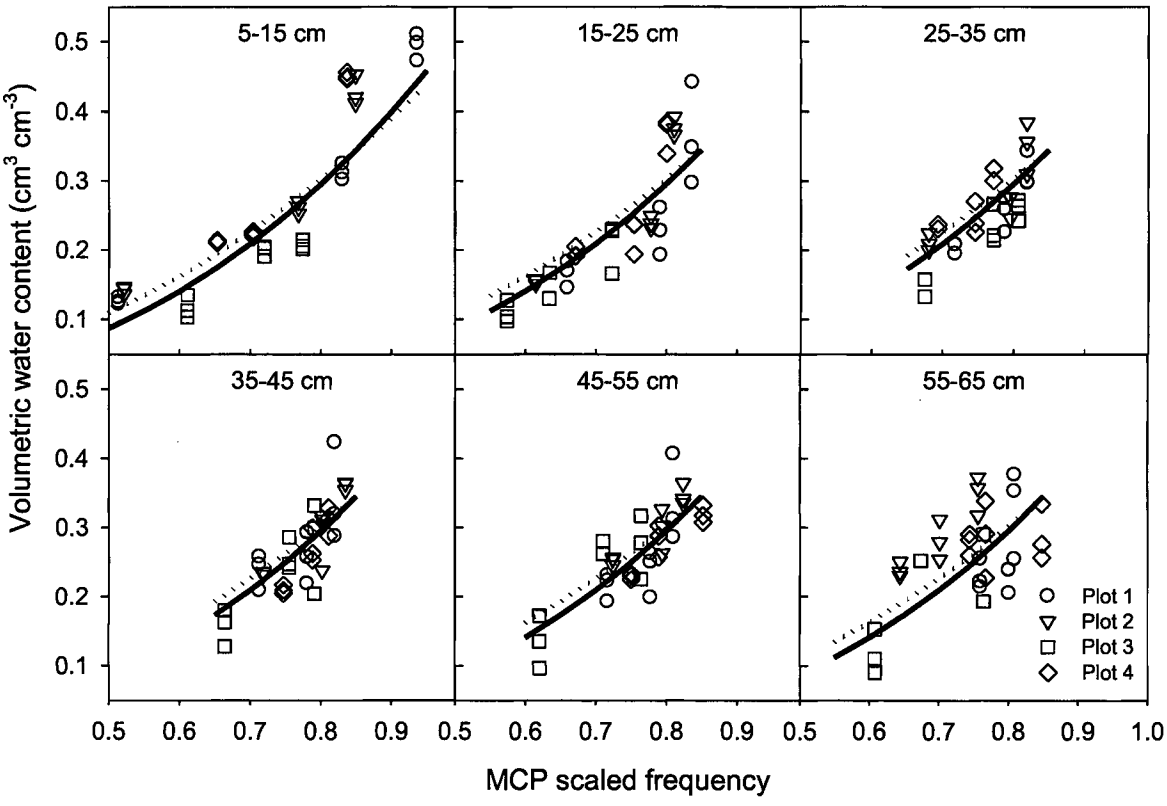

Figure B-1. Soil water contents measured in the plots (symbols) and calculated using the SENTEC (solid lines) and laboratory measured (dotted lines) MCP calibrations vs. MCP scaled frequency.

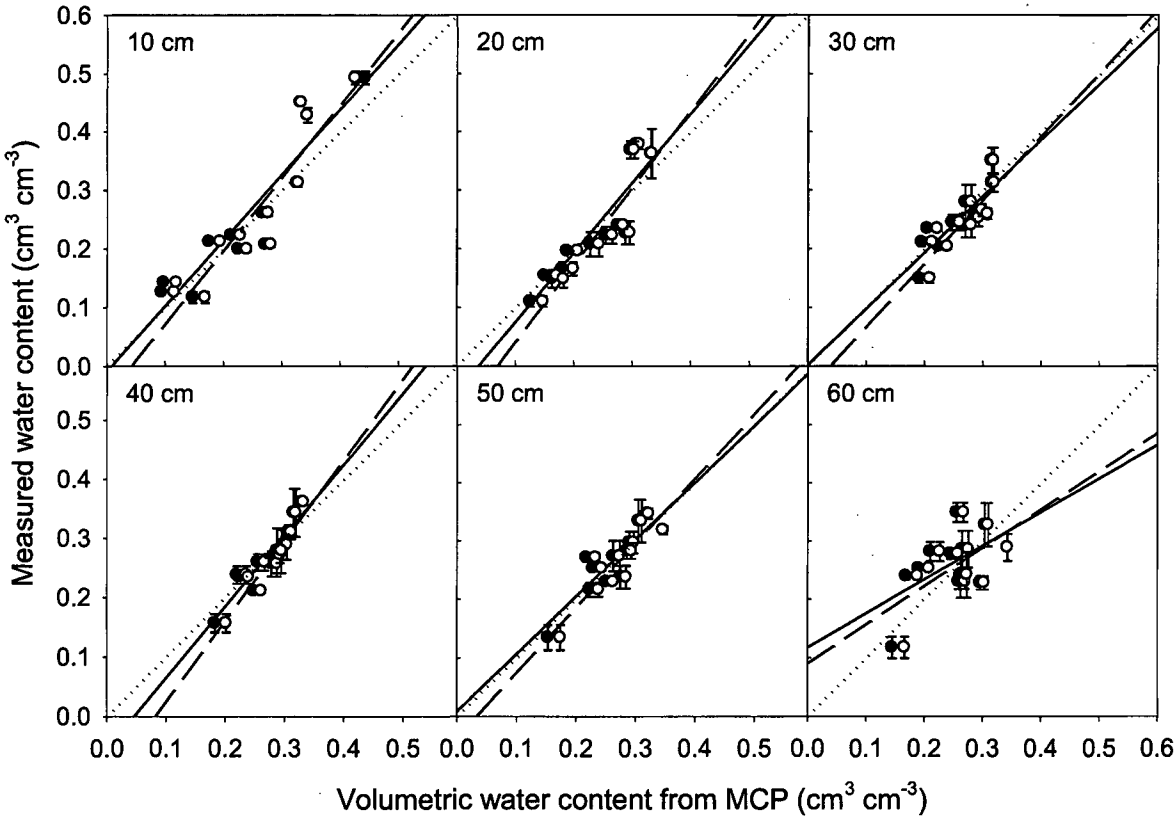

Figure B-2. Plot-averaged vs. MCP estimated soil water contents for the mesic Typic Hapludult soil. Solid and hollow symbols show estimates with the SENTEC calibration and laboratory calibrations developed by Starr and Paltineanu (1997), respectively. Solid and dash trend lines show the general relationship between plot average and MCP-estimated water contents for the SENTEC and laboratory calibrations, respectively. The dotted line shows the 1:1 line.

Table B-1. Soil texture at locations of the multisensor capacitance probes installation.

Depth cm	Clay %	Silt %	Sand %
0-15	15 ± 6[#]	24 ± 9	61 ± 4
15-25	17 ± 4	23 ± 7	60 ± 3
25-35	22 ± 3	22 ± 5	56 ± 7
35-45	23 ± 4	21 ± 4	56 ± 7
45-55	24 ± 4	22 ± 4	54 ± 6
55-65	21 ± 6	21 ± 3	58 ± 2

[#]The '±' separates the average from the standard deviation

Table B-2. Soil bulk density around the multisensor capacitance probes.

Depth cm	Location 1 g cm^{-3}	Location 2 g cm^{-3}	Location 3 g cm^{-3}	Location 4 g cm^{-3}
0-15	1.344±0.029[#]	1.516±0.033	1.557±0.031	1.455±0.007
15-25	1.691±0.112	1.649±0.020	1.689±0.130	1.674±0.038
25-35	1.822±0.040	1.722±0.058	1.843±0.046	1.831±0.019
35-45	1.741±0.109	1.694±0.009	1.787±0.079	1.828±0.031
45-55	1.764±0.097	1.731±0.023	1.828±0.038	1.805±0.019
55-65	1.782±0.099	1.726±0.044	1.952±0.062	1.885±0.062

[#]The '±' separates the average from the standard error.

Table B-3. The original SENTEC and laboratory MCP calibration equations.

Depth cm	SENTEC calibration	Beltsville laboratory calibration
	Original calibration equations	
All depths	$\theta = (0.7920SF - 0.0226)^{2.4752}$	$\theta = 0.490SF^{2.1674}$
	Corrected calibration equations	
0-65	$\theta = (0.8051SF - 0.0230)^{2.4752} + 0.0063$	$\theta = 0.6247SF^{2.1674} - 0.0704$
0-25	$\theta = (0.8373SF - 0.0239)^{2.4752} + 0.0219$	$\theta = 0.4996SF^{2.1674} - 0.0140$
25-65	$\theta = (0.7601SF - 0.0217)^{2.4752} - 0.0300$	$\theta = 0.5690SF^{2.1674} - 0.0495$
0-15	$\theta = (0.8292SF - 0.0237)^{2.4752} + 0.0084$	$\theta = 0.6109SF^{2.1674} - 0.0530$
15-25	$\theta = (0.8499SF - 0.0243)^{2.4752} + 0.0375$	$\theta = 0.6466SF^{2.1674} - 0.0919$
25-35	$\theta = (0.7906SF - 0.0226)^{2.4752} + 0.0078$	$\theta = 0.5512SF^{2.1674} - 0.0535$
35-45	$\theta = (0.8530SF - 0.0243)^{2.4752} + 0.0465$	$\theta = 0.6668SF^{2.1674} - 0.1120$
45-55	$\theta = (0.7942SF - 0.0227)^{2.4752} + 0.0002$	$\theta = 0.5579SF^{2.1674} - 0.0465$
55-65	$\theta = (0.6495SF - 0.0185)^{2.4752} - 0.1779$	$\theta = 0.3405SF^{2.1674} + 0.0801$

Table B-4. Root-mean-squared differences of plot-averaged water contents (cm^3 cm^{-3}) for the original and corrected MCP calibration equations.

Depth range cm	SENTEC calibration			Beltsville laboratory calibration	
	Original	Corrected for specific depth range	Corrected for soil texture	Original	Corrected for specific depth range
0-65	0.0458	0.0455	0.0446	0.0474	0.0459
0-25	0.0505	0.0478	0.0429	0.0535	0.0491
25-65	0.0431	0.0428	0.0454	0.0436	0.0427
5-15	0.0542	0.0488	0.0402	0.0561	0.0505
15-25	0.0464	0.0447	0.0456	0.0506	0.0451
25-35	0.0344	0.0332	0.0284	0.0390	0.0333
35-45	0.0360	0.0349	0.0354	0.0392	0.0350
45-55	0.0357	0.0356	0.0375	0.0370	0.0355
55-65	0.0616	0.0563	0.0702	0.0580	0.0560

An exploratory analysis with regression trees (Rawls and Pachepsky, 2002) was used to evaluate the possible effect of basic soil properties on apparently random deviations of plot-averaged from MCP-measured water contents at depths from 5 to 55 cm. Sand, silt, and clay contents along with bulk density and depth were introduced as potential input variables. The resulting regression tree is shown in Fig. B-3. The group of plots and depths with sand content greater than 62.2% showed on average the largest difference between the plot-averaged and MCP measured water contents (-0.030 cm^3 cm^{-3}). Where sand content was less than 62.2%, the silt content was the splitting variable. The average deviation was negligible at depths and locations where silt content was greater than 20.5%. An average difference of 0.021 cm^3 cm^{-3} was found for samples with sand content less than 62.2% and silt content less than 20.5%. Neither soil bulk density nor depth was included in the list of splitting variables of the regression tree. However, the effect of bulk density could be masked by its correlation with textural components along the soil profile (Table B-1). Using high frequency capacitance probes, Gardner et al. (1998) concluded that differences in dry bulk density were important, while clay and organic matter content were not.

We attempted to use the average deviations for the texture-based groups in Fig. B-3 to correct MCP measured water contents by subtracting group average deviations from the MCP measurement results. Improvements were observed in the RMSD values, which decreased from 0.0458 cm^3 cm^{-3} to 0.0446 cm^3 cm^{-3} for the whole soil profile, and from 0.0505 cm^3 cm^{-3} to 0.0429 cm^3 cm^{-3} for the topsoil (Table B-4). However, corrections for soil texture did not reduce the RMSD for the subsoil. Similar results were obtained for the laboratory calibration (data not shown). These results imply that correction for texture is possible and desirable if a site-specific MCP calibration is to be developed. Since texture was dependent upon depth in our case (Table B-1), it actually might have been feasible to develop depth-dependent calibration corrections.

Overall, both bias and random errors were observed when the differences between plot average and MCP-estimated soil water contents were analyzed for the top 65 cm of the coarse-loamy, siliceous, mesic Typic Hapludult. Developing a site specific calibration to remove the bias appeared to be important. However, random variations apparently dominated the differences between plot-averaged and MCP-measured water contents. A linear correction of the calibration equation improved the estimates of the plot average water contents from the MCP data, but only by 0.7 percent on average, while leaving the RMSD at 0.046 m^3 m^{-3} overall. Relationships between the water content differences and soil texture were observed. Using these relationships to correct the MCP measurements increased their similarity to plot-averaged water contents, and reducing the RMSD to 0.045 m^3 m^{-3} overall. A site-specific MCP calibration correction appears to be desirable before using a single MCP in soil water monitoring at the plot scale, but the methods used here were not adequate for such a calibration.

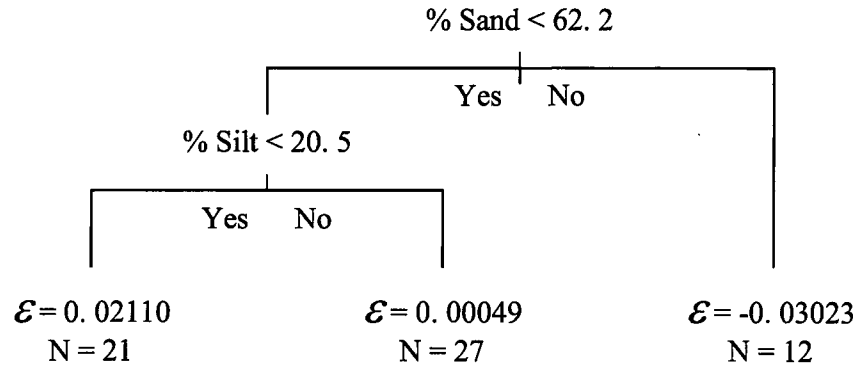

Figure B-3. Average differences between plot-averaged water contents and MCP-measured water contents as a function of texture in the upper 50-cm soil layer as expressed with a regression tree. ε is the average deviation for the group, and N is the total number of samples in the group.

APPENDIX C. FIELD-SCALE COUPLED SURFACE-SUBSURFACE FLOW AND TRANSPORT MODELING

C1.1 EQUATIONS OF THE MODEL

C1.1.1 Flow model

Overland flow may be simulated using the Saint-Venant conservation equations as (Tseng, 1999):

$$\frac{\partial Q}{\partial t}+\frac{\partial E}{\partial x}+\frac{\partial G}{\partial y}=F \qquad \text{(C-1)}$$

where $Q=(h,hu,hv)^T$,

$$E=\begin{pmatrix} hu \\ hu^2+\frac{1}{2}gh^2 \\ huv \end{pmatrix} \quad G=\begin{pmatrix} hv \\ huv \\ hv^2+\frac{1}{2}gh^2 \end{pmatrix} \quad F=\begin{pmatrix} R-I \\ gh(S_{0_x}-\frac{m^2u\sqrt{u^2+v^2}}{h^{4/3}}) \\ gh(S_{0_y}-\frac{m^2v\sqrt{u^2+v^2}}{h^{4/3}}) \end{pmatrix}$$

in which h is the flow depth on the soil surface [L]; u and v are the velocity components in the x and y directions, respectively [LT^{-1}], m/s; g is the acceleration due to gravity [L^2T^{-1}]; S_{0_x} and S_{0_y} are the surface slope in the x and y directions, respectively, t is time [T], m is Manning's roughness coefficient [$L^{-1/3}T$], R is the rainfall rate [LT^{-1}]; and I is the infiltration rate [LT^{-1}]. If the local and convective inertial terms and the momentum term owing to rainfall excess are neglected, equation (C-1) reduces to its diffusive-wave (DW) approximation (e.g.,Weill et al., 2009):

$$\frac{\partial h}{\partial t}=-\vec{\nabla}\cdot\vec{g}+R-I \qquad \text{(C-2)}$$

where $\vec{\nabla}=(\frac{\partial}{\partial x},\frac{\partial}{\partial y})$ is the gradient operator in x-y space. The surface flux $\vec{g}$ is calculated utilizing the two-dimensional form of the empirical Manning equation:

$$\vec{g}=-k_{surf}\vec{\nabla}(h+z) \qquad \text{(C-3)}$$

where $k_{surf}=\frac{h^{7/3}}{m^2\Phi}$ is the surface conductivity,

$$\Phi=\left[\left(\frac{\partial(h+z_s)}{\partial x}\right)^2+\left(\frac{\partial(h+z_s)}{\partial y}\right)^2\right]^{1/2}$$

and z_s is the land surface elevation [L].

The three-dimensional Richards equation as described and implemented in FEMWATER (Richards et al., 1997) was used to simulate water flow in variably-saturated soil. The water depth on the soil surface water depth was assumed to be equal to the pressure head p if $p>0$, otherwise $p\leq 0$. The flux boundary condition on the soil surface is

$$-K(p)\frac{\partial(p+z_s)}{\partial n}=\begin{cases}\dfrac{\partial h}{\partial t}-\dfrac{\partial}{\partial x}K_{surf}\dfrac{\partial(p+z)}{\partial x}-\dfrac{\partial}{\partial y}K_{surf}\dfrac{\partial(p+z)}{\partial y}+R_n & p>h_0\\ \dfrac{\partial h}{\partial t}+R_n & 0<p\leq h_0\\ R_n & h\leq 0\end{cases} \quad \text{(C-4)}$$

where **n** is the vector normal to the soil surface boundary, $R_n = R\cos(z,n)$ is the projection of rain on the normal **n**, and n_0 is a small parameter. Equations (C-4) can be condensed to the computationally more efficient form

$$-K(p)\frac{\partial(h+z_s)}{\partial n}=\frac{\partial\eta(h)h}{\partial t}-\frac{\partial}{\partial x}\eta(h-h_0)K_{surf}\frac{\partial(h+z)}{\partial x}-\frac{\partial}{\partial y}\eta(h-h_0)K_{surf}\frac{\partial(h+z)}{\partial y}+R_n \quad \text{(C-5)}$$

where $\eta(h)=\begin{cases}1, & h\geq 0\\ 0, & h<0\end{cases}$ is the Heaviside function.

C1.1.2 Transport model

Surface and subsurface solute transport is simulated with the three-dimensional advective-dispersive equation subject to decay, adsorption, and biodegradation in the liquid and solid phases (Richards et al., 1997). Overland transport of solutes can be described by the equation

$$\frac{\partial(ch)}{\partial t}+\frac{\partial c_{sorb}}{\partial t}+\vec{\nabla}\cdot(\vec{q}_s c-\overline{\overline{D}}_s\vec{\nabla}c)=\lambda hc+J-M \quad \text{(C-6)}$$

Here c is the solute concentration in the runoff [M L^{-3}], $c_{sorb}=K_F c^{n_F}$ is the surface density of the attached solute [M L^{-2}], K_F and n_F parameters of the Freundlich equation for the mass-exchange isotherm, $\overline{\overline{D}}=h\overline{\overline{d}}_m+\overline{\overline{\alpha}}q$ is the surface diffusion-dispersion tensor [L^3 T^{-1}], d_m is the molecular diffusive component [L^2T^{-1}], α is the dispersivity tensor [L], λ is the decay or biodegradation rate coefficient [T^{-1}], $J=cI-D_{soil}\dfrac{\partial c}{\partial n}$ is the rate of solute loss from runoff to soil with infiltration [L^{-2} T^{-1}], D_{soil} is the solute dispersion coefficient in soil [L^2 T^{-1}], $M=c_R R_n$ is the rate of the solute mass influx from rain [$ML^{-2}T^{-1}$], and c_R is the concentration of water in rain [ML^{-3}]. The solute concentration in soil water on the soil surface is assumed to be equal to the concentration in runoff.

C1.2 COUPLING SURFACE AND SUBSURFACE FLOW AND TRANSPORT IN THE NUMERICAL SOLUTION

We combined the public domain three-dimensional FEMFLOW code for saturated-unsaturated subsurface flow and transport with the two-dimensional 2DOIL (Pachepsky et al., 1993) code for modeling runoff. The 2DSOIL code as coupled with FEMWATER used to alter

the matrix coefficients of the boundary surface nodes in the flow and transport numerical equations as follows.

For the 3D mesh, the Richards equation at the surface boundary nodes was integrated using the finite element approximation:

$$\frac{\theta^{l+1}-\theta^{l}}{\Delta t}+A\cdot q^{l+1}-\frac{2(q_z^{l+1}-U^{l+1})}{\Delta z}-F=0 \qquad \text{(C-6)}$$

where A is the finite element approximation of the gradient operator $\vec{\nabla}$, and $\theta^l=\theta(x_i,y_j,z_k,t^l)$ and $p(x_i,y_j,z_k,t^l)$ are the water content and pressure heads at node *ijk*, $z=z(x_i,y_j,z_k)$ is the gravitational head for node *ijk*, $q=-k\vec{\nabla}(p+z)$ is the water flux in the horizontal direction, $q_z=-k_{z_{1/2}}(\frac{\Delta p^{l+1}}{\Delta z}+1)$ is water flux in the vertical direction, $\frac{\Delta p^{l+1}}{\Delta z}$ is pressure gradient in the vertical direction between the top surface boundary node and the next node in the vertical direction, Δz and $k_{z_{1/2}}$ are the distance and the conductivity between these two nodes; $U^{l+1}=\frac{h^{l+1}-h^{l}}{\Delta t}-\vec{\nabla}\cdot g^{l+1}+R_n$ is a surface boundary flux (which is an approximation from surface flow equation (C-6)) and $h=\begin{cases}p & p>0\\ 0 & p\le 0\end{cases}$ is surface flow depth. Equation (6) can be rewritten as

$$\frac{\ddot{\theta}^{l+1}-\ddot{\theta}^{l}}{\Delta t}+A\cdot \ddot{q}^{l+1}-\frac{2(q_z^{l+1}-U^{l+1})}{\Delta z}-F=0 \qquad \text{(C-7)}$$

where $\ddot{\theta}^l=\theta^l+2\eta(p^l)p/\Delta z$ is the corrected water content at the surface boundary nodes and $\ddot{q}^{l+1}=q^{l+1}+g^{l+1}=-\ddot{k}^{l+1}\vec{\nabla}(p^{l+1}+z)$ is the corrected flux at the surface boundary nodes in the *x* or *y* directions; $\ddot{k}=k+k_{surf}2/\Delta z$ is the corrected hydraulic conductivity of the surface boundary nodes; and $\eta(h)$ is the Heaviside function. A similar approach was used for the transport simulations.

Ponding did not generally occur simultaneously at all surface nodes, but the ponding front moved along the slope until all nodes were ponded. Similarly, the drying front (i.e., the front where runoff ceased to exist) also was moving from one node to another. Advances in the ponding and drying fronts were simulated by using upwind schemes for the nodes bracketing the front. The surface flow pressure gradient in the horizontal *x* and *y* directions could not be greater than the surface water layer gradient in those direction since the gradient is determined only of the depth of the surface water layer. For the wet or dry front for surface flow we used the limitation of surface horizontal gradient and upwind scheme for surface conductivity. Specifically, we used the control volume finite-element method for approximating the two-dimensional surface flow and mass transport equation (Baliga and Patankar, 1980, 1983). For a rectangular surface mesh with two neighboring surface nodes, horizontal surface flow $g^{l+1,s+1}$ and conductivity $k_{surf}^{s}{}_{1/2}$ during iteration process on s+1 iteration is determined as

$$g^{l+1,s+1}=-\ddot{k}_{surf_{1/2}}^{\;l+1,S}\cdot\left[\frac{\left|\max(p_1^{l+1,S},0)-\max(p^{l+1,S},0)\right|+\varepsilon}{\left|p_1^{l+1,S}-p^{l+1,S}\right|+\varepsilon}\cdot\frac{p_1^{l+1,S+1}-p^{l+1,S+1}}{\Delta e}+\frac{z_1-z}{\Delta e}\right]/\Delta z \qquad \text{(C-8)}$$

where $\frac{\left|\max(p_1^{l+1,S},0)-\max(p^{l+1,S},0)\right|+\varepsilon}{\left|p_1^{l+1,S}-p^{l+1,S}\right|+\varepsilon}$ automatically limits the value of the pressure gradient and

$$\ddot{k}_{surf_{1/2}}^{l+1,S}=\begin{cases}(k_{surf}^{l+1,S}+k_{surf_1}^{l+1,S})/2 & P^{l+1,S}>0\,\&\,P_1^{l+1,S}>0\\ k_{surf_1}^{l+1,S}/2 & P_1^{l+1,S}>0\,\&\,(P_1^{l+1,S}+z_1)>z\\ k_{surf}^{l+1,S}/2 & P^{l+1,S}>0\,\&\,(P^{l+1,S}+z)>z_1\\ 0 & otherwise\end{cases} \tag{C-9}$$

In which $\ddot{k}_{surf_{1/2}}^{l+1,S}$ determines the possible direction and rate of surface flow front movement, Δe is the step in x or y direction. Using this approximation limits the surface pressure gradient prevents the erroneous computation of the flow from dry sells. This procedure provides the numerical stability and mass conservation in the surface flow. Overall, the surface flow equation was approximated only in surface boundary nodes and was solved simultaneously with the Richards equation in subsurface. The matrix of nonlinear system algebraic Richards equations had to be modified only in boundary nodes

Two small parameters were introduced to prevent oscillations and to save the computation time. First, runoff was deemed to be formed and solution of the equations (C-7) began when the soil pressure head on the surface exceeded a small positive number h_0 that could be viewed as an initial thickness of the water film on the surface. The value of h_0 was set to 10^{-4} m. Second, the discontinuous Heaviside function and its derivative, the Dirac function, were replaced with their continuous approximations:

$$\eta_\omega(h)=\frac{1}{\pi}\operatorname{arctg}(h/\omega)\cdot h$$
$$\delta_\omega(h)=\frac{1}{\pi}\cdot\frac{\omega}{\omega^2+h^2} \tag{C-10}$$

where ω is the spread parameter. This allowed avoiding iterations to find the ponding time in each of surface nodes. The value of ω was 0.01m.

Because of relatively poor mass balances observed in the flow and transport simulations, we changed the numerical scheme and used the control volume finite-element method (Baliga and Patankar, 1983) in FEMWATER and upstream weighing in 2DSOIL as implemented in the SWMS2D model (Simunek et al., 1994). These changes provided a satisfactory mass balance.

NRC FORM 335 (9-2004) NRCMD 3.7

U.S. NUCLEAR REGULATORY COMMISSION

BIBLIOGRAPHIC DATA SHEET

(See instructions on the reverse)

1. REPORT NUMBER (Assigned by NRC, Add Vol., Supp., Rev., and Addendum Numbers, If any.)

NUREG/CR-7026

2. TITLE AND SUBTITLE

Application of Model Abstraction Techniques to Simulate Transport in Soils

3. DATE REPORT PUBLISHED

MONTH	YEAR
March	2011

4. FIN OR GRANT NUMBER

N6235

5. AUTHOR(S)

Y. Pachepsky, T. Gish, and A. Guber (USDA/ARS); A. Yakirevich and M. Kouznetsov (BGU), M. Van Genuchten (UFRJ), T. Nicholson and Ralph Cady (NRC)

(ARS- Agricultural Research Service, BGU - Ben-Gurion University of the Negev, UFRJ - Federal University of Rio de Janeiro)

6. TYPE OF REPORT

Technical

7. PERIOD COVERED *(Inclusive Dates)*

September 2005 - October 2009

8. PERFORMING ORGANIZATION - NAME AND ADDRESS *(If NRC, provide Division, Office or Region, U.S. Nuclear Regulatory Commission, and mailing address; if contractor, provide name and mailing address.)*

Agricultural Research Service
Beltsville Agricultural Research Center
10300 Baltimore Boulevard
Beltsville, MD 20705

9. SPONSORING ORGANIZATION - NAME AND ADDRESS *(If NRC, type "Same as above"; if contractor, provide NRC Division, Office or Region, U.S. Nuclear Regulatory Commission, and mailing address.)*

Division of Risk Analysis
Office of Nuclear Regulatory Research
U.S. Nuclear Regulatory Commission
Washington, DC 20555-0001

10. SUPPLEMENTARY NOTES

T.J. Nicholson, NRC Project Manager

11. ABSTRACT *(200 words or less)*

Successful understanding and modeling of contaminant transport in soils and groundwater is a precondition of risk-informed predictions of the subsurface contaminant transport. Exceedingly complex models of subsurface transport are often inefficient. Model abstraction is a methodology for reducing the complexity of a simulation model while maintaining the validity of the simulation. The objective of this work was to use model abstraction techniques to characterize and understand flow and transport in soils in the presence of shallow groundwater. We developed two case studies by carrying out two types of field tracer experiments at the USDA-ARS OPE3 Beltsville field site, and applying a sequence of model simplifications based on the HYDRUS software family and MODFLOW. Soil moisture, soil water potential, tracer concentrations in groundwater, groundwater levels, and weather data, along with ground penetration radar surveys, electric resistivity monitoring, and dilution tests complemented borehole log data and laboratory hydraulic measurements to characterize soil heterogeneity. The invoked series of model abstractions showed the important role of subsurface heterogeneity in the vadose zone and groundwater, and substantial improved the conceptualization of the subsurface. Results of this study provide techniques to aid the NRC licensing staff in their review of a licensee's abstraction of complex transport models, and to help confirm the acceptability of model abstraction assumptions used in performance assessments.

12. KEY WORDS/DESCRIPTORS *(List words or phrases that will assist researchers in locating the report.)*

field tracer experiment
flow and transport modeling
ground water
model abstraction
model simplification
pedotransfer function
soil water
subsurface contaminant transport
uncertainty
vadose zone

13. AVAILABILITY STATEMENT

unlimited

14. SECURITY CLASSIFICATION

(This Page) unclassified

(This Report) unclassified

15. NUMBER OF PAGES

16. PRICE

Federal Recycling Program

UNITED STATES
NUCLEAR REGULATORY COMMISSION
WASHINGTON, DC 20555-0001

OFFICIAL BUSINESS